AD 609059

U. S. ARMY
TRANSPORTATION RESEARCH COMMAND
FORT EUSTIS, VIRGINIA

TRECOM TECHNICAL REPORT 64-59

TANDEM CASCADE THRUST VECTORING RESEARCH PROGRAM

Project 1D121401A142
Contract DA 44-177-AMC-73(T)

November 1964

COPY 2 OF 3
HARD COPY $. 4 00
MICROFICHE $. 1 00

prepared by:

GENERAL ELECTRIC COMPANY
Flight Propulsion Division
Cincinnati, Ohio

149 p

ARCHIVE COPY

DISCLAIMER NOTICE

When Government drawings, specifications, or other data are used for any purpose other than in connection with a definitely related Government procurement operation, the United States Government thereby incurs no responsibility nor any obligation whatsoever; and the fact that the Government may have formulated, furnished, or in any way supplied the said drawings, specifications, or other data is not to be regarded by implication or otherwise as in any manner licensing the holder or any other person or corporation, or conveying any rights or permission, to manufacture, use, or sell any patented invention that may in any way be related thereto.

* * *

DDC AVAILABILITY NOTICE

Qualified requesters may obtain copies of this report from

Defense Documentation Center
Cameron Station
Alexandria, Virginia 22314

* * *

This report has been released to the Office of Technical Services, U. S. Department of Commerce, Washington 25, D. C., for sale to the general public.

* * *

The findings and recommendations contained in this report are those of the contractor and do not necessarily reflect the views of the U. S. Army Mobility Command, the U.S. Army Materiel Command, or the Department of the Army.

HEADQUARTERS
U S ARMY TRANSPORTATION RESEARCH COMMAND
FORT EUSTIS VIRGINIA 23604

This report has been reviewed by the U. S. Army Transportation Research Command, and the data contained herein are considered to be valid. The report is published for the dissemination of information.

PATRICK A. CANCRO
Project Engineer

JOHN E. YEATES
Group Leader
Aeromechanics Group

APPROVED.

FOR THE COMMANDER:

for LARRY M. HEWIN
Technical Director

Project 1D121401A142
Contract DA 44-177-AMC-73(T)
TRECOM Technical Report 64-59
November 1964

TANDEM CASCADE THRUST VECTORING RESEARCH PROGRAM

Prepared by:
Lift Fan Systems Operation
Advanced Engine and Technology Department
Flight Propulsion Division
General Electric Company
Cincinnati, Ohio 45215

for
U. S. ARMY TRANSPORTATION RESEARCH COMMAND
FORT EUSTIS, VIRGINIA

FOREWORD

This report describes an investigation to determine the aerodynamic feasibility of single and tandem cascades for vectoring the thrust of V/STOL aircraft. The investigation was conducted by the Flight Propulsion Division of the General Electric Company, Evendale, Ohio, under U.S. Army Contract Number DA 44-177-AMC-73(T). The Project Engineer was J. R. Erwin and the principal engineers conducting the investigations were D. E. Clark, R. G. Giffin, and J. G. Kirkpatrick. The experimental phases of the project began in June 1963, and were completed in June 1964.

CONTENTS

	Page
FOREWORD	iii
LIST OF ILLUSTRATIONS	vii
LIST OF TABLES	xiii
LIST OF SYMBOLS	xv
SUMMARY	1
CONCLUSIONS	3
RECOMMENDATIONS	4
INTRODUCTION	5
SCOPE OF INVESTIGATION	10
TECHNICAL DISCUSSION, PHASE I	12
TECHNICAL DISCUSSION, PHASE II	18
TECHNICAL DISCUSSION, PHASE III	23
BIBLIOGRAPHY	41
APPENDIX I, CHRONOLOGY OF RUNS	43
APPENDIX II, TABULATION OF TEST POINTS	45
APPENDIX III, SAMPLE CALCULATION	54
APPENDIX IV, DRAWINGS	59
APPENDIX V, FIGURES 1 THROUGH 67	65
DISTRIBUTION	135

BLANK PAGE

ILLUSTRATIONS

Figure		Page
1	Tandem Cascade	65
2	View of Test Section in the Transonic Cascade Tunnel	66
3	Reverse Thrust Mode	67
4	Short Take-Off and Landing (STOL) Mode	67
5	Vertical Take-Off and Landing (VTOL) Mode	67
6	Cruise Mode	67
7	Intermediate Positions	67
8	Flapped-Blade Cascade	68
9a	Articulated Inlet Guide Vanes	69
9b	Articulated Inlet Guide Vanes	70
10	Silicon Rubber Variable Camber Blades (Convex Side)	71
11a	Honeycomb Variable Camber Blades (Convex Side)	72
11b	Honeycomb Variable Camber Blades (Concave Side)	72
12	Cascade Geometry Nomenclature	73
13	Articulated Blade	74
14	Articulated-Blade Cascade - Low Camber	75
15	Articulated-Blade Cascade - High Camber	76
16	Flapped Blade	77
17	Flapped-Blade Cascade	78
18a	Flexible-Blade Dimensions	79

Figure		Page
18b	Flexible-Blade Cascade - Low Camber	80
18c	Flexible-Blade Cascade - High Camber	80
18d	Flexible Blades - Four Camber Settings	81
19	Experimental Evaluation of Expanded Honeycomb as an Aerodynamic Surface	82
20	Articulated Airfoil. Airfoil Setting Angle $\lambda = 29^{\circ}$ ...	83
21a	Articulated Airfoil. Airfoil Setting Angle $\lambda = 0^{\circ}$	84
21b	Articulated Airfoil. Airfoil Setting Angle $\lambda = 0^{\circ}$	85
22	Flapped Airfoil. Airfoil Setting Angle $\lambda = 29^{\circ}$	86
23	Flexible Airfoil. Camber $\theta^* = 17^{\circ}$. Airfoil Setting Angle $\lambda = 29^{\circ}$	87
24	Flexible Airfoil. Camber $\theta^* = 36^{\circ}$. Airfoil Setting Angle $\lambda = 17.25^{\circ}$	88
25	Flexible Airfoil. Camber $\theta^* = 66^{\circ}$. Airfoil Setting Angle $\lambda = 0^{\circ}$	89
26	Total Pressure Loss Coefficient Comparison between Airfoils	90
27	Tandem (Forward) Cascade. Camber $\theta^* = 30^{\circ}$. Airfoil Setting Angle $\lambda = 22^{\circ}$	91
28a	Tandem (Forward) Cascade. Camber $\theta^* = 45^{\circ}$. Airfoil Setting Angle $\lambda = 14.5^{\circ}$	92
28b	Tandem (Forward) Cascade. Camber $\theta^* = 45^{\circ}$. Airfoil Setting Angle $\lambda = 14.5^{\circ}$	93
29a	Tandem (Forward) Cascade. Camber $\theta^* = 60^{\circ}$. Airfoil Setting Angle $\lambda = 7^{\circ}$	94
29b	Tandem (Forward) Cascade. Camber $\theta^* = 60^{\circ}$. Airfoil Setting Angle $\lambda = 7^{\circ}$	95

Figure		Page
30a	Tandem (Forward) Cascade. Camber $\theta^* = 78^\circ$. Airfoil Setting Angle $\lambda = -2^\circ$	96
30b	Tandem (Forward) Cascade. Camber $\theta^* = 78^\circ$. Airfoil Setting Angle $\lambda = -2^\circ$	97
31	Flexible Airfoil. Single Cascade	98
32	Tandem Cascade of Flexible Blades Installed in Transonic Cascade Tunnel	99
33	Tandem Cascade. Forward Camber $\theta_A^* = 60^\circ$. Aft Camber $\theta_B^* = 8^\circ$. Turning Angle $\beta_J = \theta_B = 50^\circ$	100
34	Tandem Cascade. Forward Camber $\theta_A^* = 60^\circ$. Aft Camber $\theta_B^* = 30^\circ$. Turning Angle $\beta_J = \theta_A + \theta_B = 70^\circ$	101
35	Tandem Cascade. Forward Camber $\theta_A^* = 60^\circ$. Aft Camber $\theta_B^* = 52^\circ$. Turning Angle $\beta_J = \theta_A + \theta_B = 90^\circ$	102
36	Tandem Cascade. Forward Camber $\theta_A^* = 78^\circ$. Aft Camber $\theta_B^* = 66^\circ$. Turning Angle $\beta_J = \theta_A + \theta_B = 130^\circ$ ...	103
37	Tandem Cascade. Forward Camber $\theta_A^* = 60^\circ$. Aft Camber $\theta_B^* = 52^\circ$. Turning Angle $\beta_J = \theta_A + \theta_B = 90^\circ$	104
38	Tandem Cascade. Forward Camber $\theta_A^* = 78^\circ$. Aft Camber $\theta_B^* = 66^\circ$. Turning Angle $\beta_J = \theta_A + \theta_B = 129^\circ$ ...	105
39	Summary of Flexible-Airfoil Tandem Cascade Results Obtained in the Transonic Cascade Tunnel	106
40	Schematic of Tandem Cascade Test Facility	107
41	Scale-Model Tandem Cascade Facility - Plan View	108
42	View Looking into Cascade B Discharge	109
43	View Looking Upstream between Cascades A and B	110
44	Scale-Model Tandem Cascade Facility - Side View	111

Figure		Page
45	Flow and Pressure Rise Coefficients for 26-Inch-Tip-Diameter Fan	112
46	Fixed-Camber Cascade with Molded Plastic Blades. Camber $\theta^* = 90^\circ$. Solidity $\sigma = 2.14$	113
47	Tandem Cascade Geometry Nomenclature	114
48	Vectored Thrust	115
49	Vectored Thrust	116
50	Vectored Thrust	117
51	Vectored Thrust	118
52	Maximum Vectored Thrust for Tandem Cascade Testing, Runs 1-14	119
53	Blade Wake Profiles. Single Cascade. $\theta_A^* = 78^\circ$, $\beta_1^* = 39^\circ$, and $\gamma_A = 35^\circ$	120
54	Blade Wake Profiles. Tandem Cascade. $\theta_B^* = 78^\circ$, $\beta_1^* = 39^\circ$, and $\gamma_B = 95^\circ$	121
55	Vectored Thrust Comparison - Cascade A Shifted Aft	122
56	Vectored Thrust Comparison - Cascade B Shifted Aft	123
57	Vectored Thrust	124
58	Vectored Thrust - Ground Effect	125
59	Vectored Thrust - Ground Effect	126
60	Vectored Thrust - Ground Effect	127
61	Vectored Thrust Comparison of Simulated Flight and Static Test Conditions	128
62	Vectored Thrust	129

Figure		Page
63	Vectored Thrust	130
64	Summary of Maximum Vectored Thrust for Phase III. Tandem Cascade Testing	131
65	Flow Distribution through Tandem Cascades	132
66	Vectored Thrust - Ducted Flow	133
67	Comparison of Run 27 Vectored Thrust with Previous Runs	134

TABLES

Table		Page
1	Simulated Flight Data Comparison	38
2	Example Test Data	58

SYMBOLS

A	Flow path cross-sectional area, feet^2
C_P	Static pressure rise coefficient $= \frac{P_2 - P_1}{P_{T1} - P_1}$
d	Fan rotor diameter, d = 26 inches
F	Force, pounds
F_H	Horizontal thrust, pounds
F_V	Vertical thrust or lift, pounds
$F_H \frac{\theta}{\delta}$	Horizontal corrected thrust, pounds
$F_V \frac{\theta}{\delta}$	Vertical corrected thrust or lift, pounds
h/d	Ground plane height h divided by rotor diameter d
HP	Horsepower input, feet-pound/second^2
i	Incidence angle $(\beta_1 - \beta_1^*)$, degrees
L	Length, feet
M	Mach number
n	Rotational speed, revolutions/second
P	Pressure, pounds/feet^2
P_T	Total pressure, pounds/feet^2
p	Static pressure, pounds/feet^2
Q	Flow, feet^3/second
R	Resultant thrust force or radius, pounds
$R \frac{\theta}{\delta}$	Resultant corrected thrust force, pounds
STOL	Short take-off and landing

T	Fan inlet total temperature = temperature $^{o}F + 460^{o}R$ (Degrees Rankine)
TCT	Transonic Cascade Tunnel
U_T	Fan rotor tip speed, feet/second
$V_{10.2}$	Flow velocity at fan rotor inlet, feet/second
V_p	Wind tunnel velocity, feet/second
VTOL	Vertical take-off and landing
β_F	Angle of the resultant thrust R $\underline{\theta}$ from the fan axis $= \arctan F_V \frac{\theta}{\delta} \Big/ F_H \frac{\theta}{\delta}$, degrees$^{\delta}$
β_J	Jet efflux angle measured from fan axis during the test, degrees
β_1	Air inlet angle from cascade axis, degrees
β_2	Air exit angle from cascade axis, degrees
β_1^*	Blade inlet angle from cascade axis, degrees
β_2^*	Blade exit angle from cascade axis, degrees
γ	Cascade orientation angle measured from normal to fan discharge, degrees
δ	Air exit deviation angle, $\delta = \beta_2^* - \beta_2$, degrees
η_R	Rotor efficiency
θ	Air turning angle, $\theta = \beta_1 + \beta_2$ (degrees) or temperature correction, $\theta = \frac{\text{temperature } ^{o}F + 460^{o}F}{518.7^{o}F}$
θ^*	Blade camber angle, $\theta^* = \beta_1^* + \beta_2^*$, degrees
λ	Airfoil setting angle measured from cascade axis, degrees
π	Geometrical constant, $\pi = 3.14159$

ρ_o	Mass density at standard conditions, slugs/feet^3
σ	Solidity = $\frac{\text{blade chord length}}{\text{blade pitch}}$
ϕ	Flow coefficient
$\phi_{10.2}$	Flow coefficient measured at plane just ahead of fan rotor $\frac{V_{10.2}}{U_T}$
ψ	Pressure rise coefficient
$\psi_{10.6}$	Pressure rise coefficient measured across the fan rotor $\frac{P_{T10.6} - P_{T\ ambient}}{\frac{\rho U_T^2}{2}}$
$\bar{\omega}$	Pressure loss coefficient measured across a cascade

SUBSCRIPTS

1	Inlet plane at upstream boundary of cascade
2	Exit plane at downstream boundary of cascade
10.2	Inlet plane just ahead of fan rotor
10.6	Plane between fan rotor and fan stator
A	Denotes Cascade A
B	Denotes Cascade B

BLANK PAGE

SUMMARY

PHASE I

Variable camber airfoils of three different types -- articulated, flapped, and flexible -- were tested in the Transonic Cascade Tunnel to determine their suitability for use in thrust-vectoring tandem cascades for V/STOL aircraft. The required conditions were inlet flow angles of 30, 34 (nominal), and 38°, and inlet Mach numbers from about 0.30 to drag-rise (0.40 to 0.70), with a nominal inlet Mach number of 0.50. Only the flexible airfoil cascade was capable of producing the required turning angle (67.5°) with low loss at the nominal inlet conditions. Therefore, this type was selected for further investigation in single and in tandem cascade arrangements.

PHASE II

Single cascades of flexible airfoils were tested in a more systematic and detailed investigation to determine proper cambers and setting angles for their use in single and tandem cascades. Consistent turning angle and loss coefficient results were obtained for the camber range from 30° to 78° over a range of inlet angles from 30° to 38° and inlet Mach numbers from about 0.30 to 0.60.

Tandem cascades of flexible airfoils were tested with overall flow turning angles of 50, 70, 90 and 130°. Although the flow in the aft cascade appeared to be satisfactory during tuft studies at very low speeds ($M \approx 0.10$), the losses increased rapidly with increasing inlet Mach number and were unacceptably high at $M_1 = 0.50$. These results were believed to be due primarily to strong secondary flows occurring in the low-aspect-ratio (AR = 1) test airfoils. The porous wall technique was employed to increase the effective aspect ratio of the forward cascade. Through the use of this technique and other minor modifications, satisfactory tandem cascade results were obtained at the nominal inlet conditions for the vertical thrust and reversed thrust modes of V/STOL aircraft operation.

PHASE III

An experimental evaluation of the tandem cascade thrust vectoring system was made on a scale model of a cruise fan installation using two cascades of flexible camber airfoils.

A satisfactory level of thrust vectoring was demonstrated over the range from zero to maximum vectoring. The following significant results were obtained, described by the angle by which the thrust was vectored and

the magnitude of the resultant thrust expressed as a percent of the unvectored fan thrust:

	Vector Angle (degrees)	Thrust Vector (percent)
Basic Fan Thrust	0°	100
Single Cascade - Uncambered	0°	97.5
Single Cascade - Maximum Camber	64.4°	93.6
Tandem Cascade - VTOL	90°	92.6
Tandem Cascade - Maximum Camber	124°	86.8
Tandem Cascade - Maximum Reversal	130°	84.1

In general after the 2-1/2 percent loss incurred by inserting the first uncambered cascade in the air stream, the loss increased from 7 percent at 90° vectoring to 13 percent at 124° vectoring. A maximum of 54 percent reversed thrust was obtained.

CONCLUSIONS

The combination of transonic cascade tunnel testing and scale model system testing conclusively demonstrated that tandem cascade thrust vectoring can provide an efficient system for STOL or VTOL propulsion systems.

The performance superiority of the flexible airfoils over the flapped and articulated airfoils is clear and dramatic up to test Mach numbers encountered in V/STOL devices. After evaluation of proper testing techniques, wind tunnel cascade testing of the flexible airfoils in a tandem cascade configuration showed satisfactory operation up to test Mach numbers of 0.5.

Low-speed testing with two cascades of flexible camber blading behind a scale-model cruise fan demonstrated efficient thrust vectoring through 90^{o} suitable for VTOL operation. Efficient thrust vectoring through 67^{o} and 130^{o} with a maximum of 54 percent of reversed thrust as required for STOL operation was also demonstrated.

The demonstrated performance could clearly be improved since there were distinct deviations in the quality of the scale-model blading. Further improvement is possible as a result of discovering unexpected spreading of the free jets, which caused some of the flow to miss the deflecting cascades. The results from the cascade wind tunnel tests obtained at high Mach number prove that these low-speed results obtained at 0.1 Mach number are valid up to an operating Mach number of 0.5. Consequently, the application of the tandem cascade thrust vectoring system to V/STOL systems is feasible.

RECOMMENDATIONS

It is recommended that:

1. A similar investigation be conducted to demonstrate the design of a thrust vectoring system to maximize the efficiency at 90^{o} vectoring for VTOL and to further improve the reversed thrust capability. Tests of the fixed 90^{o} turning cascade followed by a flexible camber cascade produced 152^{o} vectoring angle with 68 percent reversed thrust.

2. A similar program be conducted to evaluate the feasibility of, and to demonstrate, a 0^{o} to 90^{o} variable camber cascade as a single deflecting cascade.

3. A high Mach number test of a suitably scaled configuration be conducted to assess aeromechanical problems of a practical design.

INTRODUCTION

Use of cruise engines as part of any V/STOL lifting system is a basic requirement. No efficient V/STOL aircraft design could afford the luxury of an independent lift system which did not utilize the cruise engines. Simple means of varying the direction of the cruise engine thrust vector is an essential requirement in practical V/STOL applications. Tilting or swivelling engines, convertible lift fans and various thrust deflection schemes are the main approaches to this requirement.

A tandem cascade exhaust system (Figure 1) is a novel thrust deflection method which has been studied by the General Electric Company. It offers the potential for efficient operation over a continuous range of flow deflections from horizontal through vertical to about 45° forward of vertical. The flow turning required varies from 0° to 135°. This same system would, therefore, be applicable to VTOL systems and include at the same time the very difficult thrust reversing capability for STOL operation.

FIXED-CAMBER AIRFOILS

The broad range of travel required of a vectored thrust system for VTOL, STOL, and reverse thrust operation (0° to 135°) is believed to be well beyond the capability of a single row of conventional airfoils. The best known performance for conventional inlet guide vanes or exit louvers (operating with 0° inlet angle) is about $\pm 20^{\circ}$. Although tandem cascades of such airfoils have not been extensively investigated, it would seem that $\pm 40^{\circ}$ would be the maximum operating range of fixed-camber airfoils that could be expected, and only then with substantial static pressure drop.

FLAPPED AIRFOILS

When thrust vectoring is being considered, it is usually desired not to affect the fan discharge pressure through the use of the vectoring device. This constant-static-pressure turning of the flow is referred to as "impulse". In order to determine the performance of exit louvers under impulse conditions, a cascade of flapped airfoils has been tested in the General Electric Transonic Cascade Tunnel (TCT), Figure 2, over a range of inlet angles and flap angles (Reference 1). The results indicate that $\pm 20^{\circ}$ of turning can be achieved with low loss without static pressure drop. The possibility exists that specially designed flapped airfoils can accomplish the range of $\pm 33\text{-}3/4^{\circ}$ of turning required of louver vanes in a typical thrust vectoring tandem cascade (Figures 3 through 7). The cascade of flapped blades is shown in Figure 8.

ARTICULATED AIRFOILS

The General Electric Company has recently conducted a limited series of tests on articulated inlet guide vanes (Reference 2), Figure 9. These articulated inlet guide vanes are of somewhat unusual design in that the fixed forward portion is a relatively small percent (about 20 percent) of the total chord length of the vanes. The pivoting flap portion made up the remaining chord length of the airfoil. Tests at a solidity of 1.50 with these articulated inlet guide vanes yielded low-loss turning angles of about $\pm 50^{\circ}$ (inlet air angle with respect to cascade, $\beta_1 = 0^{\circ}$). Substantial static pressure drop occurred. This type of airfoil has not been tested as a tandem cascade. There is reason to believe, however, that a tandem cascade of these inlet guide vanes with the second row also fully articulated might exhibit the necessary range for a thrust vectoring system to accomplish both VTOL and STOL requirements. The observed wide operating range would probably not be achieved under impulse (constant static pressure) condition. For efficient operation of articulated airfoils, a significant drop in static pressure across the cascade with a resultant increase in fan static back pressure may be required.

FLEXIBLE AIRFOILS

The success of the articulated airfoil has stimulated ideas for achieving further advances in the design of airfoils to work efficiently with very broad ranges of thrust deflections. Sometime ago the possibility of using variable-camber airfoils was considered. At that time two novel types of variable-camber airfoils were constructed. One type uses a room-temperature vulcanizing silicon rubber for one of the aerodynamic surfaces and metal shim stock (Figure 10) for the other aerodynamic surface. Figure 11 illustrates another type which has been constructed using a flexible compressed honeycomb for one of the aerodynamic surfaces and metal shim stock for the other. A variation, which could be applied to either type of material, would be to use the continuous metal shim stock for the meanline of the airfoil, and to use the expandable material for both aerodynamic surfaces. The aerodynamic performance of these flexible airfoils has not yet been measured. The metal honeycomb airfoils will be tested in both single and tandem cascades in order to establish the range of operation attainable with high efficiency.

TANDEM CASCADE ARRANGEMENT

A method for achieving continuous thrust vectoring from the horizontal cruise condition through the STOL and VTOL modes to thrust reversal with a tandem cascade system has been briefly considered. In a proposed scheme the powerplant nacelle has a transition from circular cross-section

to rectangular in the zone of the vectoring cascades, but the present investigation will use a conical nozzle and elliptical cascades.

In this system (refer to Figure 1) the first row of the cascade is fixed in one position to accommodate all operating conditions including cruise, and the second row is variable so that it can be positioned at all operating conditions for impulse turning and stowed for cruise. Both rows consist of variable-camber vanes. For the maximum flow turning required, 135°, the turning is divided equally between the two cascades. The arrangement is such that in this full-reverse-thrust position both cascades operate in the impulse condition, that is, with the inlet flow angle to the cascade equal to half the cascade turning angle as shown in Figure 3. In this case, each cascade is set at an angle of 33.75° to its inlet flow and each contributes $67\text{-}1/2^{\circ}$ of turning.

The relationship between cascade and air angles and this desired impulse condition can be shown with simple vector diagrams. Impulse conditions are present when the area of the cascade normal to inlet flow is equal to the area of the cascade normal to the discharge flow. See Figure 12 for cascade geometry nomenclature.

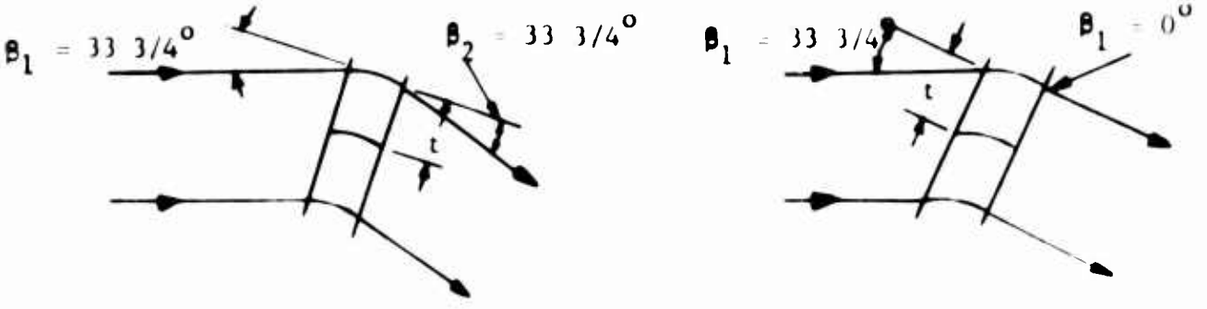

Case I Case II

In Case I, the area normal to inlet flow is a function of the product of cascade pitch "t" and cosine β_1. The discharge area is a function of the product of cascade pitch "t" and cosine β_2. As $\beta_1 = \beta_2$, there is no area change and the impulse condition is present. In Case II, the inlet area is a function of the product of cascade pitch "t" and the cosine of β_1 ($33\text{-}3/4^{\circ}$). The discharge area is a function of the product of cascade pitch "t" and the cosine of β_2 (0°). The discharge to inlet area ratio is then about 1.2 and a diffusion condition exists. Diffusion during turning is known to be detrimental to cascade performance.

MODE OF OPERATION

It is proposed that for STOL operation, only the first cascade would be used and the second cascade would be carried in a closed position aligned with the discharge flow (Figure 4). For the larger flow deflections required for VTOL operation and thrust reversal, the second cascade is in a position to intercept the discharge flow from the first cascade so that the inlet flow angle of the second cascade would equal half of the turning produced by the second cascade (Figure 5). Thus, the second cascade always operates in the impulse or constant static pressure condition. The first cascade operates with varying amounts of negative reaction (pressure rise) except during cruise or the reversed thrust condition. For cruise the first cascade is set with the vanes at zero camber and the second cascade is stowed (Figure 6). An intermediate position is shown in Figure 7.

CRITICAL OPERATING CONDITION

Although this particular configuration may not be optimum when the practical details of retraction and stowage are considered, it does exhibit certain aerodynamic advantages. Both cascades are of minimum length and have the same maximum turning requirement. The most difficult aerodynamic job (maximum static pressure rise) that the airfoils in the proposed cascade must accomplish is turning the flow by 33° ($\beta_2 = 0^{\circ}$). This condition occurs in the first cascade for the STOL position and was Case II in the previously discussed example. The cascade data obtained by Reference 3 demonstrated that a significantly more difficult job than this (turning 45° from $\beta = 45^{\circ}$) can be accomplished efficiently, so no aerodynamic breakthrough other than providing the proper effective camber is required (area ratio of 1.415 vs. 1.2 in Case II). As the turning requirement increases beyond 33.75°, the static pressure rise produced decreases until the impulse condition is reached at the maximum turning required of $67\text{-}1/2^{\circ}$ ($\beta_2 = 33.75^{\circ}$) where $\beta_1 = \beta_2$.

PRACTICAL CONSIDERATIONS

It may not be necessary to provide a physical boundary between the extremities of the first and the second cascades. (Theoretically, the static pressure between the cascades would be ambient for an impulse condition in the first stage.)

It may be of practical importance that the force vector produced by the second cascade is always radially outward from the hinge point with the exception of the aerodynamic drag. For this reason, the force required to actuate the second cascade in rotation about the hinge point will be quite small. In fact, it is possible, although perhaps not practical,

to control the airfoils of the second cascade in such a manner as to produce aerodynamic forces to assist in moving the cascade in the desired direction.

In the tandem cascade arrangement initially considered and previously described, the operating requirements of the second cascade are: (1) thrust reversal, a turning angle of 68° with an inlet angle of 34°; (2) VTOL, a turning angle of 38° with an inlet angle of 19°; (3) transition, continuous variation in turning angle from 38° to 0° and inlet air angle with inlet air angle equal to one-half of the turning angle; (4) STOL, stowed. Relatively complex mechanical problems arise as a result of the transition phase of operation because of simultaneous variations in camber of first cascade row and leading edge angle, camber and angular position of the second cascade row.

A study of the overall system was made to determine other possible schemes which would eliminate some of the mechanical problems with reasonable compromises to the system aerodynamics. The resulting scheme allowed fixing of the leading edge portion of the blading in the second cascade row and permits two-position operation of the second cascade row. The aerodynamic compromises accepted were a 15° swing in incidence angle on the second cascade row and operation of the second cascade row at a slight pressure rise during transition. (This pressure rise results from turning the flow through 19° from an inlet air angle of 19° which corresponds to an area ratio of about 1.06.) Neither of these compromises is very severe, nor is either expected to detract from system performance.

Under this more practical arrangement, the operating requirements are: (1) thrust reversal, as before; (2) VTOL, as before; (3) transition, continuous variation in turning angle from 38° to 0° at an inlet air angle of 19° by uncambering the second cascade row; (4) STOL, as before. The advantages of this arrangement are: (1) similarity of the actuation systems in the first and second cascades for camber changes, since leading-edge variation of the second cascade has been eliminated; (2) the leading edge of the second cascade can act as an integral structural member; (3) two-position operation for the second cascade; (4) simplicity in programming motions, since no simultaneous changes are required.

SCOPE OF INVESTIGATION

PHASE I - COMPARATIVE CASCADE TESTS

The present program included two phases of investigation using TCT. The first phase consisted of a comparative evaluation of the merits of flapped, articulated and flexible airfoils. The test conditions included the range of air deflection angles required to establish the relative merits of the several airfoil types at several values of inlet Mach number.

The requirements of the blading in a typical tandem cascade system are variable turning angle (0° to $67\text{-}1/2^{\circ}$) at constant inlet angle in the front cascade and variable turning angle (0° to $67\text{-}1/2^{\circ}$) with inlet angle equal to one-half of the turning angle in the second cascade. The wide operating range requirements of this system suggest the use of cascades in which the blade shape is made variable. Three possible types of blades for fulfilling this requirement are: (1) flexible blades, (2) articulated blades, and (3) flapped blades. The flexible blade is a single unit in which the shape is altered by a physical bending of the blade. The articulated and the flapped blades consist of two units (a front and a rear portion) which achieve the variable geometry by pivoting the two units relative to each other. The characteristic that distinguishes these two blade types is the motion between the front and rear portions. In the case of the flapped blade, the rear portion of the blade retracts from the front portion to form a pseudo-tandem cascade. In the articulated blade, the two units pivot but do not translate.

The present investigation consisted of the design and experimental evaluation of the three types of blades in cascade. The tests were conducted in the TCT. The test conditions covered the complete range of air deflection angles required (0° to $67\text{-}1/2^{\circ}$) and included several inlet Mach numbers.

PHASE II - TANDEM CASCADE TESTS

From the information obtained in Phase I, the optimum tandem cascades were selected to perform the total thrust deflection required, from horizontal (0°) through vertical (90°), to thrust reversal (135°). The first cascade was set for turning angles of 30°, 45°, and $67\text{-}1/2^{\circ}$ at constant inlet angles of 30°, 34°, and 38°. For each setting of the first cascade, the second was set for the appropriate inlet angle and turning angle to maintain impulse conditions. Basic cascade performance data was recorded at several values of inlet Mach number.

PHASE III - SCALE MODEL SYSTEM TESTING

After the basic cascade performance data was obtained, a low-speed, scale-model, test program to demonstrate the application of the tandem cascade principle was conducted. In this test, a representative scale model of a complete system was tested under all of the basic flight conditions possible with the tandem cascade arrangement, including normal forward flight, STOL, VTOL, and reversed thrust. Low-speed flight conditions and ground effects were simulated.

The scale-model tests employed an existing fan which is an aerodynamic scale of the X353-5 lift fan. It has been used since 1960 as a research vehicle for investigating system and internal aerodynamic effects on lift and cruise fans. It is instrumented for the measurement of thrust, power, efficiency, fan flow and pressure rise, and is equipped to operate in a free jet to simulate flight speeds equivalent to the range from 50 to 140 knots. It has recently been used to investigate the performance of a cruise fan wing-mounted nacelle with provision for thrust deflection by methods other than the use of cascades. It is obvious from these tests that the use of cascades is necessary for good performance and would permit an installation utilizing the least available space.

The basic feasibility of various tandem cascade arrangements was studied by installing both turning cascades with adjustable stagger and camber. Thrust, power, fan flow, and system efficiency were measured under static conditions and conditions of simulated, low-speed flight. Ground effect tests were run to determine the effect on the operation of the tandem cascade. The effect on the fan of the diffusing conditions (STOL) and the effect of the external flow on the diffusing cascade were determined.

A number of basic design questions required for the design of the tandem cascade system were investigated; e.g., the need for side plates and the need for confining the jet between the tandem cascades.

TECHNICAL DISCUSSION - PHASE I

GENERAL

The purpose of the Phase I investigation was to select a satisfactory variable camber airfoil type capable of turning flow having an inlet Mach number of about 0.50 through angles from 0^{o} to $67\text{-}1/2^{o}$. The tandem cascade was intended to be operated with the first cascade at a fixed inlet angle of about 34^{o} and with the camber variable as required for thrust vectoring. The second cascade would operate at variable inlet angles and with variable camber in an angular relationship such that little or no static pressure change (impulse condition) occurs across the second blade row. Since a small static pressure rise will occur across the first cascade at intermediate turning angles between 0^{o} and $67\text{-}1/2^{o}$, the first cascade is the more difficult from the standpoint of airfoil operation. Therefore, single cascade performance was measured at fixed inlet angles corresponding to the operation of the forward cascade of a tandem arrangement.

The optimum incidence angle was not known for the new airfoils to be tested in this investigation. Using the Transonic Cascade Tunnel (TCT), it is convenient to vary the inlet angle, β_1, while maintaining the setting angle, λ, of the airfoils fixed. To determine satisfactory incidence angles and to provide further operating information, each of the three different types of airfoils was tested at several inlet angles, generally 30^{o}, 34^{o}, and 38^{o}. The flapped blades did not perform well at 30^{o}, however, so the lowest inlet angle was increased to 32^{o} for this set.

Since the purpose of this phase was to select a satisfactory airfoil type, the testing was discontinued at a particular inlet angle and setting angle when it was determined that good performance could not be obtained with the airfoils being tested at an inlet Mach number of 0.50.

DESCRIPTION OF TEST BLADES

Articulated Airfoils

The articulated airfoils used in this test series were derived substantially from Reference 2. The maximum thickness used herein was 10 percent chord, and the camber of the basic section was 30^{o}. A close fit between the 20 percent chord fixed section and the 89 percent chord flap was specified, since the presence of a gap or slot had not proven beneficial in the reported inlet guide vane tests (Figure 13 and drawing 4012154-997, Appendix II, page 60). Photographs showing the articulated airfoils in two positions are given in Figures 14 and 15.

The articulated airfoils concentrate the camber at the hinge point for the high camber cases and produce passage area distributions that enlarge suddenly and then contract when used at positive inlet flow angles other than zero. These characteristics are not favorable to wide operating range, but their excellent performance as inlet guide vanes suggested that they might be satisfactory for impulse turning vanes. The excellent performance of the articulated inlet guide vane was probably attributable to the ability to design the passage without the sudden area enlargement because of the 0° inlet air angle. As inlet guide vanes, the articulated airfoils operated under conditions of increasing static pressure drop as the flap angle was increased from zero.

Flapped Airfoils

The flapped airfoils designed and tested in this program are required to operate efficiently over a wider range of turning angles than the flapped airfoil cascade reported in Reference 1. The movable portion (flap) of these airfoils was about 60 percent in length of the total airfoil chord. The flap could be rotated about a fixed pivot external to the airfoil through an angle of about 30° while maintaining a configuration meeting accepted requirements for slotted airfoil design. Some increase in effective chord length, and therefore cascade solidity, resulted during this rotation. The rotation permissible with these flaps was not considered nearly sufficient for the present purposes.

Several attempts were made to derive flapped airfoils capable of conforming to established design practices while deflected 70° to 75° (to achieve $67\text{-}1/2^{\circ}$ of flow turning). Flaps of lengths approaching the total airfoil chord length would be required to obtain the desired flow deflection. A sharp curvature resulted at the airfoil-flap juncture. The passage area distribution between adjacent blades in cascade showed rapid and large increases and then decreases in area. The slot width of the large deflection positions becomes unacceptably large. Good performance could not be expected under these conditions.

A new approach to the solution was then taken. Flapped airfoils consisting of a fixed lenticular section and a full-chord-length movable flap were examined. As the length of the lenticular section was increased, the effective chord length of each airfoil increased and the radius of rotation increased, but the required section thickness increased to obtain required flap deflection. As the lenticular section length was decreased, the reverse was true. A section best meeting the various requirements including a satisfactory passage area distribution was selected (drawing 4012160-033, Appendix II, page 61 and Figures 16 and 17). The airfoil in the nested 0° flap extension position was 10 percent thick and of 30° camber.

Flexible Airfoils

Derivation

The airfoil shape selected for the flexible airfoils was the NACA 65 series section of 10 percent thickness. The basic design was constructed using a 30° circular arc meanline. Studies of the flexible airfoils in various cambered and staggered arrangements were conducted. It was found that precambering of the shim stock forming the convex surface influenced the shape of the airfoil as the camber was varied. The passage area distribution was examined at cambers of 40°, 50°, 60°, and 70°. An airfoil yielding satisfactory passage area distribution was achieved when the shim stock for the 5-inch-chord airfoils was precambered $38\text{-}1/2^{\circ}$ with a radius of 5.50 inches (Figure 18a and drawing 4012154-988, Appendix II, page 59. The flexible airfoils are shown in the different cambered positions in Figures 18b, 18c, and 18d.

Construction

Flexible airfoils for testing in the TCT were constructed using thin (0.15 inch) brass shim stock for the convex airfoil surface. A machined airfoil leading edge and a triangular trailing edge were used. A brass bar located at approximately mid-chord location provided a third support point for the airfoils. The remainder of each airfoil, including the concave surface, consisted of closely packed sheet-metal strips commercially available from a manufacturer of honeycomb materials. In order to provide flexibility of the airfoil, it was necessary to attach the metal foil in a slightly expanded condition for the uncambered airfoil. A series of tests of a flat surface of the metal foil at various amounts of extension was conducted to determine the aerodynamic loss (Figure 19). In these tests it was found that the total pressure loss increased linearly as the honeycomb was extended from zero to 200 percent. At the 200 percent extension, the total pressure loss was about twice that of the smooth surface alone. Therefore, it was concluded that the small extension required to produce the flexible airfoil, about 15 percent, would not have a significant effect on the drag coefficient of the airfoils.

There are a number of methods for controlling the contour and setting angle of a flexible airfoil. If the leading and trailing edges only are used, it is necessary to apply a couple at the leading and trailing edges and to displace one edge in the axial and tangential directions with respect to the other edge. It is believed that this actuation system will be more complicated to use than the method selected: the use of three pin joints. Obviously, two of the pins must be moved with respect to one fixed pin in the tangential

direction; furthermore, provision for a small axial movement of the pins must also be made.

It was found during the course of the tests that the pin joints were not perfectly free and that modifications to the camber shape could be made. As will be pointed out subsequently, the test results indicated that the original circular arc meanline selected was not necessarily optimum.

TEST RESULTS

Articulated Airfoils

The articulated airfoils were tested in the zero flapped deflection case with a setting of 29°. This cascade was tested at inlet air angles of 30°, 34°, and 38° over the inlet Mach number range from 0.35 to about 0.70 (Figure 20). At the nominal inlet air angle of 34°, the loss coefficient remained low (0.030) to Mach numbers of about 0.60. The turning angle produced at a Mach number of 0.50 was 11.1°.

The flap angle of the articulated airfoils was set with an angle of 0°, and the cascade was tested at inlet angles of 30°, 34°, and 38°. At an inlet Mach number of 0.50, the turning produced at the nominal inlet air angle was 39.3° (Figure 21). The loss coefficient at this condition was 0.051.

An attempt was made to produce a turning angle of about 70° with the articulated blades. At the nominal inlet air angle and an inlet Mach number of 0.50, the loss coefficient was about 0.35. Attempts to improve performance by changing the inlet air angle were made but were unsuccessful. Therefore, it was concluded that the articulated airfoils were unsatisfactory for the present purposes.

Flapped Airfoils

The flapped airfoils were first tested in the 0°-flap-angle condition with a setting angle of 29°. This cascade performance was measured at inlet air angles of 32°, 34°, and 38° since poor performance was observed at $\beta_1 = 30^{\circ}$. At the nominal condition of 34°, the loss coefficient had the low value of 0.030 at Mach number of 0.38 and 0.51 (Figure 22). At higher Mach numbers the loss coefficient increased rapidly. The turning angle at the nominal conditions was 10.3° at a Mach number of 0.50.

Attempts were made to obtain satisfactory performance with the flapped blades set for turning angles of about 55°. Several setting angles were tried, and the inlet angle was varied over the range from 30° to 38°.

However, it did not appear possible to obtain a loss coefficient less than 0.160 at an inlet Mach number of 0.50. Therefore, it was concluded that the flapped airfoils were not satisfactory for operation in tandem cascades with high turning as required in the present program.

Flexible Airfoils

The flexible airfoils were tested with a setting angle of 29° and inlet angles of 30°, 34°, and 38°. At the nominal inlet air angle, the drag coefficient was 0.030 at an inlet Mach number of 0.60 (Figure 23). The turning angle at this condition was about 14.5°. At the reduced incidence angle obtained at an inlet angle of 30°, a lower turning angle (about 11°) was achieved with low drag values up to a Mach number of 0.57. At 38° inlet angle, the airfoils appeared to operate very well, with total pressure loss coefficients less than 0.030 up to an inlet Mach number of 0.63, turning angles of about 17° and a positive static pressure rise coefficient of from 0.20 to 0.15.

The camber of the flexible airfoils was then increased to a value of about 36° and set in the cascade at an angle of 17.25° from the axial direction (see Figure 24) to obtain maximum static pressure rise. At the nominal inlet angle, the turning produced was 30.3° with a loss coefficient of 0.034 at $M_1 = 0.62$, and a pressure coefficient of +0.15. The performance was also satisfactory at inlet angles of 30° and 38°, with the highest angle showing slightly better performance at inlet Mach numbers above 0.62.

The flexible airfoils were then reset with a camber of about 66° and with the lower-surface tangent parallel to the axial direction (setting angle $\lambda = 0^{\circ}$). At the nominal inlet angle, the turning was 55° for $M_1 = 0.50$, with a loss coefficient of $\varpi = 0.060$ obtained at $M_1 = 0.62$ (Figure 25). Satisfactory results were also obtained at $\beta_1 = 30^{\circ}$. The losses increased at $\beta_1 = 38^{\circ}$ rapidly above an inlet Mach number of 0.40 due to the combination of high turning (56°) and a significant static pressure rise, C_p.

CONCLUSIONS

The conditions at which the flexible airfoils were set in cascade, with 65° camber and 0° setting angle, produced an incidence angle of about -3° at the inlet angle of 34°. With 55° of turning observed, the difference in angle between the trailing edge direction and exit flow direction (the deviation angle) is about 7°. This amount of deviation is somewhat larger than would be expected for optimum airfoils of this camber operating with these inlet conditions at the solidity $\sigma = 1.50$ used. This result suggests that modifying the meanline to move the

point of maximum camber forward and thus to produce a more nearly straight trailing edge would be beneficial to performance.

A comparison of the loss coefficients as a function of turning angle as obtained with all three types of variable-camber airfoils is presented for the nominal inlet angle of 34° and an inlet Mach number of 0.50 on Figure 26. Only the flexible airfoils are capable of turning the flow more than 40° with low loss under these inlet conditions. For this reason, the flexible airfoils were selected for further investigation in tandem cascades under Phases II and III of this program.

TECHNICAL DISCUSSION - PHASE II

SINGLE CASCADE RESULTS

Following the selection of flexible airfoils for further investigation, and before the fabrication of the second set of blades required for tandem cascade testing was completed, a more detailed series of single-blade-row cascade tests was conducted to provide further information for selecting flexible airfoil cascade configurations. In this series, care was taken to set the camber of the airfoil to particular values of 30°, 45°, 60°, and 75° (actually 78° was set) so that the relationship between camber and turning angle could be defined more exactly. Inlet angles $\beta_1 = 30^\circ$, 34°, and 38° were again used to conform with previous runs and to provide similar information.

The results obtained (Figures 27 through 30) were quite consistent with the earlier flexible airfoil results. Rather than recite individual test point values, a general summary of the results will be presented: The loss levels are much more affected by the increase in area that occurs through the blade row (and the static pressure rise that is attempted) rather than the turning angle (θ) that is produced. Thus the condition of turning to axial direction ($\theta = \beta_1$) yields larger loss coefficients than $\theta = 2\beta_1$.

The effect of increasing Mach number is to accentuate the effects of diffusion. These relatively thick, high-cambered sections have a critical (drag-rise) Mach number of about 0.65 when operating with the nominal inlet angle and the solidity (1.50) of these tests. The condition for which the turning angle increases with Mach number (78° camber) has a large static pressure drop, and the increased turning appears to occur more as a function of the increasing pressure decrease than of the increasing Mach number.

The turning angle and loss coefficient as a function of camber at the nominal inlet conditions are summarized on Figure 31. The turning increases linearly with increasing camber and with an increasing deviation

The trailing edge direction β_2^* is

$$\beta_2^* = \beta_1 - i - \theta^*.$$

Since i has been set at -3° for the nominal inlet angle, β_2^* is known. β_2 is

$$\beta_2 = \beta_1 - \theta.$$

and the deviation δ is

$$\delta = \beta_2 - \beta_2^*.$$

Therefore, the deviations observed are 2.7, 2.0, 7.3, and 10.0 for cambers of 30^o, 45^o, 60^o, and 78^o. These values for the higher cambers seem larger than necessary for these test conditions and could be reduced by using airfoils having less curvature in the trailing edge region.

TANDEM CASCADES

The thrust vectoring cascades being investigated in the present program are intended for use in high-aspect-ratio arrangements like the exit louvers on the XV-5A aircraft. With aspect ratios of four or higher, the end effects, that is, the non-two-dimensional flows near the juncture of the vanes and the cascade boundaries, would not be expected to influence the main flow or to seriously affect the overall thrust vectoring performance. For the single-row cascade tests (aspect ratio one), the secondary flows dominated the flow in a region 1/4 to 1/3 of the blade span near the walls. The loss measurements were made in the central region of the cascade since the two-dimensional performance was of primary interest. Occasional spanwise surveys were made to determine that a significant percentage of the flow was uniform.

For the early tandem cascade tests (see Figure 32), no attempt was made to reduce the secondary flows occurring in the test section. Tuft surveys were made with the system operating at atmospheric discharge pressure and with the air flow at low speed. These studies indicated that generally satisfactory flow conditions existed. It was assumed, therefore, that the losses due to the secondary flows in the upstream cascade were not large and that essentially complete mixing of the primary flow and the secondary flow had occurred by the time the second cascade was encountered. When the TCT facility was closed and the Mach number increased to 0.40 and higher, it was found that unacceptably high losses were occurring. It was, there, decided to reduce the secondary flow and to increase the effective aspect ratio of the first cascade by employing the porous-wall technique reported in Reference 4. In the interval during the construction of the porous walls, tandem cascade testing continued, and the results obtained are presented in Figures 33 through 36. The desired turning angles were obtained.

VERTICAL THRUST

Because of conflicts of other programs using the TCT, it was not possible to conduct porous-wall tandem cascade tests for all of the turning angle

conditions required. It was decided to concentrate upon the two most critical conditions of vertical thrust ($\theta = 90^{\circ}$) and thrust reversal ($\theta = 135^{\circ}$). The early tandem cascade tests had indicated better performance with the forward cascade having slightly greater camber and turning than the aft cascade. For the 90° turning case, the camber of the forward cascade was set at 60° and aft cascade camber was set at 52°. The powerful effect of boundary layer removal through the porous wall is illustrated in Figure 37. For minimum bleed flow, high loss coefficients were again observed with inlet Mach numbers of 0.40 and above. With the nominal bleed flow, which was selected to yield equal upstream and downstream pressures at low Mach numbers, the loss coefficients were reduced significantly. For example, the early tandem cascade tests indicated a loss coefficient of 0.24 at an inlet Mach number of 0.50 for the 90° turning condition. With nominal bleed, the loss coefficient was reduced to 0.15 at the same inlet Mach number and turning angle. It would be expected that the tandem cascade losses would be two to three times the magnitude of the single cascade loss for a turning angle equal to half of the tandem cascade turning. Since the single cascade loss coefficient was 0.055, the observed tandem cascade result is quite reasonable. These results indicate that 92 percent to 93 percent of the horizontal thrust could be obtained as vertical lift using a tandem cascade thrust vectoring system.

The fact that the loss coefficient increases rapidly with increasing Mach number suggests that improvements to the tandem cascade can be made or that, if it is possible to operate the thrust vectoring system at a lower Mach number than 0.50, improved thrust vectoring performance can be achieved with the present configuration.

THRUST REVERSAL

A number of difficulties were encountered in obtaining satisfactory flow conditions for the thrust reversal case. For the very high turning angles, there was some impingement of the exit flow on the stationary structure supporting the lower floor of the cascade tunnel. Attempts were made to measure the static pressure at the exit of the second cascade to determine whether a static pressure gradient occurred in the direction from the apex of the tandem cascade along the trailing edges of each blade to the blade farthest from the apex. The static pressure appeared to be constant at a value equal to the tank static pressure. A significant static pressure gradient was observed in the zone between the forward and the aft cascades along the line bisecting the two cascades.

Several attempts were made to relieve the observed static pressure gradient. The position of the second cascade was changed relative to

the first cascade. A fairing block was installed on the lower floor to prevent flow from passing through the blade passage closest to the apex to reduce the impingement. A slight reduction in the total turning by decreasing the second-row camber was followed by an adjustment in the incidence angle of the second cascade. In each case the static pressure gradient remained. Tuft surveys at low speeds indicated a generally satisfactory flow; however, as Mach number was increased, the total pressure rake showed a rapid deterioration of the flow. These results indicated that a rather drastic change would be required to improve the performance.

The inlet angle to the second cascade was reduced from 34^{o} to 24^{o}, boundary layer bleed was applied through a slot in front of the second cascade row, and the blade shape was altered to conform more closely to that of a typical impulse turbine blade by moving the camber forward to provide a straight trailing-edge region. Tuft surveys at low speed showed a generally satisfactory configuration. A static pressure gradient was still in evidence between the two cascades, but the magnitude of this gradient was greatly reduced from that observed on the earlier runs. Measurement of the exit flow direction yielded a total turning of 129^{o}. It is significant to note that the deviation angle of the second cascade with the modified meanline shape was approximately 3^{o}, as compared to about 10^{o} for similar camber levels with the original blade meanline.

The effect of applying boundary layer control was to significantly reduce secondary flow occurring in the first cascade. Applying bleed did not seem to make a significant difference in the performance of the second blade row at low speed. At Mach numbers above 0.40, however, a very significant reduction in the total loss occurred (Figure 38). The loss coefficient measured in the early tandem cascade running without boundary layer control was 0.345. With nominal boundary layer control, the loss coefficient was reduced to the acceptable value of 0.148. With the tandem cascade arrangement, it was not convenient to make spanwise loss measurements at high speed. A few points were taken at low speed, however, with the indication that the losses away from the tunnel centerline were not greatly different from those observed on the tunnel centerline. A summary plot comparing single and tandem cascade losses without tunnel-wall boundary layer control with tandem cascades having nominal bleed is presented in Figure 39.

CONCLUSIONS

The tandem cascade tests employing boundary layer control are believed to represent the conditions that occur with a high-aspect-ratio thrust vectoring system. The results obtained using the TCT prove that satis-

factory tandem cascade operation can be obtained at inlet Mach numbers up to 0.50. Improvements in vertical thrust performance can probably be achieved by modifications to the meanline shape of the airfoils used. Reversed thrust equal to about 60 percent of the forward thrust can be achieved with a thrust vectoring tandem cascade. The achievement of these satisfactory results at high speed is important to the investigation conducted as Phase III of this program since these tests are run at low speed.

TECHNICAL DISCUSSION - PHASE III

GENERAL

The purposes of Phase III of this program are to determine: (1) the performance of a practical-construction thrust-vectoring tandem cascade operating in conjunction with a typical cruise fan installation; (2) performance improvement by confining the jet flow with ducts from the fan nacelle exit nozzle to the first cascade and to the second cascade, by providing flow boundaries at the blade ends, and by the combined use of ducts and end walls; (3) the effects of simulated flight velocity on thrust vectoring performance; (4) ground effects at various distances of from one to three fan diameters from the fan axis.

DESCRIPTION OF TEST EQUIPMENT

Facility

Scale-model testing of the tandem cascade principle was accomplished using a 26-inch-tip-diameter, low-speed scale-model fan installed in a nacelle exhausting into the tandem cascade assembly. Tests using a single cascade of flexible blades were made, as well as tests of two cascades in a tandem arrangement. Ground effects were evaluated by locating a large plane surface parallel to the fan axis of rotation and at various distances from the cascade assembly. A large rectangular free jet was used to simulate the external flow resulting from low-speed flight conditions. The fan is driven by a 25-horsepower induction motor through a belt drive. The entire fan assembly and drive are mounted on a cable-suspended frame. Three Wianco load cells constrain the movable frame and form the force measurement system. One of the cells (#1) is on the fan centerline and thus reads thrust (drag). The other cells (#2 and #3) together read the side force (lift). The motor is supported on bearings, and a lever arm connected to it rests on a scale. This arrangement reads input torque.

The general arrangement of the facility is shown schematically in Figure 40. Photographs of the facility arrangement are shown in Figures 41, 42, 43, and 44.

Model Fan

The model fan is a geometric scale of the X353-5 lift fan. It is a single-stage fan consisting of a rotor and a stator. The flow path in the vicinity of the rotor and stator is cylindrical at both hub and casing. A low-speed inlet cowl and bulletnose constitute the front parts of the nacelle. The aft part of the nacelle tapers to a 24-inch-diameter exit.

The fan absorbs approximately 14.5 horsepower at 1782 rpm and delivers 102.5 pounds of thrust at standard conditions. The velocity at the rotor inlet face is 115 feet/second. The radial variation of rotor inlet velocity, normalized with fan tip speed to give the flow coefficient (ϕ), is shown in Figure 45. A design feature of the original X353-5 fan was the use of a higher loading in the tip region than at the hub. This feature is incorporated in the scale-model fan. The radial variation in rotor pressure rise, normalized with a dynamic head based on tip speed squared ($\rho U_{T/2}^2$) to give the pressure rise coefficient $\Psi_{10.6}$, is shown in Figure 45.

Simulated Conditions

For ground effect tests, a 4-foot by 8-foot sheet of plywood, mounted to a frame, was located parallel to the fan axis at various distances from the deflecting cascades.

For simulated flight tests, the output from an 82,000 cfm, 4-foot-diameter blower was diffused to a 4-foot by 9-foot rectangular duct. Pressure drop screens were used to make the jet reasonably uniform. The actual velocity level of the free jet, 38 feet/second, is 33 percent of the low-speed scale-model fan inflow velocity. The inflow velocity of the full-scale X353-5 fan is 410 feet/second. Therefore, the free jet velocity ratio is equivalent to 135 feet/second or a flight speed of 80 knots.

Construction of Tandem Cascades

The airfoil blades used in the tandem cascades were fabricated as shown in drawing 4012150-92 and -93*. The 0.008-inch-thick brass shim stock forming the suction surface was first put in a die which shaped the leading edge. The shim stock was then soldered to the steel leading-edge bar and the steel trailing-edge bar. Next, the steel center bar was fastened to the brass stock with screws. Finally, the 0.006-inch thick nichrome pressure surface was spot-welded to the steel center bar. The camber was set at the required angle, then the nichrome was taped to the leading and trailing edges. The camber was held by applying force on the studs at the ends of the blade by means of the end fixtures depicted in drawing 4012160-97**.

The camber was set on each blade by first setting one of the blades at a given camber and making a template of the airfoil which was transferred

*Appendix IV, pages 62, 63
**Appendix IV, page 64

to paper. The camber line was then constructed, and tangent lines were drawn to the meanline at the leading and trailing edges. The camber angle was measured and corrected to the required value. The angle on the brass or suction side was measured with a protractor and held so its legs were tangent to the first 1/4 inch of the leading and trailing edges.

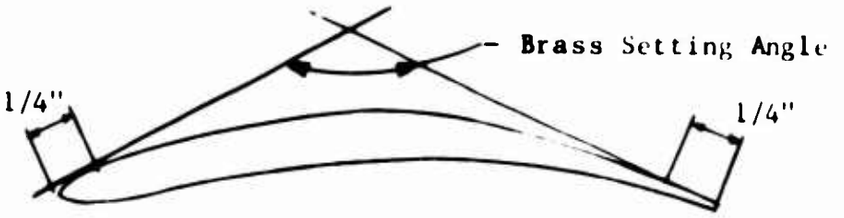

This brass setting angle was used to set the camber on the ends and middle of all the blades.

The cascade blades were mounted in an elliptical frame with a solidity of 1.5. The solidity is defined as a ratio of blade chord to blade pitch.

Inspection of the test blading as fabricated and when constrained to produce the required camber revealed a number of discrepancies. A small variation in camber from end to end, while not serious in itself, produced local regions where the sheet metal buckled, resulting in locally poor profile shapes. The soldering of the brass suction surface to the leading- and trailing-edge bars resulted in generally poor leading-edge quality. These effects resulted in an uneven blade quality ranging from good to poor.

Although the test sequence was selected to minimize the cambering and uncambering of the blading, some distortion due to permanent set was gradually built into the blading as testing evolved.

As an interesting comparison, a fixed-camber cascade of 90^{o} camber was also tested (see Figure 46). It has molded plastic blades and a solidity of 2.14. The frame of the cascade was also molded and shaped so that the air passing through the cascades at the blade ends went through the same turning geometry as that at the center.

CHRONOLOGY OF RUNS

In general, the test was conducted in two phases. The first 14 runs

were without ground plane or simulated flight speed. Then the procurement, assembly, and testing of the diffuser and plenum for the 82,000-cfm blower was completed. Because of the space occupied by this additional equipment, the test vehicle had to be relocated. The second series of tests, Runs 16 through 27, included ground effect and simulated flight testing. A tabulation of all the runs is given in Appendix I. A complete listing of all the runs with data readings taken at each test point is given in Appendix II.

MEASUREMENTS AND DATA REDUCTION

The measurements taken on all data points consisted of the following:

a) Forces in the axial direction F_H and in the lateral direction F_V.

b) Torque through a lever arm (connected to the fan drive motor) which rests on a Toledo scale.

c) Fan inlet temperature and barometric pressure.

d) Fan inlet static pressure at rotor inlet $P_{10.2}$ consisting of two rakes of six elements each.

e) Fan inlet total pressure at rotor inlet $P_{T10.2}$ consisting of two rakes of six elements each.

f) Fan rotor discharge total pressure $P_{T10.6}$ consisting of two rakes of six elements each.

g) Jet nozzle peripheral static pressure consisting of eight wall static pressures around circumference of jet exit.

h) Air exit angle (β_2) at discharge of final cascade.

i) Static pressure ahead of cascade in central region of the cascade.

j) Total pressure profile of wake from blade elements using a 13-element wake rake (occasionally).

These data were reduced to standard and nondimensional form as described below. An example of the data reduction process is described in Appendix III, page 54.

The three load cells were calibrated by taking scale readings resulting from application of standard weights at each of the three load cells. The force was applied at an elevation corresponding to the fan center

through a pulley and cable arrangement. These corrections were applied to the scale readings of each test point.

For any test configuration, the fan develops a force which is proportional to the density of the ambient air. Therefore, all forces are corrected to standard density condition by the factor θ/δ as:

$$F_{corrected} = F_{test} \times \frac{\text{Density, std.}}{\text{Density, test}}$$

$$F_{corrected} = F_{test} \times \frac{P_{std.}\ T_{test}}{P_{test}\ T_{std.}}$$

$$F_{corrected} = F_{test} \times \frac{\theta}{\delta}$$

where

θ is the ratio of test temperature to standard temperature of $518.6^{\circ}R$.

δ is the ratio of test barometric pressure to standard barometric pressure of 29.92 inches of Mercury at $518.6^{\circ}R$.

The fan runs at a constant speed of 1782 rpm and for a given configuration absorbs a power which is proportional to ambient density. Consequently, the power absorbed expressed as a corrected horsepower is:

$$HP\ \theta/\delta = \frac{F\theta n 2\pi L}{\delta\ 550}$$

where

F is the lever arm force (pounds)

L is the lever arm length (feet)

n is the rotational speed (revolutions/second).

The fan inlet static pressure was used to calculate an inlet axial velocity $V_{10.2}$ at the rotor inlet. The velocity is normalized by the fan tip speed U_T to obtain the flow coefficient ϕ:

$$\phi = V_{10.2}/U_T$$

Fan inlet total pressure is used to obtain the velocity V_p of the external flow.

The average rotor discharge total pressure is used to express the rotor total pressure rise above ambient relative total pressure. The total pressure rise is reduced to coefficient form by dividing the pressure rise by a dynamic head based on fan tip speed squared ($\rho U_{T/2}^2$) to obtain the pressure rise coefficient:

$$\Psi_{10.6} = \frac{P_{T10.6} - P_{T\ amb.}}{\rho U_{T/2}^2}$$

No total pressure elements were located behind the stator; consequently, the stage total pressure rise is not available.

The jet exit nozzle static pressures were equal to ambient static pressure for all test configurations.

An efficiency η_R can be obtained, crediting the fan with the total pressure rise to rotor discharge as follows:

$$\eta_R = \frac{Q\Delta P}{\text{Power in}};$$

since $$Q = A_{10.2}\left(\frac{V_{10.2}}{U_T}\right) \times U_T = A\ U_T\ \phi$$

and $$\Delta P = \Psi\ \rho\ U_{T/2}^2$$

and $$P_{in} = (HP\ \theta/\delta)\ \delta/\theta\ 550,$$

then $$\eta_s = \left[\frac{\rho_o A\ U_T^3}{2\quad 550}\right]\ \frac{\phi\Psi}{(HP\ \theta/\delta)}$$

where ρ_o standard density

A = effective flow area at rotor inlet.

All the angles of interest are depicted in Figure 47. For each test point, the geometrical angles of cascade orientation (γ), blade camber (θ^*), and leading-edge angle (β_1^*) are recorded as well as air discharge angle (β_2). The angles measured relative to the fan axis are the cascade orientation angle (γ) and the jet efflux angle (β_J). The latter is defined as follows:

$$\beta_{JA} = \gamma_A + \beta_{2A} \quad \text{for Cascade A.}$$

$$\beta_{JB} = \gamma_B + \beta_{2B} \quad \text{for Cascade B.}$$

Angles relative to the cascade are either hardware angles or air angles. Given the leading-edge angle (β_1^*) and the camber angle (θ^*), the trailing-edge angle (β_2^*) is found from

$$\beta_2^* = \theta^* - \beta_1^*.$$

The inlet air angle (β_1) is found from

$$\beta_{1A} = \gamma_A \quad \text{for Cascade A}$$

$$\beta_{1B} = \gamma_B - \beta_{JA} \quad \text{for Cascade B.}$$

The incidence angle (i) and the deviation angle (δ) and turning angle (θ) for either cascade are found from

$$i = \beta_1 - \beta_1^*$$

$$\delta = \beta_2^* - \beta_2$$

$$\theta = \beta_1 + \beta_2.$$

The test data for all test points are tabulated in Appendix II, page 45 and include the following for almost every point:

F_H θ/δ = Horizontal Corrected Force

F_V θ/δ = Vertical Corrected Force

R θ/δ = Total Corrected Thrust Force

β_F = Force Vector Direction

β_J = Jet Efflux Angle

$\Psi_{10.6}$ = Rotor Pressure Rise Coefficient

$\phi_{10.2}$ = Rotor Inlet Flow Coefficient

HP θ/δ = Corrected Input Horsepower

η = Rotor Efficiency

γ = Cascade Orientation Angle

θ^* = Blade Camber ($\beta_1^* + \beta_2^*$)

β_1^* = Leading-Edge Orientation Angle

β_2 = Discharge-Air Angle

PRESENTATION OF RESULTS

The force results from Runs 1 through 14 are shown in Figures 48 through 51.

In a typical test involving a single cascade, a series of test points would be taken with the cascade orientation angle (γ) as the only variable. For these points, the camber angle (θ^*) and the orientation of the blading within the cascade would be held constant. In the presentation of results, these data points are connected by a curve. In a typical test involving tandem cascades, the first cascade is fixed while the orientation of the second cascade is varied. In the presentation of data, these points are connected by a curve.

Runs 1 through 14 involve blade settings of various cambers which are roughly symmetrical so that the leading-edge angle (β_1^*) and trailing-edge angle (β_2^*) are about equal. At some particular cascade orientation angle, operation under impulse conditions (no increase or decrease in static pressure across the cascade) occurs.

The results for single-cascade operation are shown in Figures 48 and 49 and include results for the various blade cambers (θ^*) of 0^o, 25^o, 35^o, 48^o, 56^o, 78^o, and 80^o each at a number of cascade orientation angles.

The force results for tandem operation during Runs 1 through 14 are shown in Figures 50 and 51. For all of these runs, the first cascade (A) is unchanged and is held at 35^o cascade orientation producing 64^o of turning at roughly impulse conditions. The cambers of the second cascade (B) include 0^o, 35^o, 48^o, 56^o, 78^o, and 80^o each tested at a number of cascade orientation angles. A locus of the optimum values forming the envelope of maximum resultant force is shown in Figure 52.

An interesting result is obtained using the 90^o fixed-camber cascade shown in Figure 44 as the first cascade and a 78^o camber cascade as the tandem cascade. The single test point is depicted in Figure 51 and shows approximately 0 percent reversed thrust at a vectoring angle of 152^o.

Local values of blade loss coefficient were obtained by measuring local profiles of total pressure immediately behind the blades at a number of locations around the cascade package. Twelve values in the periodic distance from one blade wake to the next were measured. From these a profile and average of loss coefficient were calculated as follows:

$$\bar{\omega} = \frac{P_{T,\ \text{free stream}} - P_{T,\ \text{local}}}{P_{T,\ \text{free stream}} - P_{\text{ambient}}}$$

These loss coefficient profiles, the average loss coefficient, and a schematic showing the location at which the measurement was made are

shown in Figure 53. The loss coefficients shown in this figure are for the cascade in position A which is immediately behind the fan. The same cascade set was then located in position B, where it was fed by the other cascade upstream. Similar loss profiles were measured at some of the same locations previously measured. These are shown in Figure 54.

As an interesting comparison, the loss coefficient for the fixed cascade with 90° cambered plastic blades set at 90° averaged 0.043. The loss coefficients of flexible cambered blade cascade in the upstream position averaged 0.075 and in the downstream position averaged 0.077. The greater losses of the flexible blades are due to simplified construction, since the honeycomb-surfaced flexible blades tested in the transonic cascade tunnel showed low-speed loss coefficients in the range of 0.030 to 0.040.

The effect of distance between the fan and the reverser assembly was investigated by translating the assembly 12 inches aft (1/2 fan exit diameter). The force results (from Run 12) for both single and tandem operation are shown in Figures 55 and 56. This showed no appreciable change in thrust level.

Due to the fact that a small but appreciable amount of the air effluxing from the first cascade went past and was not deflected by the second cascade, an attempt to increase the camber of the first cascade beyond the levels tested in the cascade wind tunnel was made. With 80° camber in the first cascade (A), better results were obtained compared to having 78° camber in the first cascade (A) as depicted in Figure 57.

The force results from Runs 16 through 27 are shown in Figures 58 through 63. These runs combined simulated flight tests, ground effect tests and cascade settings in which the leading-edge angle (β_2*) were not equal.

The force results for ground effect testing for Runs 16 through 26 are shown in Figures 58 through 60.

The force results for simulated flight tests for Runs 14 through 26 are shown in Figure 61.

Finally, the force results for cascade operation statically for Runs 18 through 27 are shown in Figures 62 and 63.

EVALUATION OF RESULTS

Thrust Vectoring Performance

The initial test phase, Runs 1 through 14, involved cascades with the

blading adjusted to various cambers and oriented within the cascade so that the leading- and trailing-edge angles, β_1^* and β_2^*, were essentially equal.

By variation of its camber, operation with a single cascade is capable of thrust vectoring from 0° to 64°. The thrust loss is 2-1/2 percent at zero turning, and the loss increases with increasing turning to 6 percent loss at 64° of vectoring.

Further vectoring is accomplished by operation with the tandem cascade inserted in the discharge of the first cascade and varying the camber of the aft cascade. Insertion of the second cascade, with zero addition turning, causes an additional 2 percent thrust loss at 64° vectoring. With increasing turning from the tandem cascade, the losses increase to 7-1/2 percent at 90° vectoring, and to 12 percent loss at 124° vectoring. These levels are depicted in Figure 64, which shows the envelope of maximum thrust vector over the range of thrust vectoring angles from zero to maximum. On this envelope near maximum vectoring, several points beyond 124° vectoring are shown. These include a point of maximum reversal thrust and maximum vector angle. The reduction in thrust vector for these points results primarily from flow bypassing the second cascade due to the cascade orientation.

For much of this operation, the cascade operates near impulse conditions so that the static pressure before and after the cascade is equal to ambient pressure. As a consequence, the operation of the fan is unchanged since its back-pressure is unchanged by the insertion of the cascade system. The basic fan thrust (R_1) is reduced by the losses in the cascade to a resultant thrust (R_2). The cascade loss coefficient can be estimated from these thrust levels by

$$\bar{\omega} \quad 1 - \left[\frac{R_2}{R_1}\right]^2 .$$

Based on this, the loss coefficients for the cascade system can be estimated as a function of total vectoring angle as follows:

0°	0.049
64°	0.116
90°	0.144
125°	0.225

It is seen that the loss for two cascades at maximum turning is about double that of the single cascade. Thus, the loss of each cascade used in series is simply additive with no further interaction loss.

At maximum camber, the overall loss coefficient is about 0.12. From the results of local wake measurements depicted in Figures 53 and 54, the average local loss coefficient is about 0.07. This ratio of overall loss coefficient to local loss coefficient is reasonable, and the difference is due to the end losses of the cascade assembly.

The blade ends are uncontained and open as is visually apparent in the photographs of Figures 41 through 44. Consequently, the flow at the tips of the blades develops appreciable spanwise or lateral components, resulting in thrust losses and poor cascade operation.

The mixing of the free jets and the ambient air is shown in Figure 65. Profiles of the dynamic head in the region of the edge of the free jet were made at five locations in the stream direction: at the fan discharge, at the inlet and discharge of the first cascade, and at the inlet and discharge of the tandem cascade. These profiles are located in the figure at positions corresponding to the actual streamwise locations of the measuring planes. The figure forms a physical picture of the mixing zone. The mixing zone has a half-angle of about $4\text{-}1/2^{o}$. The mixing zone is about 2 inches thick at the first cascade and about 5 inches thick at the tandem cascade. Some of the lateral or spanwise displacement of the high-velocity flow resulting from the passage of the air through the cascade is apparent from comparison of the profiles at the inlet and discharge of each cascade. The use of end plates on the blade tip to reduce this loss and the use of ducting to contain the free jets and reduce the mixing zone thickness at the edge of the jet were investigated. The results of this phase of testing are depicted in Figure 66.

The following observations can be drawn from these results:

a) Addition of end plates alone does not reduce losses.

b) Addition of a duct from the first cascade to the tandem cascade makes an improvement, which is probably a result of ducting the fraction of flow from the first which usually bypassed the tandem cascade.

c) With ducting of the free jets, there is a substantial improvement with the addition of end plates.

A physical model which is consistent with these results can be presented.

Compared to a normal boundary layer for a flow in a duct, the mixing-zone thickness of the free jet is very large. Consequently, the addition of an end plate on the tips of the blade is ineffective. Since the mixing at the edge of the free jet occurs at constant momentum, there is no inherent thrust loss so long as all the flow is effectively turned. The thin boundary layer of the contained flow offers the potential of more efficient turning when end plates are used. This seems to be the case, as the combination of both ducting and plates obtains the greatest improvement. Thus the ducting from the fan to the first cascade and end plates on the blading of the first cascade improves the thrust 1-1/2 percent to 2 percent. The 2-1/2 percent to 3 percent improvement due to the ducting between the first and tandem cascades can be discounted because it merely prevents the flow's bypassing the tandem cascade - an improvement having nothing to do with aerodynamic efficiency. The addition of the ducting to the tandem cascade plus end plates on the tandem cascade obtains another 2 percent improvement. In a practical arrangement, the ducting to only the first cascade might be used to obtain a 2 percent improvement in vectored thrust.

Practical System

The features of a possible arrangement for a more practical thrust vectoring system have been discussed earlier in the report. In the STOL phase, only the first cascade is used. It is operated at fixed cascade orientation ($\gamma_{A_*} = 35^\circ$) and with the blade leading edge fixed relative to the cascade ($\beta_{1_*} = 37^\circ$). The range of turning is obtained by increasing the camber by variation in the blade trailing-edge angle. At the maximum camber the turn is an impulse turn. At intermediate settings the discharge area of the cascade is larger than the fan area and the cascade acts as a diffuser. This tends to lower the static pressure behind the fan to induce more air flow through the fan, but it causes the cascade to operate under adverse conditions. At the most extreme diffusion the flow discharges perpendicularly from the cascade, resulting in a vector angle of 35°. This condition was tested* and shows a 7-1/2 percent increase in air flow along with the reduction in pressure rise and power input which is characteristic of the fan. The gain in thrust due to the increased weight flow is not offset by any apparent loss in cascade performance. Other points were tested with higher turning with a good level of thrust. These form the envelope of Figure 40.

In the proposed practical system, the tandem cascade operates in the transition mode with a constant cascade orientation ($\gamma_B = 73^\circ$) and with

*Run 20, Reading 4, Appendix II

the leading-edge angle fixed relative to the tandem cascade ($\beta_1^* = 25^\circ$). The additional vectoring is accomplished by variation of the trailing-edge angle through transition to the VTOL mode of 90° vectoring. This latter point was tested*. Vectoring beyond this point requires variation in the cascade angle of the tandem cascade. A point beyond 90° vectoring was obtained in this manner. The tandem cascade operating at 10° positive angle of attack shows satisfactory performance**.

Ground Effect Testing

Ground plane testing (Runs 16 through 26) are shown in Figures 58 through 60. Figure 58 has plotted all the ground plane tests for a single cascade. In most cases, there was little significant change in the thrust level. The tendency is for 1 percent decrease in thrust and a 1° to 3° increase in turning angle with the addition of a ground plane at an average distance of 1.75 fan diameters and parallel to the fan axis. The run with $\theta_A^* = 90^\circ$, $\beta_1^* = 45^\circ$ (see Figure 58) was made with the plastic-bladed cascade at ground-plane distances varying from 1.7 fan diameters average distance to 2.9 fan diameters. This "S"-shaped plot seems to be typical for a series of ground-plane readings at various distances and may be partly due to reingestion of the cascade discharge back into the fan. No record of reingestion was made at this point, although reingestion was observed using tufts.

In Figure 59, the tandem cascade runs for $\left[\theta_A^* = 61^\circ, \beta_1^* = 37^\circ \text{ and } \theta_B^* = 48^\circ, \beta_1^* = 25^\circ\right]$, $\left[\theta_A^* = 78^\circ, \beta_1^* = 39^\circ \text{ and } \theta_B^* = 42^\circ, \beta_1^* = 37^\circ\right]$, and $\left[\theta_A^* = 78^\circ, \beta_1^* = 39^\circ \text{ and } \theta_B^* = 48^\circ, \beta_1^* = 37^\circ\right]$ show approximately a 5 percent decrease in deflected thrust with the addition of a ground plane approximately one fan diameter away. The tandem cascade run for $\left[\theta_A^* = 78^\circ, \beta_1^* = 39^\circ \text{ and } \theta_B^* = 48^\circ, \beta_1^* = 25^\circ\right]$ shows only 1 to 2 percent decrease in deflected thrust. Although this is at a greater turning angle, we are not certain why the difference exists.

In Figure 60, the tandem cascade runs for $\left[\theta_A^* = 80^\circ, \beta_1^* = 39.5^\circ \text{ and } \theta_B^* = 78^\circ, \beta_1^* = 39^\circ\right]$ at two different cascade angles seem to show an "S" shape again as the ground effect varies from no ground plane to 3.3 fan diameter average distance to ground plane to only 1.8 fan diameter.

---

*Run 26, Reading 4, Appendix II
**Run 24, Reading 11, Appendix II

The reason for this is probably due to reingestion. With tufts the flow direction was determined. This showed that the discharge from the cascades went first up one side of the wind tunnel plenum ahead of the fan, then back out the opposite side, which caused reingestion on one side. This flow depended greatly on ground height and cascade exit angle interacting with the wind tunnel duct and would not be present in an actual situation with an aircraft.

Simulated Flight Conditions

The free jet used to simulate a flight speed equivalent to 80 knots has a dynamic head which is only 11 percent of the fan jet dynamic pressure. This is true for the X353-5 lift fan at 80 knots and for the scale model fan, with a free jet velocity of 38 feet/second. Tuft observations of the flow field of the model in simulated flight did not show any perceptible effects of the types that might be anticipated, namely:

a) No stalling of the second cascade.

b) No back pressuring of the second cascade causing the flow from the first to spill around the second cascade.

c) No deflection of the efflux from the first cascade.

d) No appreciable throttling or reduction of the fan flow.

Some deflection of the free jet downstream from the second cascade was observed which would be of only secondary interest.

The relationship between the forces developed by a given configuration statically and in simulated flight is depicted on Figure 61 for a number of configurations. Under the constant ram conditions existing for all the simulated flight test points, the fan flow was higher by an almost constant amount than its value under static conditions. The values of flow coefficient are about 0.565 for static conditions and 0.595 for simulated flight conditions. Since the weight flow and simulated flight speed are reasonably constant, it is possible to compute a ram drag for standard conditions of 33.7 pounds. If this drag is credited to the measured net horizontal thrust, one obtains the horizontal thrust component of the gross thrust vector. From the horizontal and vertical components, the angle of the gross force vector (β_F) can be computed and compared with the value for static test of the same configuration. Moreover, the gross thrust vector of a vectored test point can be computed and its magnitude expressed as a fraction of the gross thrust of the fan in simulated flight bare of any thrust vectoring equipment. This thrust ratio (R/Ro) can then be compared to the ratio derived in

TABLE 1

SIMULATED FLIGHT DATA COMPARISON

Cascade	θ^*	$\beta_1{}^*$	γ	Flight Speed (Knots)	β_2	R/Ro
A	42	37	40	0	38.2	0.952
				80	39.4	0.963
A	61	37	40	0	53.6	0.954
				80	54.2	0.975
A	80	39	35	0	65.7	0.950
				80	66.7	0.963
A	61	37	35	0	86.1	0.920
B	48	25	68	80	83.7	1.000
A	78	39	35	0	112.8	0.925
B	48	37	94	80	113.4	0.963
A	78	38	35	0	100.4	0.910
B	48	25	99	80	112.2	0.968

the manner for the static tests of the same configuration. This procedure was applied to a number of points of increasing vectoring, and the gross vector angle (β_F) and gross vector magnitudes expressed on a fraction of the basic fan thrust (R/Ro) are tabulated in Table 1.

It can be noted that the gross thrust vector angles for a given configuration agree within 1^o or 2^o. A small 2- or 3-pound drag, as might be due to the external geometry, would reduce this difference still further. For the single cascade tests the fraction of basic thrust obtained as gross thrust (R/Ro) is about the same for a given configuration both in simulated flight and statically. With the tandem cascade, the fraction of basic thrust obtained as gross thrust (R/Ro) is 4 to 5 percent higher in simulated flight than statically. This may be due to these possible effects:

a) Some effect of external flow on the second cascade.

b) Some induced lift resulting from an interaction between the external flow and the deflected fan jet.

It should be mentioned that all these results have been interpreted for a simulated flight speed of 80 knots. This was based on the 1.10 pressure ratio fan of the X353-5 lift fan. Basically the results apply for all incompressible cases where the flight speed is 33 percent of the fan jet velocity. Consequently, the flight speed equivalent to these tests is higher than 80 knots for fans higher in pressure ratio than that of the X353-5 lift fan.

Discussion of Thrust Discrepancy

A number of factors are known to occur in the test facility that contribute to a random variation of results for the same configuration. Among these are:

a) A diametrical variation of fan inlet air temperature of an amount ranging from 2^oF to 8^oF.

b) Varying torque and thrust of the fan due, in part, to random swirl variations of the air ingested by the fan.

c) The finite size (4 feet x 9 feet) of the free jet used to simulate the external flow.

These effects do not invalidate the conclusions reported as a result of these tests.

The test discrepancy which caused the most concern in this particular test, however, is apparent from considering Figures 52 and 64. These compare the results of Runs 1 through 14, and Runs 16 through 26. In the range of vector angles between 20° and 90°, the results from Runs 16 through 26 are 4 to 5 percent higher than the earlier runs.

The test vehicle and its thrust stand were relocated after Runs 1 through 14 were completed. Thrust stand calibrations were made at the beginning of these tests and at the end before relocations. These calibrations, while not identical, did not show differences sufficient to explain this much difference. Similarly, thrust calibrations made during Runs 16 through 26 did not show any changes of this magnitude except where anticipated.

There is the possibility that the interaction between the cascade and fan of the configurations tested in Runs 16 through 26, which were in the direction of increasing weight flow, may have caused a significant rise in thrust. This would occur unless offset by lower jet velocity due to larger effective area, or lower cascade efficiency. Some configurations near impulse operation were rerun in Run 27. These results were also 4 to 5 percent higher than the previous impulse configurations of Runs 1 through 14, as shown in Figure 67. It must be observed that these higher levels for the single cascade are most consistent with all the double or tandem cascade results, and that the overall loss coefficient of 0.12 implied that these results are more consistent with the local blade coefficients of 0.07 as shown in Figure 53. The wake measurements of Figure 53 were made at the completion of Runs 1 through 14 as part of an investigation to find the cause of the high loss implied by the single cascade results of Runs 1 through 14. The 10 percent thrust loss of these runs implied a 0.20 loss coefficient, which is very high and not consistent with the double cascade results obtained during these same tests.

We have concluded that the single cascade measurements of Runs 1 through 14 are low for reasons we are unable to re-create or determine, and that the results of Runs 16 through 26 are valid.

BIBLIOGRAPHY

1. Simonson, M.R., Cascade Tests of an Airfoil Section Incorporating a Variable Slotted Flap, R62FPD273, General Electric Company, Flight Propulsion Laboratory Department, Cincinnati 15, Ohio, June 13, 1962.

2. Giffin, R.G., Cascade Tests of Simple and Articulated Variable Inlet Guide Vanes, R63FPD193, General Electric Company, Flight Propulsion Laboratory Department, Cincinnati 15, Ohio, April 1963.

3. Emery, J.C., Herrig, L.J., Erwin, J.R., Felix, A.R., Systematic Two-Dimensional Cascade Tests of NACA 65-Series Compressor Blades at Low Speeds, 1368, National Advisory Committee for Aeronautics, Langley Aeronautical Laboratory, Langley Field, Virginia, January 1958.

4. Erwin, J.R., Emery, J.C., Effect of Tunnel Configuration and Testing Technique on Cascade Performance, 1016, National Advisory Committee for Aeronautics, Langley Aeronautical Laboratory, Langley Field, Virginia, 1951.

BLANK PAGE

APPENDIX I - CHRONOLOGY OF RUNS

Run	Date	Test Points	Single Cascade	Tandem Cascade	Notes
1	4/20/64	4	-	-	-
2	4/21/64	3	25 (13.5)*	-	-
3	4/23/64	10	78 (39)	-	-
4	4/24/64	5	-	78 (39) & (0)	-
5	4/27/64	14	35 (16.5)	78 (39) & 35 (16.5)	-
6	4/28/64	14	48 (22)	78 (39) & 48 (22)	-
7	4/29/64	14	56 (31.5)	78 (39) & 56 (31.5)	-
8	4/30/64	25	78 (39)	78 (39) & 78 (39) 90 (45) & 78 (39) Trial end plates (tape)	-
9	5/4/64	2	78 (39) 90 (45)	Wake measurement Wake measurement	-
10	5/5/64	2	-	Wake measurement	-
11	5/8/64	12	-	78 (39) & 78 (39) Duct & end plate combination	-
12	5/11/64	15	78 (39)	78 (39) & 78 (39) Relocate cascade B	-
13	5/12/64	5	-	78 (39) & 78 (39) Relocate cascade B and spill plates	-
14	5/13/64	21	80 (39.5)	78 (39) & 80 (39.5) 80 (39.5) & 78 (39)	-
15	5/15/64	2	-	80 (39.5) & 78 (39)	GP

*Denotes θ^* (β_1^*). θ^* is actual blade camber; β_1^* is leading-edge angle.

APPENDIX I - CHRONOLOGY OF RUNS (Continued)

Run	Date	Test Points	Single Cascade	Tandem Cascade	Notes
16	5/19/64	15	80 (39.5)	80 (39.5) & 78 (39)	GP & V_p**
17	5/20/64	7	-	80 (39.5) & 78 (39)	GP & V_p
18	5/20/64	5	80 (39.5)	-	GP & V_p
19	5/21/64	7	90 (45)	-	GP & V_p
20	5/25/64	9	42 (37)	-	GP & V_p
21	5/25/64	6	-	78 (39) & 42 (37)	GP & V_p
22	5/27/64	6	-	78 (39) & 48 (37)	GP & V_p
23	5/27/64	9	48 (37)	-	GP & V_p
24	5/28/64	12	-	78 (39) & 48 (25)	GP & V_p
25	6/1/64	9	61 (37)	-	GP & V_p
26	6/1/64	14	-	61 (37) & 48 (25)	GP & V_p
27	6/6/64	10	78 (39) 60 (35)	78 (39) & 60 (35)	-
28	6/8/64	4	90 (45)	Wake measurement only	-

**GP denotes ground plane tests. V_p denotes simulated flight.

APPENDIX II TABULATION OF TEST RESULTS

RUN NUMBER	READING NUMBER PER RUN	CASCADE A: BLADE CAMBER ANGLE θ_A^c (DEGREES)	CASCADE A: BLADE INLET ANGLE θ_1^c (DEGREES)	CASCADE A: AIR EXIT ANGLE θ_2 (DEGREES)	CASCADE A: BLADE SETTING ANGLE γ (DEGREES)	CASCADE A: CASCADE ANGLE γ_A (DEGREES)	CASCADE B: BLADE CAMBER ANGLE θ_A^c (DEGREES)	CASCADE B: BLADE INLET ANGLE θ_1^c (DEGREES)	CASCADE B: AIR EXIT ANGLE θ_2 (DEGREES)	CASCADE B: BLADE SETTING ANGLE γ (DEGREES)	CASCADE B: CASCADE ANGLE γ_A (DEGREES)	HORIZONTAL CORRECTED THRUST $F_{H\frac{a}{\rho}}$ (LB)	VERTICAL CORRECTED THRUST $F_{V\frac{a}{\rho}}$ (LB)	RESULTANT CORRECTED THRUST $R\frac{a}{\rho}$ (LB)	RESULTANT THRUST ANGLE θ_F (DEGREES)	JET EFFLUX ANGLE θ_J (DEGREES)	PRESSURE RISE COEFFICIENT $\Psi_{10.6}$	FLOW COEFFICIENT $\phi_{10.2}$	CORRECTED FAN RPM $\frac{N}{\sqrt{T}}$	ROTOR EFFICIENCY η_R	WIND TUNNEL VELOCITY V_p (FT SEC)	GROUND PLANE DISTANCE (h d)
1	1	0	0	0	0	0	-	-	-	-	-	99.7	4.3	99.8	2.5	0	.431	.565	14.11	.939	-	-
	2	NO CASCADES WERE MOUNTED										102.8	.4	102.8	.2	0	.432	.569	14.37	.931	-	-
	3	25	13.5	10	0	10	-	-	-	-	-	90.7	31.7	96.08	19.3	20	.427	.561	14.20	.918	-	-
	4	25	13.5	10	0	11	-	-	-	-	-	91.0	34.4	97.28	20.7	21	.424	.556	14.32	.896	-	-
2	1	25	13.5	10	0	9	-	-	-	-	-	91.6	30.5	96.5	18.4	19	.427	.561	14.1	.924	-	-
	2	25	13.5	10	0	8	-	-	-	-	-	92.8	30.5	97.7	18.2	18	.434	.568	14.4	.935	-	-
	3	25	13.5	10	0	12	-	-	-	-	-	90.2	36.1	97.2	21.8	22	.432	.569	14.4	.931	-	-
3	1	75	39	28	0	37	-	-	-	-	-	41.6	82.3	92.2	63.2	65.5	.438	.568	13.8	.981	-	-
	2	75	39	28	0	35	-	-	-	-	-	42.9	80.4	91.1	61.9	63	.435	.569	13.6	.992	-	-
	3	75	39	29	0	32.5	-	-	-	-	-	46.6	79.2	92.0	59.4	61.5	.434	.568	13.6	.986	-	-
	4	75	39	30	0	30	-	-	-	-	-	49.8	76.9	91.6	57.1	60	.439	.569	13.5	1.004	-	-
	5	75	39	30	0	25	-	-	-	-	-	56.6	71.6	91.3	51.7	55	.434	.564	13.5	.983	-	-
	6	75	39	29	0	20	-	-	-	-	-	60.6	66.5	90.0	47.7	49	.436	.560	14.3	.928	-	-
	7	75	39	29	0	15	-	-	-	-	-	65.2	55.4	85.6	40.4	44	.431	.551	14.0	.929	-	-
	8	75	39	28	0	10	-	-	-	-	-	68	42.8	80.4	32.2	38	.429	.538	13.6	.917	-	-
	9	75	39	26	0	5	-	-	-	-	-	71.1	34.7	79.1	26.1	31	.434	.528	13.5	.919	-	-
	10	75	39	27	0	0	-	-	-	-	-	68.9	31.3	73.9	25.1	27	.426	.502	13.0	.895	-	-
4	1	75	39	29	0	35	0	0	3	0	64	34.1	83.5	90.4	67.4	67	.440	.570	13.9	.985	-	-
	2	75	39	29	0	35	0	0	3	0	67	29.9	84.1	89.3	70.4	70	.439	.570	13.8	.989	-	-
	3	75	39	29	0	35	0	0	2.5	0	72	22.1	86.1	88.9	75.6	74.5	.441	.572	13.7	1.009	-	-
	4	75	39	29	0	35	0	0	4	0	61	38.0	81.4	89.8	65.0	65	.441	.571	13.6	1.012	-	-
	5	75	39	29	0	35	0	0	3	0	59	40.9	79.3	89.2	62.7	62	-	-	13.6	-	-	-
5	1	75	39	29	0	35	35	16.5	19	0	79	-10.2	87.4	87.8	97.6	98	.102	.571	14.5	.941	-	-
	2	75	39	29	0	35	35	16.5	19	0	83	-18.4	87.4	89.3	101.9	102	.106	.572	13.8	.939	-	-
	3	75	39	29	0	35	35	16.5	18	0	87	-22.9	84.2	87.3	105.2	105	.418	.570	13.5	.937	-	-
	4	75	39	29	0	35	35	16.5	20	0	75	-6.1	87.3	87.5	94	95	.117	.569	14.4	.941	-	-
	5	75	39	29	0	35	35	16.5	20.5	0	70	1.4	86.9	86.9	89.1	90.5	.119	.568	13.3	.941	-	-
	6	75	39	29	0	35	35	16.5	20	0	60	18.1	83.5	85.0	79.1	80	.114	.567	13.1	.930	-	-
	7	35	16.5	21	0	20	-	-	-	-	-	77.6	53.7	94.5	34.6	31	.119	.565	13.4	.940	-	-
	8	35	16.5	16	0	25	-	-	-	-	-	72.1	78.6	92.9	39.1	31	.118	.570	13.3	.952	-	-
	9	35	16.5	14	0	30	-	-	-	-	-	65.4	81.8	91.6	51	51	.116	.570	13.3	.939	-	-

APPENDIX II TABULATION OF TEST RESULTS (CONTINUED)

RUN NUMBER	READING NUMBER PER RUN	CASCADE A					CASCADE B															
		BLADE CAMBER ANGLE θ_1' (DEGREES)	BLADE INLET ANGLE β_1' (DEGREES)	AIR EXIT ANGLE θ_2 (DEGREES)	BLADE SETTING ANGLE λ (DEGREES)	CASCADE ANGLE γ_A (DEGREES)	BLADE CAMBER ANGLE θ_1' (DEGREES)	BLADE INLET ANGLE β_1' (DEGREES)	AIR EXIT ANGLE θ_2 (DEGREES)	BLADE SETTING ANGLE λ (DEGREES)	CASCADE ANGLE γ_A (DEGREES)	HORIZONTAL CORRECTED THRUST $F_{H\frac{1}{2}}$ (LB)	VERTICAL CORRECTED THRUST $F_{V\frac{1}{2}}$ (LB)	RESULTANT CORRECTED THRUST $R_{\frac{1}{2}}$ (LB)	RESULTANT THRUST ANGLE θ_T (DEGREES)	JET EFFLUX ANGLE θ_J (DEGREES)	PRESSURE RISE COEFFICIENT $\psi_{10.6}$	FLOW COEFFICIENT $\phi_{10.2}$	CORRECTED FAN RPM $\frac{RPM}{\sqrt{\theta}}$	ROTOR EFFICIENCY η_R	WIND TUNNEL VELOCITY V_F (FT/SEC)	GROUND PLANE DISTANCE (h/d)
5	10	36	16.5	17	0	18	-	-	-	-	-	79.0	50.8	93.9	40	35	.441	.567	14.3	.949	-	-
	11	36	16.5	-	0	16	-	-	-	-	-	81.7	49.2	96.4	37.1	-	.440	.566	14.3	.961	-	-
	12	36	16.5	19	0	18	-	-	-	-	-	79.9	41.2	89.9	31	29	.437	.562	14.3	.936	-	-
	13	36	16.5	18	0	5	-	-	-	-	-	90.2	33.1	95.1	21.8	23	.436	.560	14.3	.930	-	-
	14	36	16.5	17	0	0	-	-	-	-	-	89.7	23.9	92.8	15.5	17	.439	.552	14.6	.913	-	-
6	1	40	22	-	0	0	-	-	-	-	-	82.9	33.1	83.5	15.6	-	.435	.534	13.7	.920	-	-
	2	40	22	20	0	10	-	-	-	-	-	83.2	42.6	93.5	27.1	30	.435	.586	14.1	.933	-	-
	3	40	22	19	0	20	-	-	-	-	-	75	56.9	94.1	37.2	39	.433	.563	14.1	.939	-	-
	4	40	22	18	0	22	-	-	-	-	-	73	58.5	93.6	38.7	40	.430	.57	14.2	.937	-	-
	5	40	22	18	0	24	-	-	-	-	-	70.2	60.2	92.5	40.6	42	.433	.567	14.2	.943	-	-
	6	40	22	17	0	26	-	-	-	-	-	68.4	61.9	92.3	42.2	43	.434	.569	14.4	.934	-	-
	7	40	22	16	0	30	-	-	-	-	-	64.2	67.3	93.0	46.4	46	.442	.575	14.3	.970	-	-
	8	70	30	30	0	35	40	22	30	0	70	1.0	85.6	85.6	89.4	90	.442	.568	14.6	.934	-	-
	9	70	30	29	0	35	40	22	30	0	78	-11.9	87.1	87.9	97.8	98	.439	.57	14.6	.931	-	-
	10	70	30	29	0	35	40	22	30	0	82	-17.4	88.4	88.1	101.4	102	.439	.572	14.6	.935	-	-
	11	70	30	29	0	35	40	22	30	0	84	-20.2	85.8	88.1	103.2	104	.444	.574	14.7	.946	-	-
	12	70	30	29	0	35	40	22	30	0	88	-23.4	85.3	88.5	105.3	106	.438	.572	14.6	.931	-	-
	13	70	30	29	0	35	40	22	30	0	90	-27.6	83.2	87.7	108.4	110	.439	.572	14.5	.944	-	-
	14	70	30	29	0	35	40	22	15	0	98	-33.1	77.1	83.9	113.2	113	.438	.572	14.6	.934	-	-
7	1	70	30	29	0	35	56	31.5	18	0	105	-40.4	68.5	79.5	120.5	124	.452	.584	15.0	.959	-	-
	2	70	30	29	0	35	56	31.5	-	0	98	-40.8	75.8	86.1	118.3	-	.439	.573	14.7	.933	-	-
	3	70	30	29	0	35	56	31.5	24	0	91	-35.4	81.6	88.9	113.5	115	.44	.576	14.6	.960	-	-
	4	70	30	29	0	35	56	31.5	24	0	88	-31.0	82.2	87.9	108.2	112	.439	.572	14.5	.941	-	-
	5	70	30	29	0	35	56	31.5	25	0	85	-28.5	82.8	87.6	109	110	.438	.571	14.5	.938	-	-
	6	70	30	29	0	35	56	31.5	25	0	78	-18.1	83.9	85.8	102.2	103	.443	.573	14.7	.938	-	-
	7	70	30	29	0	35	56	31.5	25	0	70	-4.5	83.9	84.0	93.1	95	.445	.572	14.5	.952	-	-
	8	56	31.5	-	0	33	-	-	-	-	-	54.8	74.9	92.8	53.8	-	.440	.571	14.5	.949	-	-
	9	56	31.5	24	0	30	-	-	-	-	-	59	75.1	95.5	51.9	54	.437	.57	14.4	.940	-	-
	10	56	31.5	-	0	27	-	-	-	-	-	63.2	70.6	94.8	48.2	-	.435	.568	14.4	.933	-	-
	11	56	31.5	23	0	24	-	-	-	-	-	66.3	68.1	95	45.8	47	.438	.57	14.5	.934	-	-
	12	56	31.5	24	0	21	-	-	-	-	-	69.2	62.8	93.5	5.2	45	.441	.564	14.4	.918	-	-

APPENDIX II TABULATION OF TEST RESULTS (CONTINUED)

RUN NUMBER	READING NUMBER PER RUN	CASCADE A					CASCADE B					HORIZONTAL CORRECTED THRUST $F_R \frac{\theta}{T}$ (LB)	VERTICAL CORRECTED THRUST $F_V \frac{a}{T}$ (LB)	RESULTANT CORRECTED THRUST $R \frac{a}{T}$ (LB)	RESULTANT THRUST ANGLE θ_F (DEGREES)	JET EFFUX ANGLE θ_J (DEGREES)	PRESSURE RISE COEFFICIENT $\Psi_{10.6}$	FLOW COEFFICIENT $\phi_{10.2}$	CORRECTED FAN RPS $\frac{RPS}{\sqrt{\theta}}$	ROTOR EFFICIENT η_R	WIND TUNNEL VELOCITY V_p (FT SEC)	GROUND PLANE DISTANCE (I d)
		BLADE CAMBER ANGLE θ^*_A (DEGREES)	BLADE INLET ANGLE θ^*_1 (DEGREES)	AIR EXIT ANGLE θ_2 (DEGREES)	BLADE SETTING ANGLE γ (DEGREES)	CASCADE ANGLE γ_A (DEGREES)	BLADE CAMBER ANGLE θ^*_A (DEGREES)	BLADE INLET ANGLE θ^*_1 (DEGREES)	AIR EXIT ANGLE θ_2 (DEGREES)	BLADE SETTING ANGLE γ (DEGREES)	CASCADE ANGLE γ_A (DEGREES)											
7	13	56	31.5	23	0	10	-	-	-	-	-	77.1	44.4	89	29.9	33	.439	.552	14.1	.933	-	-
	14	56	31.5	23	0	0	-	-	-	-	-	77.5	27.6	82.3	19.6	23	.436	.526	13.8	.904	-	-
8	1	78	39	38	0	0	-	-	-	-	-	68.4	31.2	75.2	24.5	28	-	.501	13.4	-	-	-
	2	78	39	38	0	10	-	-	-	-	-	69.5	44.8	83.7	32.8	38	-	.538	13.8	-	-	-
	3	78	39	38	0	20	-	-	-	-	-	61.5	63.4	88.3	45.8	48	-	.555	14.1	-	-	-
	4	78	39	38	0	30	-	-	-	-	-	50	75.8	90.8	56.6	58	-	.568	14.3	-	-	-
	5	78	39	38	0	35	-	-	-	-	-	41.9	81.6	91.7	62.8	63	-	.569	14.7	-	-	-
	6	78	39	37	0	40	-	-	-	-	-	37.1	82.8	90.7	65.9	67	-	.572	14.5	-	-	-
	7	78	39	30	0	45	-	-	-	-	-	33.6	78.1	85.0	66.7	65	-	.572	14.5	-	-	-
	8	78	39	29	0	35	78	39	34	0	50	11.1	69	69.9	80.9	84	-	.568	14.6	-	-	-
	9	78	39	29	0	35	78	39	32	0	60	4.8	73.3	73.5	93.8	92	-	.568	14.5	-	-	-
	10	78	39	29	0	35	78	39	30	0	70	-9	77.9	78.4	96.6	100	-	.571	14.5	-	-	-
	11	78	39	29	0	35	78	39	30	0	80	+26.2	79	83.2	108.3	110	-	.57	14.5	-	-	-
	12	78	39	29	0	35	78	39	29	0	90	+41.2	75.5	86.0	118.6	119	-	.574	14.4	-	-	-
	13	78	39	29	0	35	78	39	29	0	95	+46.9	72.2	86.1	123	124	-	.568	14.6	-	-	-
	14	78	39	29	0	35	78	39	28	0	100	+50.3	69.9	86.1	125.7	128	-	.59	15.0	-	-	-
	15	78	39	29	0	35	78	39	27	0	105	+48.6	64.4	80.7	127.1	132	-	.591	15.2	-	-	-
	16	78	39	29	0	35	78	39	25	0	110	+42	58.9	72.3	125.5	135	-	.583	14.9	-	-	-
	17	78	39	29	0	35	78	39	23	0	115	+32.9	57.8	66.5	119.6	138	-	.584	15.0	-	-	-
	18	78	39	29	0	35	78	39	28	0	100	+48.4	66.2	82.0	126.1	128	-	.592	15.1	-	-	-
	READINGS 19- 23 IN RUN 8 WERE MADE WITH VARIOUS PORTIONS OF THE CASCADE FRAME TAPED.																					
	19	78	39	29	0	35	78	39	-	0	100	+45.8	71.1	84.6	122.8	-	-	-	-	-	-	-
	20	78	39	29	0	35	78	39		0	100	+46.8	71.5	85.5	123.2	-	-	-	-	-	-	-
	21	78	39	29	0	35	78	39	-	0	100	+46.8	71.8	85.7	123.1	-	-	-	-	-	-	-
	22	78	39	29	0	35	78	39	-	0	100	+47.2	72.7	86.7	121	-	-	-	-	-	-	-
	23	78	39	29	0	35	78	39	-	0	100	+47.1	72.8	86.9	121.1	-	-	-	-	-	-	-
	24	78	39	29	0	32	78	39	28	0	85	+31.4	78.2	85.0	111	113	-	.572	14.1	-	-	-
	25	90	45	-	0	45	78	39	-	0	-	+69.9	18	79.6	151.1	-	-	-	-	-	-	-
9	1	90	45	45	0	45	-	-	-	-	-	11	87.4	88.1	-	-	-	-	-	-	-	-
	DURING RUN 9 TWO WAKE READINGS WERE TAKEN TO GET THE TOTAL PRESSURE LOSS COEFFICIENT																					
10	1	78	39	29	0	35	-	-	-	-	-	30.7	82.7	92.2	64.7	64	-	.567	14.1	-	-	-

APPENDIX II TABULATION OF TEST RESULTS (CONTINUED)

RUN NUMBER	READING NUMBER PER RUN	CASCADE A					CASCADE B					HORIZONTAL CORRECTED THRUST $F_{H_{\frac{q}{p}}}$ (LB)	VERTICAL CORRECTED THRUST $F_{V_{\frac{q}{p}}}$	RESULTANT CORRECTED THRUST $R_{\frac{q}{p}}$ (LB)	RESULTANT THRUST ANGLE θ_F (DEGREES)	JET EFFLUX ANGLE θ_J (DEGREES)	PRESSURE RISE COEFFICIENT $\Psi_{10\,6}$	FLOW COEFFICIENT $\phi_{10\,2}$	CORRECTED FAN HORSEPOWER $HP_{\frac{q}{p}}^{c}$	ROTOR EFFICIENCY η_R	WIND TUNNEL VELOCITY V_p (FT/SEC)	GROUND PLANE DISTANCE (h d)
		BLADE CAMBER ANGLE θ_A^c (DEGREES)	BLADE TILT ANGLE θ_1^c (DEGREES)	AIR EXIT ANGLE θ_2 (DEGREES)	BLADE SETTING ANGLE γ (DEGREES)	CASCADE ANGLE γ_A (DEGREES)	BLADE CAMBER ANGLE θ_A^c (DEGREES)	BLADE TILT ANGLE θ_1^c (DEGREES)	AIR EXIT ANGLE θ_2 (DEGREES)	BLADE SETTING ANGLE γ (DEGREES)	CASCADE ANGLE γ_A (DEGREES)											
10	2	70	39	29	0	35	-	-	-	-	-	41.6	81.9	91.9	63	64	-	.566	-	-	-	-
	RUN 10 WAS A COMPARISON BETWEEN TWO CASCADE ASSEMBLIES BOTH AT THE SAME SETTINGS.																					
	DURING RUN 11 DUCTS AND END PLATES WERE ADDED TO THE TANDEM CASCADE IN																					
	VARIOUS COMBINATIONS - SEE FIGURE 67																					
11	1	70	39	29	0	35	70	39	29	0	95	-48.6	76.9	89.4	120.7	124	-	.615	15.3	-	-	-
	2	70	39	29	0	35	70	39	29	0	95	-52	79.6	95.1	123.0	124	-	.612	15.3	-	-	-
	3	70	39	29	0	35	70	39	29	0	95	-48.5	72.3	87.1	123.9	124	-	.585	14.3	-	-	-
	4	70	39	29	0	35	70	39	29	0	95	-51.7	77.6	93.3	123.7	124	-	.585	14.9	-	-	-
	5	70	39	29	0	35	70	39	29	0	95	-51.6	78.5	93.9	123.3	124	-	-	15.2	-	-	-
	6	70	39	29	0	35	70	39	29	0	95	-49.3	74.7	89.5	123.4	124	-	.587	14.9	-	-	-
	7	70	39	29	0	35	70	39	29	0	95	-46	73.1	86.4	122.2	124	-	.584	14.8	-	-	-
	8	70	39	29	0	35	70	39	29	0	95	-46.8	74.6	88.1	122.1	124	-	.580	15.7	-	-	-
	9	70	39	29	0	35	70	39	29	0	95	-5' 9	76.3	92.3	124.2	124	-	.580	14.9	-	-	-
	10	70	39	29	0	35	70	39	29	0	95	-50.4	74.9	90.3	123.9	124	-	587	15.0	-	-	-
	11	70	39	29	0	35	70	39	29	0	95	-49.8	75.5	92.8	123.1	124	-	605	15.1	-	-	-
	12	70	39	29	0	35	70	39	29	0	95	-	-	-	-	-	-	.609	-	-	-	-
	DURING RUN 12, THE CASCADES A AND B WERE SHIFTED 12 INCHES DOWNSTREAM FROM																					
	THE FAN EXIT.																					
12	1	70	39	28	0	0	-	-	-	-	-	74.6	30.5	80.6	22.2	28	-	.563	14.1	-	-	-
	2	70	39	29	0	10	-	-	-	-	-	70.2	45.9	83.9	33.2	39	-	567	11.1	-	-	-
	3	70	39	30	0	20	-	-	-	-	-	62.1	63	88.1	45.4	5[illegible]	-	566	11.3	-	-	-
	4	70	39	29	0	34	-	-	-	-	-	48.5	77	91	57.8	61	-	569	11.2	-	-	-
	5	70	39	25	0	39	-	-	-	-	-	35	82	89.2	66.9	64	-	571	11.4	-	-	-
	6	70	39	22	0	44	-	-	-	-	-	31.3	80	85.9	68.6	66	-	572	11.3	-	-	-
	7	70	39	28	0	25	-	-	-	-	-	52.6	74	90.8	54.6	53	-	570	11.4	-	-	-
	8	70	39	28	0	20	-	-	-	-	-	61.3	65.2	89.5	46.8	48	-	568	11.2	-	-	-
	9	70	39	29	0	35	70	39	31	0	75	-15.4	80.1	81.5	100.9	106	-	566	11.4	-	-	-
	10	70	39	29	0	35	70	39	31	0	85	-32.7	79.6	86	112.1	116	-	569	11.4	-	-	-
	11	70	39	29	0	35	70	39	30	0	90	-38.2	78.9	86.3	116.1	120	-	570	11.4	-	-	-
	12	70	39	29	0	35	70	39	30	0	95	-41.1	71.6	85.8	121	125	-	574	11.2	-	-	-
	13	70	39	29	0	35	70	39	30	0	100	-47.1	70.2	83.6	124.8	130	-	577	11.3	-	-	-

APPENDIX II TABULATION OF TEST RESULTS (CONTINUED)

RUN NUMBER	READING NUMBER PER RUN	CASCADE A					CASCADE B					HORIZONTAL CORRECTED THRUST F_H (LB)	VERTICAL CORRECTED THRUST F_V (LB)	RESULTANT CORRECTED THRUST R (LB)	RESULTANT THRUST ANGLE θ_F (DEGREES)	JET EFFLUX ANGLE θ_J (DEGREES)	PRESSURE RISE COEFFICIENT $\Psi_{10.6}$	FLOW COEFFICIENT $\phi_{10.2}$	CORRECTED FAN HORSEPOWER $HP\frac{\sigma}{\delta}$	ROTOR EFFICIENCY η_R	WIND TUNNEL VELOCITY V_p (FT SEC)	GROUND PLANE DISTANCE (h d)
		BLADE CAMBER ANGLE θ_A^* (DEGREES)	BLADE INLET ANGLE θ_1^* (DEGREES)	AIR EXIT ANGLE θ_2 (DEGREES)	BLADE SETTING ANGLE $\setminus$ (DEGREES)	CASCADE ANGLE γ_A (DEGREES)	BLADE CAMBER ANGLE θ_A^* (DEGREES)	BLADE INLET ANGLE θ_1^* (DEGREES)	AIR EXIT ANGLE θ_2 (DEGREES)	BLADE SETTING ANGLE $\setminus$ (DEGREES)	CASCADE ANGLE γ_A (DEGREES)											
12	14	78	39	29	0	35	78	39	27	0	105	-49.4	66.6	82.9	126.6	132	-	.586	14.6	-	-	-
	15	78	39	29	0	35	78	39	26	0	110	-44.6	61.6	76	125.9	136	-	.587	14.8	-	-	-
13	1	78	39	29	0	35	78	39	26	0	90	-36.8	65.3	75.0	119.4	-	-	-	13.5	-	-	-
	2	78	39	29	0	35	78	39	31	0	95	-43.8	73.4	85.5	120.8	126	-	-	14.4	-	-	-
	3	78	39	29	0	35	78	39	31	0	100	-49.8	70.2	86.1	125.4	131	-	-	14.4	-	-	-
	4	78	39	29	0	35	78	39	27	0	105	-52.8	63.2	82.4	129.9	132	-	-	14.6	-	-	-
	5	78	39	29	0	35	78	39	25	0	110	-51.3	57.7	77.2	131.6	135	-	-	14.9	-	-	-
14	1	78	39	29	0	35	80	39.5	30	0	70	-7.4	76.3	76.7	95.5	100	-	-	14.4	-	-	-
	2	78	39	29	0	35	80	39.5	30	0	80	-24.7	76.9	80.8	107.8	110	-	-	14.4	-	-	-
	3	78	39	29	0	35	80	39.5	31	0	90	-40.9	80.3	90.1	117	121	-	-	14.5	-	-	-
	4	78	39	29	0	35	80	39.5	32	0	95	-47.5	71.7	86.0	123.5	127	-	-	14.6	-	-	-
	5	78	39	29	0	35	80	39.5	32	0	100	-51.8	64.6	82.8	128.7	132	-	-	14.6	-	-	-
	6	78	39	29	0	35	80	39.5	30	0	105	-50.6	61.4	79.6	129.5	135	-	-	14.6	-	-	-
	7	78	39	29	0	35	80	39.5	26	0	110	-44.3	56.8	72.0	127.9	136	-	-	15.1	-	-	-
	8	80	39.5	25	0	0	-	-	-	-	-	61.9	28.6	68.2	24.8	25	-	-	12.8	-	-	-
	9	80	39.5	20	0	10	-	-	-	-	-	64.2	41.1	76.2	32.6	30	-	-	13.5	-	-	-
	10	80	39.5	23	0	20	-	-	-	-	-	58.8	58.3	82.8	44.7	43	-	-	13.9	-	-	-
	11	80	39.5	31	0	30	-	-	-	-	-	45	79.7	91.5	60.5	61	-	-	14.2	-	-	-
	12	80	39.5	0	0	35	-	-	-	-	-	38	84.3	92.5	65.7	66	-	-	14.5	-	-	-
	13	80	39.5	30	0	40	-	-	-	-	-	32	86.5	92.2	69.7	70	-	-	14.5	-	-	-
	14	80	39.5	30	0	45	-	-	-	-	-	29.9	83.5	88.7	70.3	75	-	-	14.5	-	-	-
	15	80	39.5	30	0	38	78	39	32	0	70	-8.8	78.3	78.8	96.4	102	-	-	14.5	-	-	-
	16	80	39.5	30	0	38	78	39	31	0	80	-25.9	80.3	84.4	107.9	111	-	-	14.5	-	-	-
	17	80	39.5	30	0	38	78	39	32	0	90	-40.1	79.4	89.1	117	122	-	-	14.5	-	-	-
	18	80	39.5	30	0	38	78	39	-	0	95	-49.4	74.7	89.6	123.5	-	-	-	14.9	-	-	-
	19	80	39.5	30	0	38	78	39	32	0	100	-53.2	70.6	88.4	127	100	-	-	15.1	-	-	-
	20	80	39.5	30	0	38	78	39	31	0	105	-55.5	65.9	86.2	130.1	136	-	-	15.1	-	-	-
	21	80	39.5	30	0	38	78	39	30	0	110	-53.7	60.5	80.9	131.6	140	-	-	14.9	-	-	-
15	1	THESE READINGS WERE DUPLICATED																				
	2	IN RUN 16																				

APPENDIX II TABULATION OF TEST RESULTS (CONTINUED)

RUN NUMBER	READING NUMBER PER RUN	CASCADE A					CASCADE B					HORIZONTAL CORRECTED THRUST $F_{B,T}$ (LB)	VERTICAL CORRECTED THRUST $F_{V,T}$ (LB)	RESULTANT CORRECTED THRUST R (LB)	RESULTANT THRUST ANGLE θ_R (DEGREES)	JET EFFLUX ANGLE θ_J (DEGREES)	PRESSURE RISE COEFFICIENT $\Psi_{10.8}$	FLOW COEFFICIENT $\phi_{10.2}$	CORRECTED FAN RESPONSE $\frac{N}{\sqrt{\theta}}$	ROTOR EFFICIENCY η_R	WIND TUNNEL VELOCITY V_p (FT/SEC)	GROUND PLANE DISTANCE (D/d)
		BLADE CAMBER ANGLE θ_C (DEGREES)	BLADE INLET ANGLE θ_I (DEGREES)	AIR EXIT ANGLE θ_E (DEGREES)	BLADE SETTING ANGLE 1 (DEGREES)	CASCADE ANGLE γ_A (DEGREES)	BLADE CAMBER ANGLE θ_C (DEGREES)	BLADE INLET ANGLE θ_I (DEGREES)	AIR EXIT ANGLE θ_E (DEGREES)	BLADE SETTING ANGLE 1 (DEGREES)	CASCADE ANGLE γ_A (DEGREES)											
16	1	NO CASCADES MOUNTED, NO FAN RUNNING										-45	- 3	4 5	3 8	-	-	-	- 5	-	38	-
	2	NO CASCADES MOUNTED										102 8	- 8	102 8	179 6	-	-	-	14 4	-	0	-
	3	NO CASCADES MOUNTED										79	-1 2	79	179 2	-	418	583	14 1	956	38	-
	4	80	39 5		0	35	NO FAN RUNNING					-8 2	5 0	9 6	148 6	-	-	-	- 5	-	38	-
	5	80	39 5	30	0	35						9 3	99 5	99 9	84 7	65	419	59	14 0	961	38	-
	6	80	39 5	30	0	35	DURING POINT 16-6, NO FAN RUNNING 78	30	31	0	95	-11 9	11 7	16 7	135 3	126	-	-	- 5	-	38	-
	7	80	39.5	30	0	35	78	30	32	0	95	-91 0	87 8	126 5	136	127	419	580	14 2	945	38	-
	8	80	39 5	30	0	35	78	30	29	0	95	-45 1	73	86 2	121 7	124	432	572	14 6	899	0	1 83
	9	80	39 5	30	0	35	78	30	29	0	95	-	-	-	-	124	-	-	-	-	38	1.83
	10	80	39 5	30	0	35	78	30	31	0	95	-48.6	72.9	87 6	123 7	124	.434	.580	14 8	925	0	2 00
	11	80	39 5	30	0	35	78	30	31	0	95	-48 1	74 9	89 0	122 7	124	.432	578	14 8	918	0	2 41
	12	80	39.5	30	0	35	78	30	31	0	95	-45.8	74.6	87 5	121 6	126	.433	565	14.6	.918	0	2 69
	13	80	39 5	30	0	35	78	30	31	0	95	-43 7	76 1	87 8	119 8	126	424	573	14 4	918	0	2 94
	14	80	39.5	30	0	35	78	30	31	0	95	-44 4	77	88.9	120	126	437	577	14 7	.933	0	3 32
	15	80	39 5	30	0	35	78	30	32	0	95	-86 5	86 8	125 4	134 9	127	417	580	14 1	946	38	3 32
17	1	78	39	DURING POINT 17-1	0	35	NO FAN RUNNING 80	30.5		0	105	+13 9	5 4	14 9	158 6	-	-	-	- 34	-	38	-
	2	80	39 5	30	0	35	78	30	30	0	105	+51 7	65 8	83 7	128 1	135	-	-	14 2	-	0	3 32
	3	80	39 5	30	0	35	78	30	30	0	105	+49 8	65 9	82 6	127 1	135	-	-	14 4	-	0	2 81
	4	80	39 5	30	0	35	78	30	29	0	105	+53 6	67 5	86 2	128 6	134	-	-	14 9	-	0	2 48
	5	80	39 5	30	0	35	78	30	29	0	105	+55 3	65 7	85 9	130 1	134	-	-	15 0	-	0	2 11
	6	80	39 5	30	0	35	78	30	28	0	105	+47 1	66 8	81 7	125 2	133	-	-	14 7	-	0	1 76
	7	80	39 5	30	0	35	78	30	30	0	105	+94 3	83 1	125 7	138 6	135	421	59	14 2	982	38	-
18	1	80	39 5	30	0	35	-	-	-	-	-	44 4	83 9	94 9	62 1	110	-	-	14 4	-	0	1 7
	2	80	39 5	30	0	35	-	-	-	-	-	10 2	106 8	107 3	84 5	110	419	580	14 6	920	38	-
	3	80	39 5	30	0	35	-	-	-	-	-	39 5	84 1	92 9	64 8	110	-	-	14 6	-	0	2 18
	4	80	39 5	30	0	35	-	-	-	-	-	9 1	105 4	105 8	85 1	110	419	59	11 7	915	38	-
	5	80	39 5	30	0	35	-	-	-	-	-	41 6	89 0	98 2	64 9	110	-	-	14 1	-	0	-
19	1	90	45	45	0	45	(FIXED CAMBER CASCADE)					12 1	105 1	105 8	83 4	90	-	-	11 8	-	0	-
	2	90	45	45	0	45	-	-	-	-	-	21 8	118 7	121 2	79 6	90	118	595	11 2	953	38	-

APPENDIX II TABULATION OF TEST RESULTS (CONTINUED)

RUN NUMBER	READING NUMBER PER RUN	CASCADE A					CASCADE B					HORIZONTAL CORRECTED THRUST F_{H_c} (LB)	VERTICAL CORRECTED THRUST F_{V_c} (LB)	RESULTANT CORRECTED THRUST R (LB)	RESULTANT THRUST ANGLE θ_T (DEGREES)	JET EFFLUX ANGLE θ_J (DEGREES)	PRESSURE RISE COEFFICIENT $\Psi_{10\,6}$	FLOW COEFFICIENT $\phi_{10\,2}$	CORRECTED FAN HORSEPOWER HP_c^*	ROTOR EFFICIENCY η_R	WIND TUNNEL VELOCITY V_p (FT SEC)	GROUND PLANE DISTANCE (h/d)
		BLADE CAMBER ANGLE θ_2 (DEGREES)	BLADE INLET ANGLE θ_1 (DEGREES)	AIR EXIT ANGLE θ_2 (DEGREES)	BLADE SETTING ANGLE γ (DEGREES)	CASCADE ANGLE γ_A (DEGREES)	BLADE CAMBER ANGLE θ_2 (DEGREES)	BLADE INLET ANGLE θ_1 (DEGREES)	AIR EXIT ANGLE θ_2 (DEGREES)	BLADE SETTING ANGLE γ (DEGREES)	CASCADE ANGLE γ_A (DEGREES)											
19	3	90	45	45	0	45	NO FAN RUNNING					12 8	10	16 2	141 9	90	-	-	-	-	18	-
	4	90	45	45	0	45	-	-	-	-	-	12 5	91 3	92 2	82 1	90			14 1		0	1 7
	5	90	45	45	0	45	-	-	-	-	-	11 5	91 5	92 2	82 9	90			14 1		0	2 04
	6	90	45	45	0	45						11 0	95 6	92 2	83 4	90			14 4		0	2 48
	7	90	45	45	0	45	-	-	-	-	-	13 0	95 7	96 6	82 3	90			14 2		1	2 89
20	1	42	37	0	15	30	-	-	-	-	-	85	48 8	98	29 9	30			14 1		0	-
	2	42	37	0	15	30	-	-	-	-	-	59 5	56 4	82	43 5	30	416	597	14 0	965	18	
	3	42	37	0	15	30	-	-	-	-	-	83 5	48 7	96 7	30 3	30	418	609	14 8	936	0	1 75
	4	42	37	0	15	35	-	-	-	-	-	80 5	54 6	97 1	34 9	35	418	609	14 1	982	0	
	5	42	37	0	15	35	-	-	-	-	-	56	82 4	83 8	48 1	35	418	597	14 2	956	18	
	6	42	37	0	15	35	-	-	-	-	-	79 6	54 6	96 5	34 4	35			14 1		0	1 74
	7	42	37	-1	15	40	-	-	-	-	-	77 1	60 1	97 8	37 9	39			14 4			
	8	42	37	-2	15	40	-	-	-	-	-	50 2	68 9	85 1	53 9	38	419	598	14 6	1 002	18	
	9	42	37	-1	15	40	-	-	-	-	-	75 2	59 1	95 6	38 2	39			14 2		0	2 71
21	1	78	39	29	0	35	42	37	1	15	85	8 7	87 4	87 8	84 3	84			14 1		0	
	2	78	39	28	0	35	42	37	-10	15	90	1	90 4	90 1	89 8	80			14 2		0	
	4	78	39	29	0	35	42	37	1	15	90	17 7	107 2	111 6	109 4	89	1 [illegible]	[illegible]	14 [illegible]	96	18	
	5	78	39	29	0	35	12	37	1	15	90	1 9	84 5	84 1	88 7	87			14 4			
	6	78	39	29	0	35	42	37	2	15	95	6 4	92 5	92 7	94	94			14			
	7	78	39	29	0	35	42	37	2	1	99	11 6	90 6	91 1	97 5	97			14			
22	1	78	39	29	0	35	18	37	6	12	98	17 2	91 6	95 2	100 5	10			14			
	2	78	39	29	0	35	48	37	6	12	98	56 5	106 1	1 0	118	100	1 8	92	14 4	968	18	
	3	78	39	29	0	35	48	37	6	12	94	12 7	105 1	103 9	96 9	97			14 2			8
	4	78	39	29	0	35	48	37	6	12	99	16 6	82 9	88 5	101 1	104			14 2			
	5	78	39	29	0	35	48	37	6	12	99	20	90 8	94 1	102 2	100			14 1			
	6	78	39	29	0	35	48	37	6	12	94	61 7	101 7	119 0	121 1	100	1 0	9	15	984	18	
23	1	48	17	7	5	30	-	-				78 7	58 2	97 9	36	37			14 1			
	2	48	17	6	12	30	-	-				2 9	63 7	84 1	1	36	119	93	1	9	18	
	4	48	17	7	1	30						78 1	61 1	99	38	1			14 1			
	5	48	17	7	1	1						7	68	100	1	1			14 1			
	6	48	17	7		1						2 1	66	100	1	1			14			

APPENDIX II TABULATION OF TEST RESULTS (CONTINUED)

RUN NUMBER	READING NUMBER PER RUN	CASCADE A					CASCADE B					HORIZONTAL CORRECTED THRUST $F_{H_{\frac{B}{T}}}$ (LB)	VERTICAL CORRECTED THRUST $F_{V_{\frac{B}{T}}}$ (LB)	RESULTANT CORRECTED THRUST R $_{\frac{B}{T}}$ (LB)	RESULTANT THRUST ANGLE θ_R (DEGREES)	JET EFFLUX ANGLE θ_J (DEGREES)	PRESSURE RISE COEFFICIENT $\Psi_{10.6}$	FLOW COEFFICIENT $\phi_{10.2}$	CORRECTED FAN HORSEPOWER $HP_V^{\frac{B}{T}}$	ROTOR EFFICIENCY η_R	WIND TUNNEL VELOCITY V_p (FT SEC)	GROUND PLANE DISTANCE (h d)
		BLADE CAMBER ANGLE θ_A^* (DEGREES)	BLADE INLET ANGLE θ_1^* (DEGREES)	AIR EXIT ANGLE θ_2 (DEGREES)	BLADE SETTING ANGLE γ (DEGREES)	CASCADE ANGLE γ_A (DEGREES)	BLADE CAMBER ANGLE θ_A^* (DEGREES)	BLADE INLET ANGLE β_1^* (DEGREES)	AIR EXIT ANGLE β_2 (DEGREES)	BLADE SETTING ANGLE γ (DEGREES)	CASCADE ANGLE γ_A (DEGREES)											
23	6	48	37	7	12	35	-	-	-	-	-	47 8	78 4	90 1	58	42	416	596	13 9	970	38	-
	7	48	37	7 5	12	40	-	-	-	-	-	69 5	70 8	99.2	45 5	47 5	-	-	14 3	-	0	-
	8	48	37	7	12	40	-	-	-	-	-	41 8	89 1	98 4	84 9	47	420	597	14 2	961	38	-
	9	48	37	7	12	40	-	-	-	-	-	68 6	122 7	140 6	60 8	47 5	-	-	-	-	0	1 74
24	1	78	39	29	0	35	48	25	18	0	84	-20 6	93 5	95 7	102 4	102	-	-	14 4	-	0	-
	2	78	39	29	0	35	48	25	18	0	84	-60 8	108 8	124 6	119 2	102	416	591	14 0	955	38	-
	3	78	39	29	0	35	48	25	18	0	84	-20 4	92	94 2	102 5	102	-	-	15 3	-	0	2 21
	4	78	39	29	0	35	48	25	17 5	0	89	-25 1	88 2	91 7	105 9	106 5	-	-	15 4	-	0	2 21
	5	78	39	29	0	35	48	25	17 5	0	89	-24 4	90 6	93 8	105 1	106 5	-	-	14 5	-	0	-
	6	78	39	29	0	35	48	25	17 5	0	89	-68 5	106 8	126 9	122 7	106 5	421	589	14 2	950	38	-
	7	78	39	29	0	35	48	25	16	0	94	-29 4	88 4	93 2	108 4	110	-	-	14 3	-	0	-
	8	78	39	29	0	35	48	25	16	0	94	-73 2	99 3	123 4	126 4	110	418	592	13 5	987	38	-
	9	78	39	29	0	35	48	25	15	0	94	-30	87 9	92 9	108 8	109	-	-	15 2	-	0	2 21
	10	78	39	29	0	35	48	25	12	0	99	-35 1	83 7	90 8	112 8	111	-	-	15 2	-	0	2 21
	11	78	39	29	0	35	48	25	14	0	99	-33 9	87 3	93 7	111 2	113	-	-	14 3	-	0	-
	12	78	39	29	0	35	48	37	15	0	84	-76 8	100	126 1	127 5	99	441	588	14 2	993	38	-
25	1	61	37	15	8	30	-	-	-	-	-	70 2	69	98 1	44 5	45	-	-	14 6	-	0	-
	2	61	37	15	8	30	-	-	-	-	-	43 2	78 5	89 6	61 2	45	421	592	14 5	935	38	-
	3	61	37	15	8	30	-	-	-	-	-	67 7	70 6	97 8	46 2	45	-	-	14 2	-	0	1 76
	4	61	37	13	8	35	-	-	-	-	-	63 5	77 1	-	46 2	50	-	-	14 6	-	0	1 76
	5	61	37	13	8	35	-	-	-	-	-	64 6	75 2	99	49 3	50	-	-	14 6	-	0	
	6	61	37	13	8	35	-	-	-	-	-	36 4	84 5	92	66 7	50	419	594	14 4	940	38	-
	7	61	37	12	8	40	-	-	-	-	-	58 3	79 2	98 1	53 6	52	-	-	14 6	-	0	-
	8	61	37	11	8	40	-	-	-	-	-	30 6	89 1	94 4	71 7	51	419	594	14 4	940	38	-
	9	61	37	11 5	8	40	-	-	-	-	-	55 8	79 4	97 1	54 9	51 5	-	-	14 1	-	0	1 76
26	1	61	37	13	8	35	48	25	18	0	88	11 5	86 1	86 9	82 1	86	-	-	13 8	-	0	1 97
	2	61	37	11	8	35	48	25	18	0	88	6 5	94 5	94 7	86 1	86	-	-	13 6	-	0	
	3	61	37	11	8	35	48	25	19	0	88	-29 9	111 1	115 1	105 1	87	117	495	13 1	957	38	
	4	61	37	11	8	35	38	25	18	0	73	0	95 1	95 1	0	91	-	-	13 6	-	0	

APPENDIX II TABULATION OF TEST RESULTS (CONTINUED)

RUN NUMBER	READING NUMBER PER RUN	CASCADE A: BLADE CAMBER ANGLE θ_A (DEGREES)	CASCADE A: BLADE INLET ANGLE β_1^* (DEGREES)	CASCADE A: AIR EXIT ANGLE θ_2 (DEGREES)	CASCADE A: BLADE SETTING ANGLE γ (DEGREES)	CASCADE A: CASCADE ANGLE γ_A (DEGREES)	CASCADE B: BLADE CAMBER ANGLE θ_B (DEGREES)	CASCADE B: BLADE INLET ANGLE β_1^* (DEGREES)	CASCADE B: AIR EXIT ANGLE θ_2 (DEGREES)	CASCADE B: BLADE SETTING ANGLE γ (DEGREES)	CASCADE B: CASCADE ANGLE γ_A (DEGREES)	HORIZONTAL CORRECTED THRUST F_{H_2} (LB)	VERTICAL CORRECTED THRUST F_{V_2} (LB)	RESULTANT CORRECTED THRUST R_2 (LB)	RESULTANT THRUST ANGLE θ_p (DEGREES)	JET EFFLUX ANGLE θ_j (DEGREES)	PRESSURE RISE COEFFICIENT Ψ_{10-6}	FLOW COEFFICIENT θ_{10-6}	CORRECTED FAN HORSEPOWER HP_2^θ	ROTOR EFFICIENCY η_R	WIND TUNNEL VELOCITY V_p (FT SEC)	GROUND PLANE DISTANCE (ft d)
26	5	61	37	13	N	35	48	25	18	0	73	+18.9	99.N	107.1	111.1	91	.417	.594	14.1	.956	18	
	6	61	37	13	N	35	48	25	18	0	73	-.2	88.3	88.3	91.1	91			14.4		0	2.19
	7	61	37	13	N	35	48	25	16	0	78	-3.9	86.2	86.1	92.6	94			15		0	2.18
	8	61	37	13	N	35	48	25	17	0	78	-3.2	92.6	92.7	92	95			14.4		0	
	9	61	37	13	N	35	48	25	17	0	78	+44.2	108.4	117.1	112.2	95	.420	.596	14.2	.959	18	
	10	61	37	13	N	35	48	25	16	0	83	-4.N	89.1	89.2	91.1	99			14.4		0	
	11	61	37	13	N	35	48	25	16	0	83	+47.1	104.1	114.4	114.1	99	.418	.594	14.1	.958	18	
	12	61	37	13	N	35	48	25	17	0	81	-4.5	82.1	82.2	91.1	100			14.1		0	2.14
	13	NO CASCADE MOUNTED										102.1	.2	102.1	1.1						0	
	14	90	45	-	-	45	FIXED CAMBER CASCADE					9.2	100.4	100.N	N4.N						0	
27	1	78	39	26	0	30						52.7	N1.5	97.1	57.1	56			14.1			
	2	78	39	26.5	0	35						46.7	N4.7	96.7	61.1	61.5			13.1			
	3	78	39	26.5	0	40						41.7	N6.N	96.1	64.1	66.5			14.1			
	4	60	35	15	0	40						4N.1	N3.7	96.6	60	55			13.1			
	5	60	35	20	0	30						60.6	77.1	98.2	51.9	50			14.4			
	6	60	35	17.5	0	35						54.9	N1.2	98	55.9	52.4			14.1*			
	7	60	35	17.5	0	35	78		26		N5	+28	N7.5	91.9	107.7	111			14.6			
	N	78	35	26	0	35	60	19.1	20	0	90	+29.2	N6.9	91.7	108.5	110			13.4			
	9	78	35	26	0	35	60	19	19	0	95	+12.1	N5.7	91.5	100.4	114			14.5			
	10	78	39	26	0	35	60	19	17	0	100	+11.9	N1.6	N7.6	101.4	117			13.5			

APPENDIX III - SAMPLE CALCULATIONS

A sample calculation using the data reduction procedure outlined in the Technical Discussion, Phase III, Measurements and Data Reduction, is illustrated in this appendix. The data from Run 16, Reading 7 is chosen for illustration.

FORCE RESULTS

The load cell readings receive calibration corrections and ambient density corrections. Lift and thrust are defined as positive forces in the vertical and horizontal directions and correspond to a tension force in Load Cell Number 1 and compression forces in Load Cell Numbers 2 and 3.

	Number 1	Number 2	Number 3
Direction	Compression	Tension	Compression
Scale Reading	-79.0	-6.5	+83.5
Calibration	- 5.3	- .7	+ 5.1
Force	-84.3	-7.2	+88.6
			- 7.2
Total Force	-84.3		+81.4

Density correction:

$$\rho = 1.0654 = \frac{94 + 460}{518.7}$$

$$\delta = 0.9868 = \frac{29.525}{29.92}$$

$$\frac{\rho}{\delta} = 1.0796$$

Corrected forces:

Horizontal $\quad F_H \frac{\rho}{\delta} = -91.0 = -84.3\ (1.0796)$

Vectored $\quad F_V \frac{\rho}{\delta} = +87.9 = +81.4\ (1.0796)$

Resultant $R\frac{\theta}{\delta} = 126.5$

Vector Angle $\beta_F = 136^o = \arctan \frac{-91}{87.9}$

FAN POWER

The fan power consumption is computed from the torque developed by the 6.385 foot lever arm exerting a net force of 6.05 pounds at a rotational speed of 1782 r.p.m. The power is corrected for inlet density:

$$HP\frac{\theta}{\delta} = F\frac{\theta}{\delta} n\ 2\ \pi \frac{L}{550}$$

$$HP\frac{\theta}{\delta} = \frac{(6.05)(1.0796)(29.7)(6.28)(6.385)}{550}$$

$$HP\frac{\theta}{\delta} = 14.15.$$

PRESSURE DATA

The pressure data consists mainly of six-element rakes except for the eight nozzle wall static pressures at the fan nozzle exit. All of these pressures are measured by calibrated inclined manometers of approximately 4:1 slope. The six-element rakes read on center of equal annular areas to facilitate area averaging. The manometer readings are processed by a simple IBM program which converts each reading into pressure coefficient form. For the purposes of this sample calculation, one element will be taken as typical of all 44 elements:

Manometer Reading	23.15	inches
Manometer Reference	11.05	inches
Inclined Deflection	12.10	inches
Manometer Slope	.2389	
Vertical Deflection	2.89	inches
Pressure Difference	15.02	pounds per square foot

$$\Psi = \frac{\Delta P \frac{g}{\delta}}{\left(\frac{\rho_o}{2}\right) U_T^2}$$

$$\Psi = \frac{(15.02)(1.0796)}{(.00119)(202)^2}$$

$$\Psi = 0.334$$

Average pressures at the four locations in the fan and references to ambient static pressure expressed in this coefficient form are:

(a) Fan inlet static pressure = -.3145

(b) Fan inlet total pressure = +.034

(c) Rotor discharge total pressure = +.452

(d) Nozzle wall static pressure = +.007

The fan inlet flow coefficient is found from (a) and (b) above using

$$\Phi = \frac{V_{10.2}}{U_T}$$

$$\Phi = (0.034 + 0.3145)^{.5}$$

$$\Phi = 0.589.$$

The velocity of the force jet (V_o) normalized with fan tip speed is obtained from (b) above by

$$\frac{V_o}{U_T} = (0.034)^{.5}$$

$$\frac{V_o}{U_T} = 0.184$$

$$U_T = 202 \text{ feet/second}$$

$$V_o = 37.4 \text{ feet/second.}$$

The fan rotor total pressure rise coefficient is found from (b) and (c) above as

$$\Psi_{10.6} = 0.452 - 0.034$$

$$\Psi_{10.6} = 0.418.$$

The fan rotor efficiency is found from

$$\eta_R = \left[\frac{\rho_o A U_T^3}{2(550)}\right] \frac{\phi\Psi}{HP \frac{\theta}{\delta}}$$

$$\eta_R = 54.4 \frac{\phi\Psi}{HP \frac{\theta}{\delta}}$$

where

standard density $\rho_o = 0.00238$

for annular area $A = 3.1$

fan tip speed $U_T = 202.$

For this test point the rotor efficiency is calculated.

$$\eta_R = \frac{(54.4)(0.589)(0.418)}{(14.15)}$$

$$\eta_R = 0.945$$

ANGLES

All angles of interest are defined in Figure 48. The angles are measured as shown in Table 2.

TABLE 2

EXAMPLE TEST DATA

Description			Cascade A	Cascade B
Angles Relative to Fan				
(a) Cascade Orientation Angle	γ	(Measured)	35°	95°
(b) Jet Efflux Angle	β_J	(Equation 1)*	65°	127°
Hardware Angles				
(c) Leading-Edge Angle	β_1^*	(Measured	39.5°	39°
(d) Trailing-Edge Angle	β_2^*	(Equation 2)*	40.5°	39°
(e) Camber Angle	θ^*	(Measured)	80°	78°
(f) Orientation Angle	β_m^*	(Measured)	0°	0°
Air Angles				
(g) Inlet-Air Angle	β_1	(Equation 3)*	35°	30°
(h) Discharge-Air Angle	β_2	(Measured)	30°	32°
(i) Turning Angle	θ	(Equation 4)*	65°	62°
(j) Incidence Angle	i	(Equation 5)*	-4.5°	-9°
(k) Deviation Angle	δ	(Equation 6)*	10.5°	7°

*where:

Equation 1 $\beta_J = \gamma + \beta_2$

Equation 2 $\beta_2^* = \theta^* - \beta_1^*$

Equation 3 $\beta_{1A} = \gamma_A$

$\beta_{1B} = \gamma_B - \beta_{JA}$

Equation 4 $\theta = \beta_1 + \beta_2$

Equation 5 $i = \beta_1 + \beta_1^*$

Equation 6 $\delta = \beta_2^* - \beta_2$

APPENDIX IV

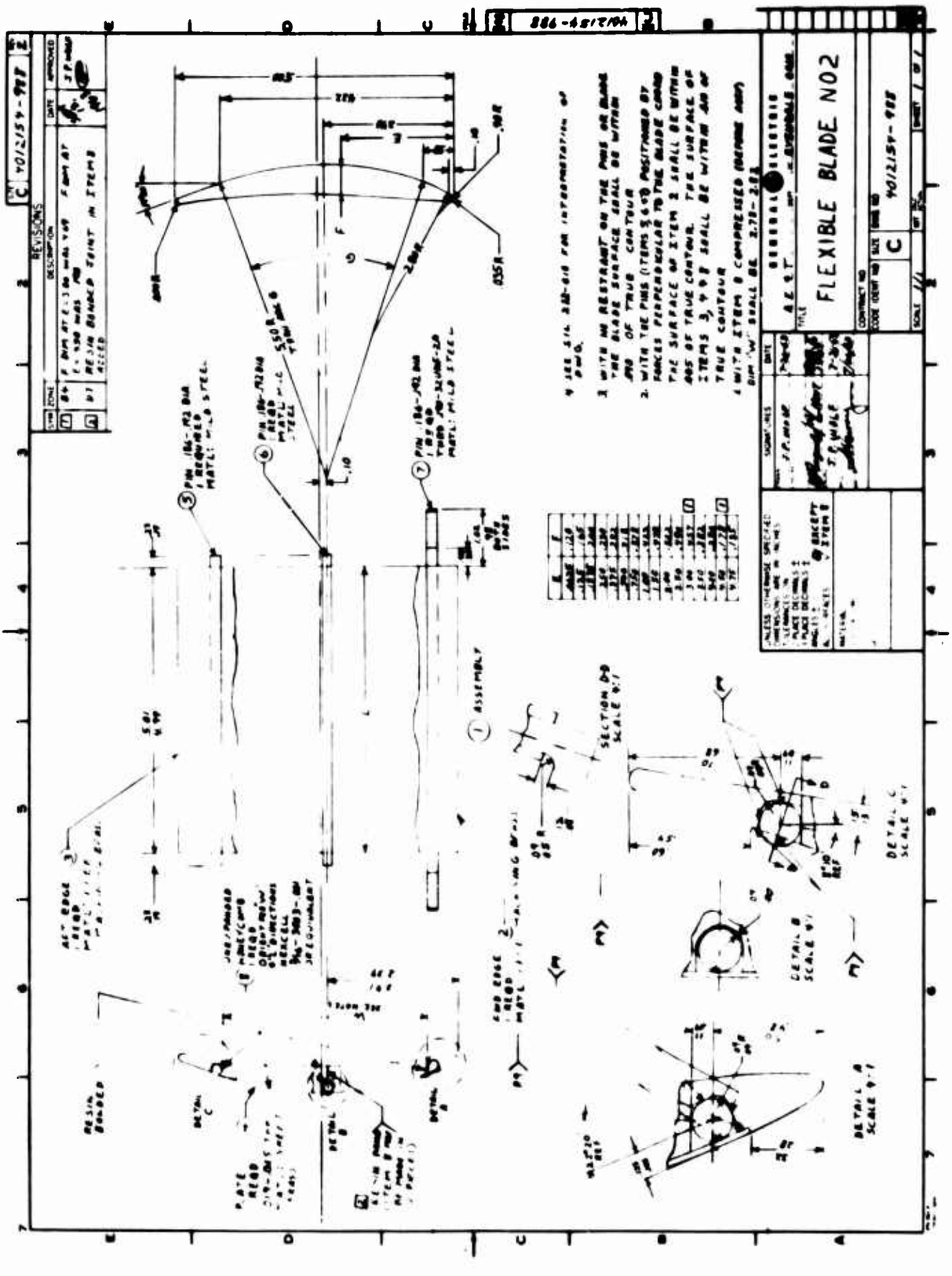
FLEXIBLE BLADE NO2
REVISIONS
SECTION D-D
SCALE 1/1
DETAIL C
SCALE 1/1
DETAIL B
SCALE 1/1
DETAIL A
SCALE 1/1
ASSEMBLY

REVISIONS					SIZE C	4012154-997
ZONE	SYM	DESCRIPTION	DATE	APPROVAL	CONT ON SHEET	SH NO 1

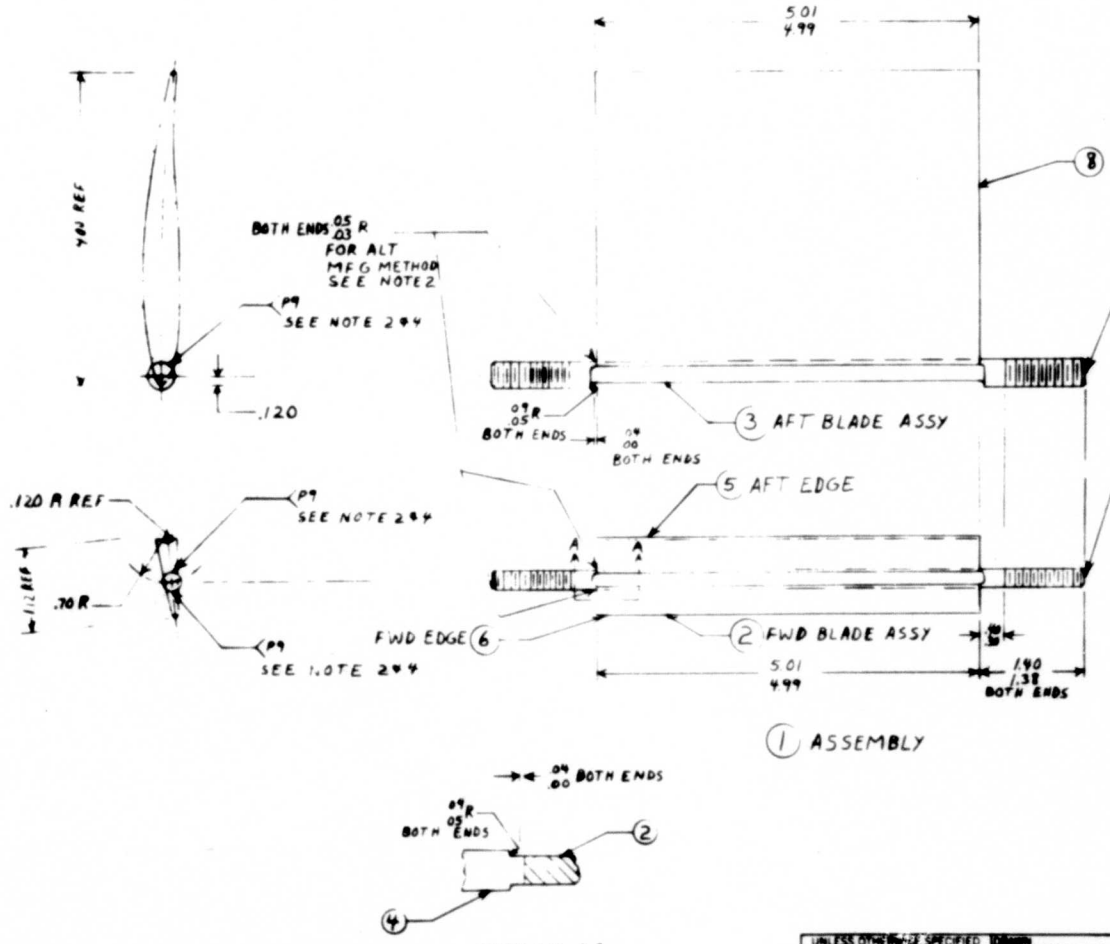

SECTION AA
SCALE 2:1

4. P9 FILLET MATL: AMS 4770. FLUX, IF REQD, AMS 3410D
3. BLADE CONTOUR MUST BE WITHIN .005 OF TRUE CONTOUR AS DEFINED BY GLASSINE 4012241-241
2. BRAZED JOINTS MAY BE ELIMINATED MAKING ITEMS 2 & 3 EACH 1 PIECE MACH. PARTS. IF THIS ALT. MFG. METHOD IS USED, INCORPORATE .03-.05 RADII.
1. SEE SIL 212-010 FOR INTERPRETATION OF DWG.

UNLESS OTHERWISE SPECIFIED DIMENSIONS ARE IN INCHES TOLERANCES ON FRACTIONS DECIMALS ANGLES ± ± ± ALL SURFACES
MATERIAL GOVT OR COML 321 S.S.
DRAWN T.P. NOBLE
DATE 8-24-62

ARTICULATED BLADE 2

SCALE 1/1 WT (lbs)
SIZE C 4012154-997 SHT NO 1

4012154-997

REVISIONS					SIZE C	4012160 – 33	REV
ZONE	SYM	DESCRIPTION	DATE	APPROVAL	CONT ON SHEET	SH NO 1	

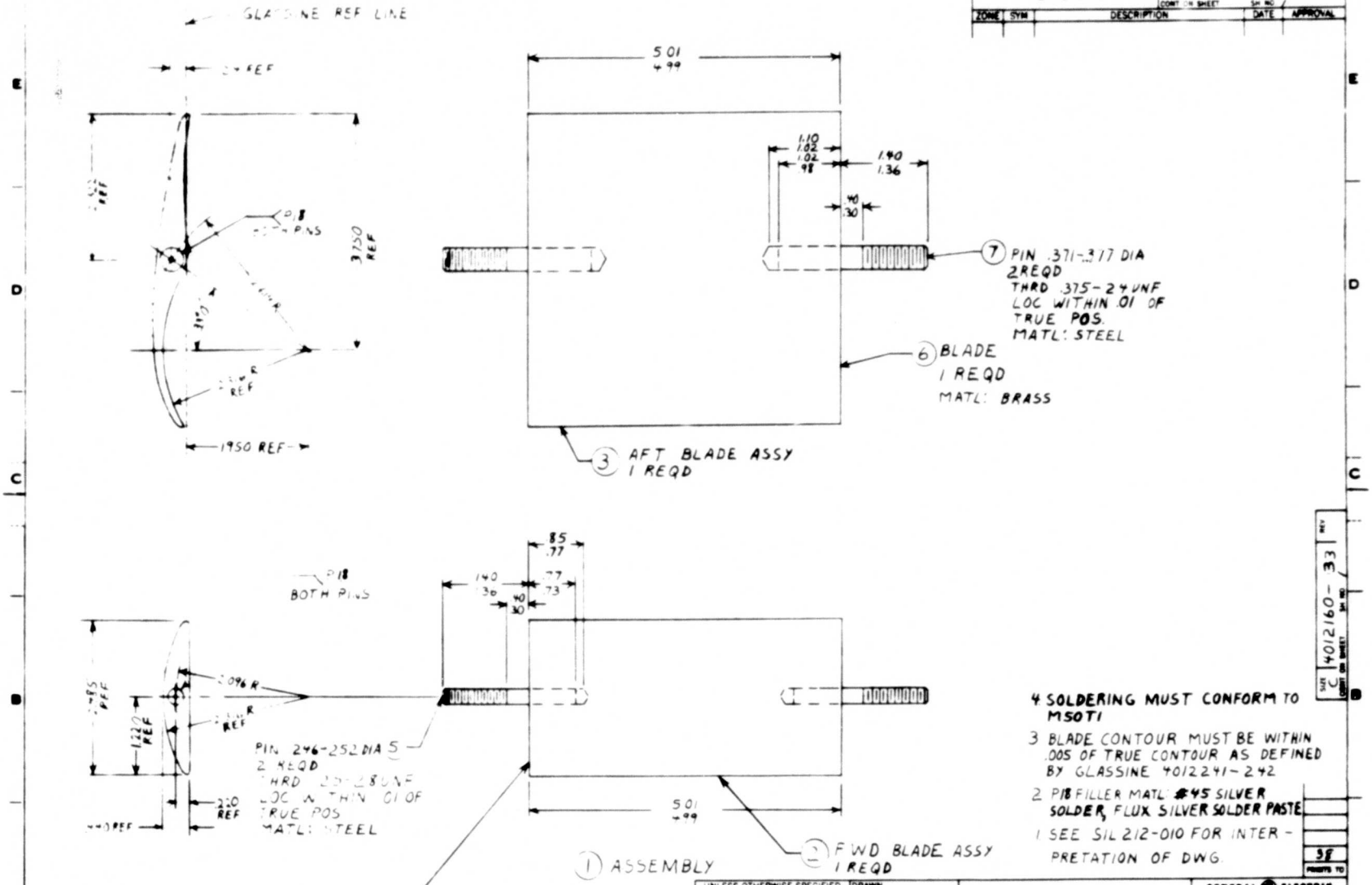

4 SOLDERING MUST CONFORM TO MSOTI

3 BLADE CONTOUR MUST BE WITHIN .005 OF TRUE CONTOUR AS DEFINED BY GLASSINE 4012241-242

2 PIN FILLER MATL: #45 SILVER SOLDER, FLUX SILVER SOLDER PASTE

1 SEE SIL 212-010 FOR INTERPRETATION OF DWG.

SIZE C 4012160-33 REV

SH NO 1 CONT ON SHEET

SH PRINTS TO

UNLESS OTHERWISE SPECIFIED DIMENSIONS ARE IN INCHES TOLERANCES ON FRACTIONS ± DECIMALS ± ANGLES ± ALL SURFACES 63	DRAWN T.P. WOLF	FLAPPED BLADE	GENERAL ELECTRIC AEFT EVENDALE, OHIO LOCATION
MATERIAL	DATE 7-6-63		SIZE C 4012160-33
NEXT ASSY	APPD		CONT ON SHEET SH NO 1
USED ON	ISSUED		
	ENGR		
	MFG		
	MATL	SCALE 1/1	WT

GENERAL ELECTRIC A-4012160-93

REV NO

CONT ON SHEET SH NO

TITLE
ALTERNATE MANUFACTURE FOR LEADING & TRAILING EDGES
FIRST MADE FOR TANDEM CASCADE

CONT IN SHEET SH NO

REVISIONS

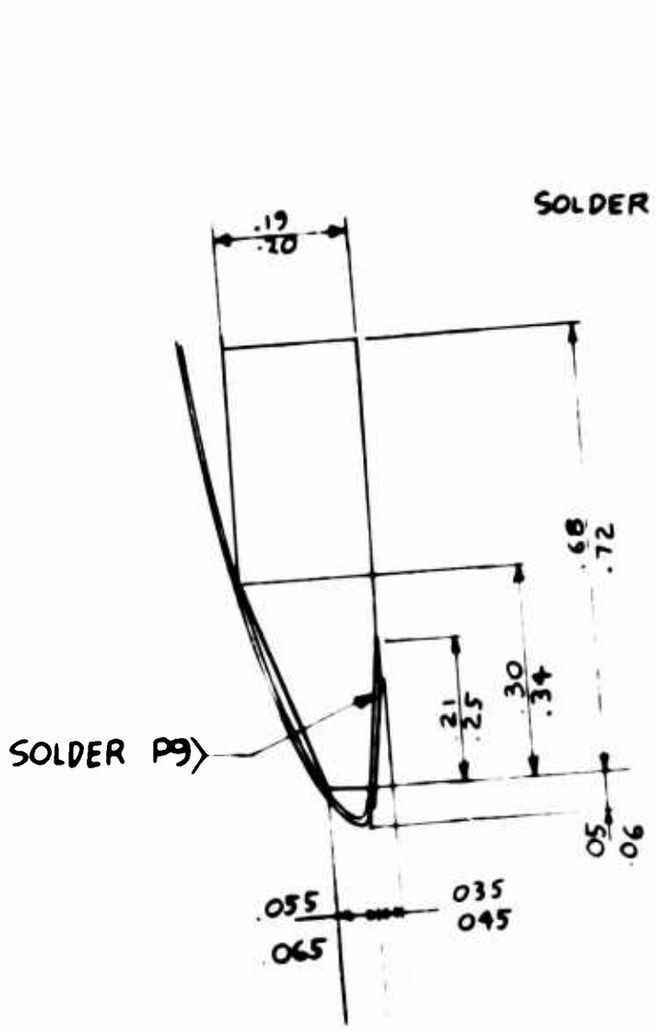

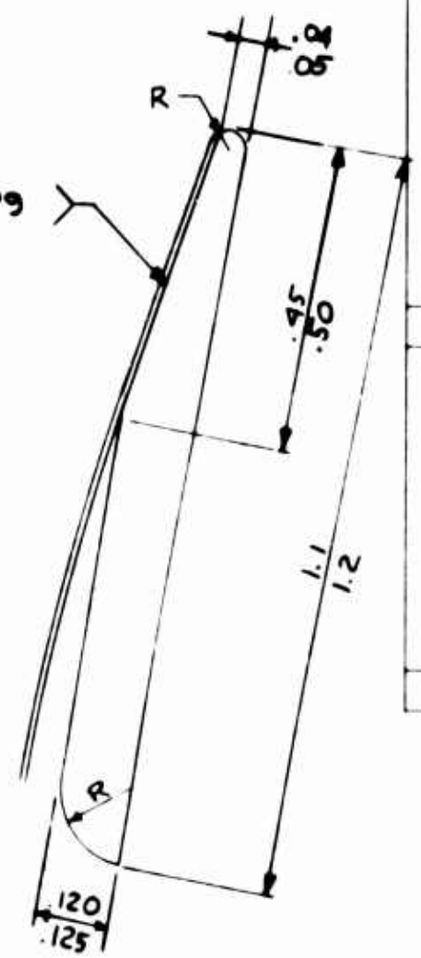

© LEADING EDGE

Ⓓ TRAILING EDGE

IF THIS METHOD OF MANUFACTURE IS USED ALL NOTES & VIEWS ON SHEET 1 STILL APPLY.

38

PRINTS

ISSUED NOV. 9 1966

APPROVALS

AETD

EVENDALE, OHIO

A-4012160-93

SH NO

PP-603-WA (9-61)
PRINTED IN U.S.A.

GENERAL ELECTRIC

A4012160-97

A-4012160-97

TITLE HOLDER - FLEXIBLE BLADE

FIRST MADE FOR TANDEM CASCADE

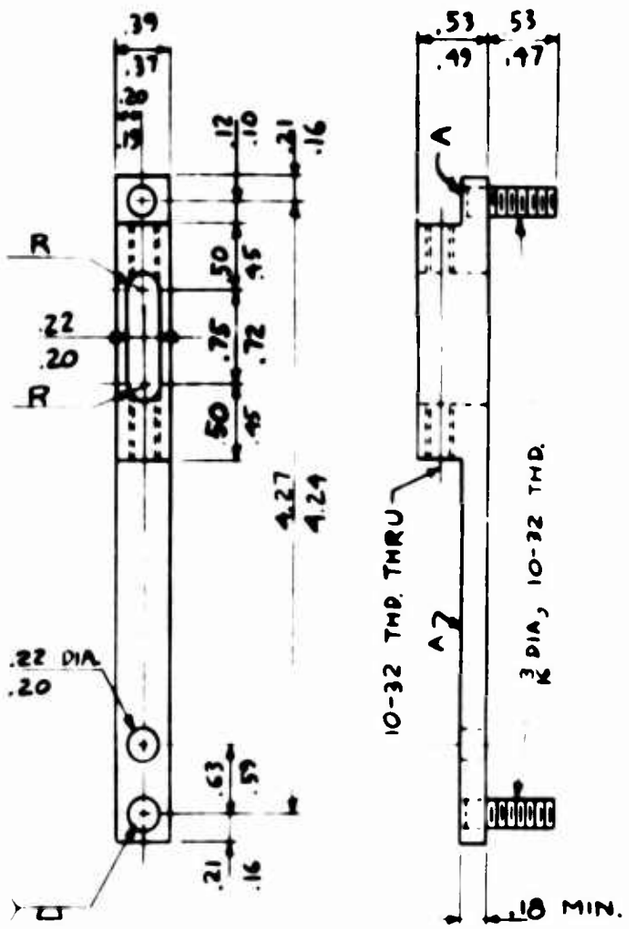

REVISIONS

5. WELDING PER GE M50T1
4. PAINT WITH ONE COAT MACHINERY GRAY PAINT EXCEPT THREADS.
3. SEE SIL 212-000 FOR DWG. INTERPRETATION
2. ALL MATERIAL MILD STEEL
1. SAW MAY BE USED TO GET SURFACE A

24
38
PRINTS TO

DRAWN J.S. Hollenbeck MAR 13, 1969	APPROVALS M.T. Bozzuto	A&TP EVENDALE, OHIO	DIV OR DEPT	A 4012160-97
ENGR H.L. Hoyt MAR 29 1969	M.C. Yuill		LOCATION	CONT ON SHEET SH NO

FP-000-WA (9-61)
PRINTED IN U.S.A.

APPENDIX V

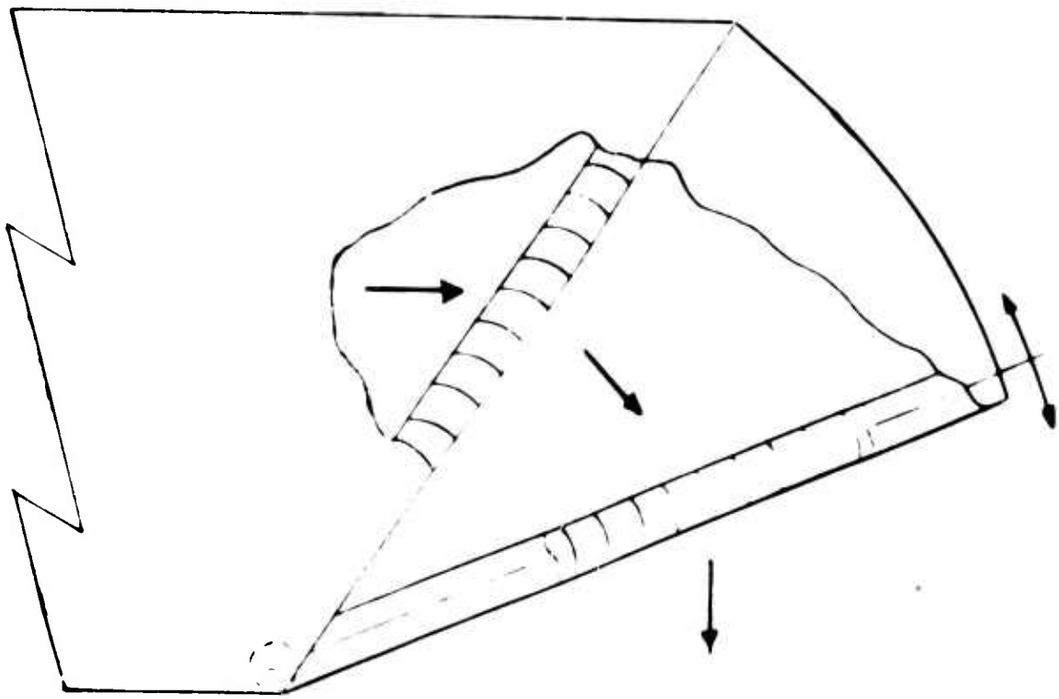

Figure 1. Tandem Cascade.

Figure 2. View of Test Section in the Transonic Cascade Tunnel.

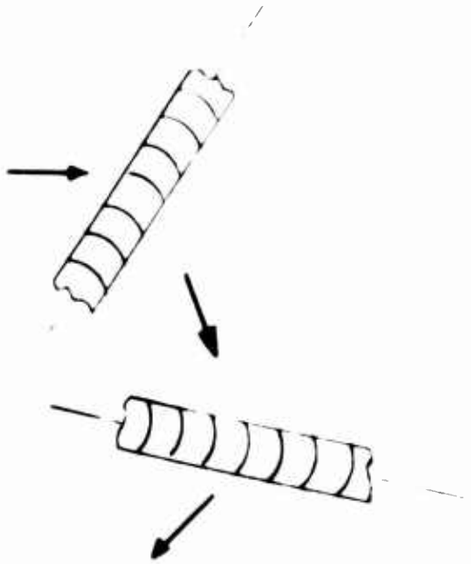

Figure 3. Reverse Thrust Mode.

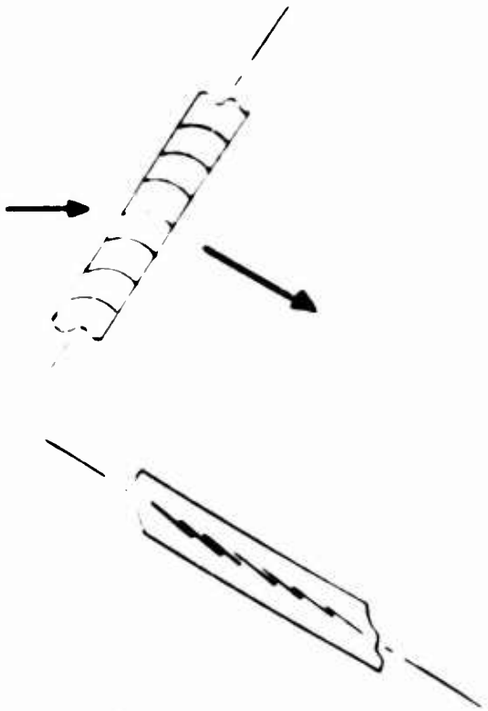

Figure 4. Short Take-Off and Landing (STOL) Mode.

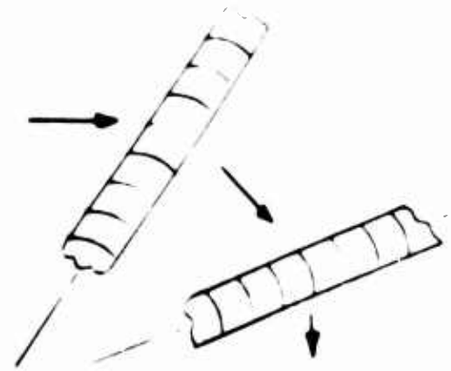

Figure 5. Vertical Take-Off and Landing (VTOL) Mode.

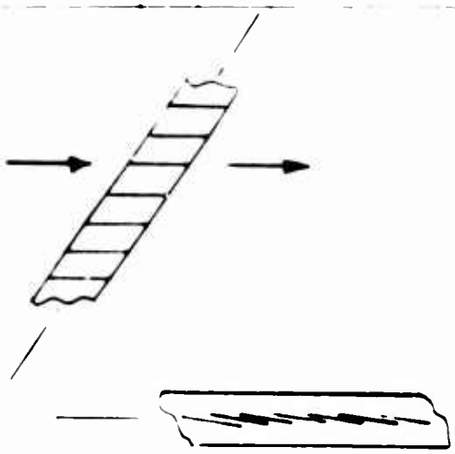

Figure 6. Cruise Mode

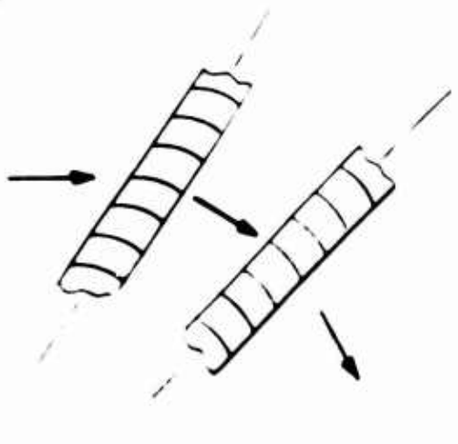

Figure 7. Intermediate Positions.

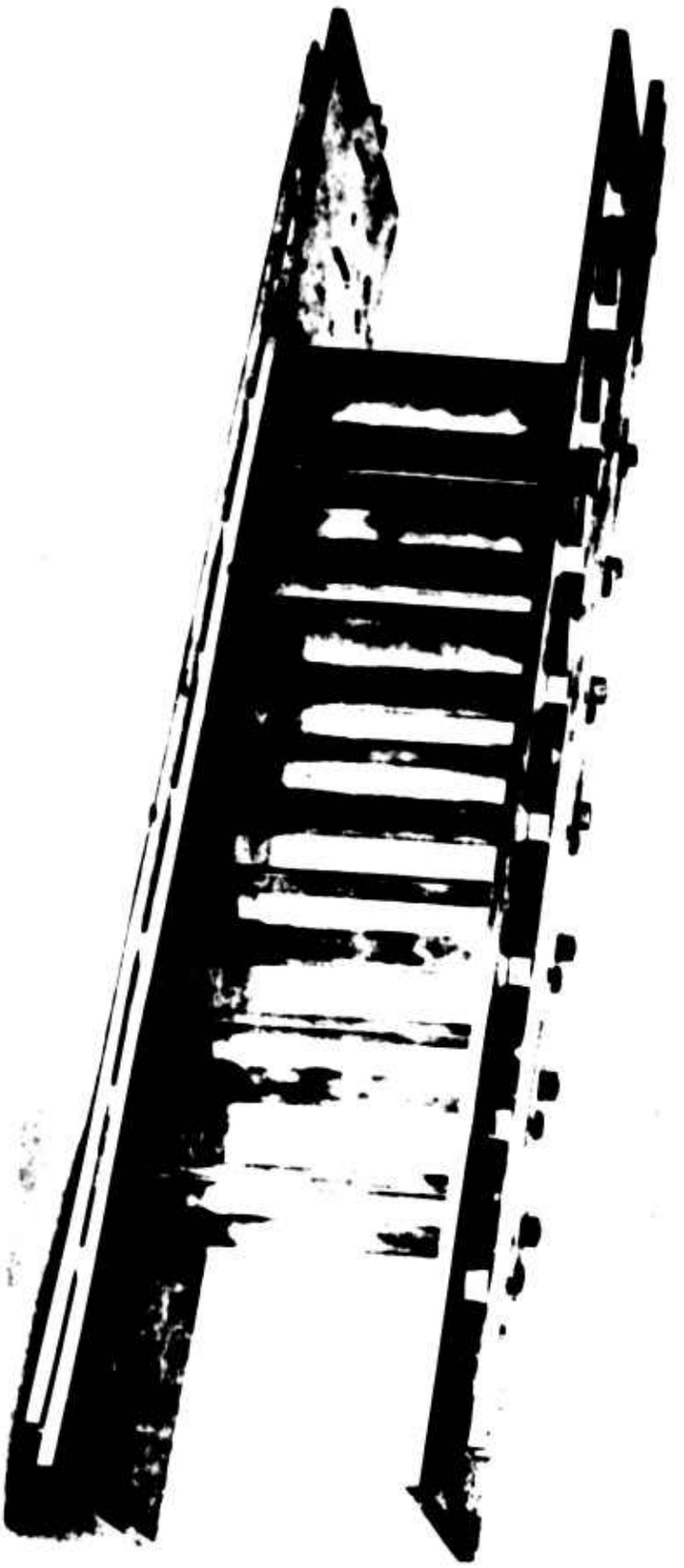

Figure 8. Flapped-Blade Cascade

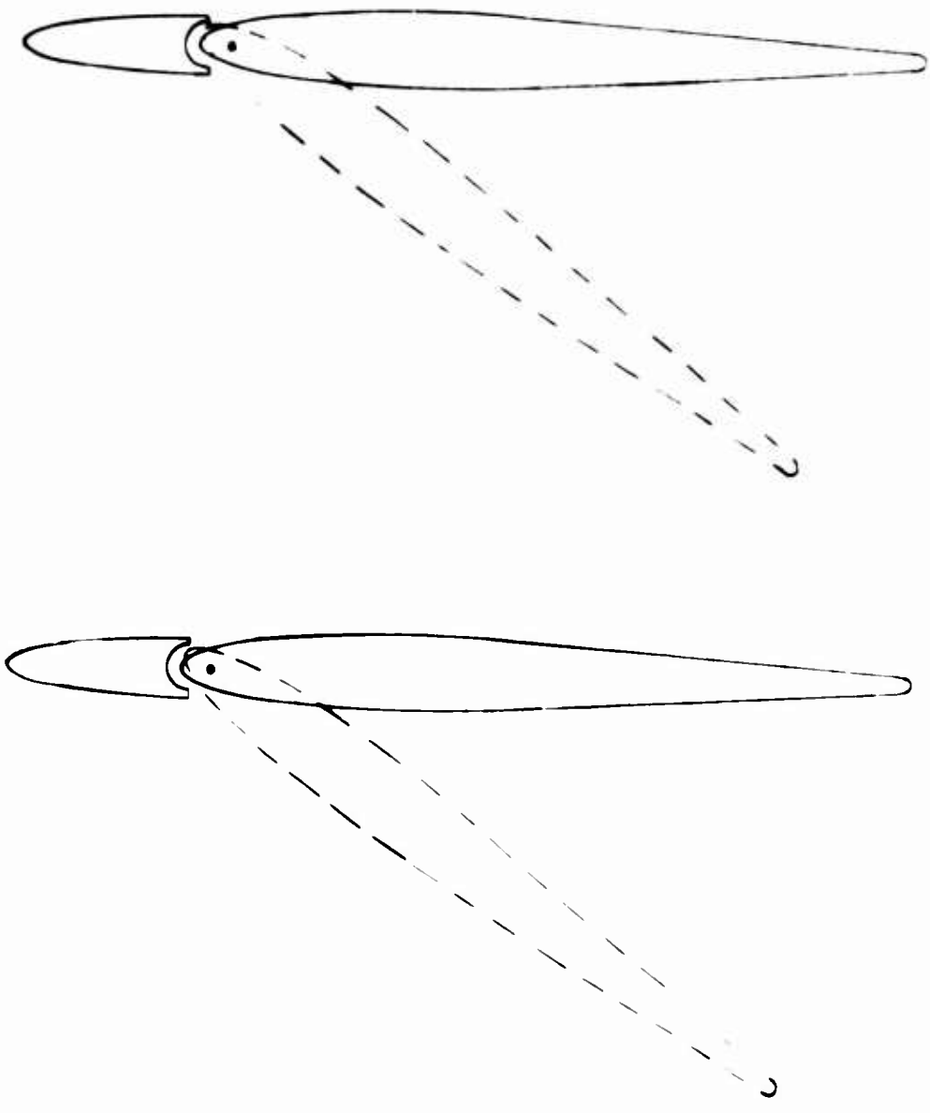

Figure 9a. Articulated Inlet Guide Vanes.

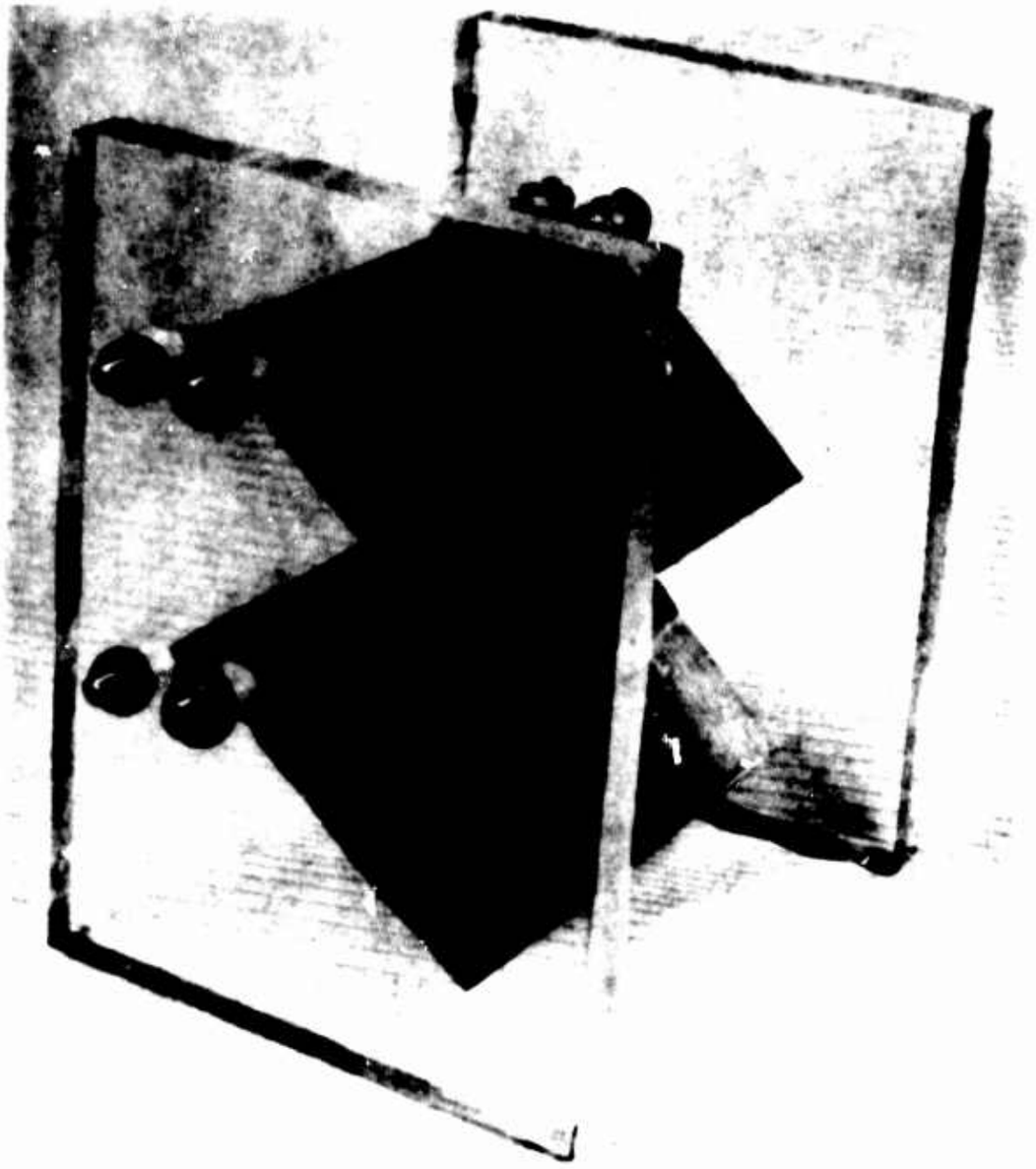

Figure 9b. Articulated Inlet Guide Vanes

Figure 10. Silicon Rubber Variable Camber Blades (Convex Side)

Figure 11a. Honeycomb Variable Camber Blades (Convex Side).

Figure 11b Honeycomb Variable Camber Blades (Concave Side).

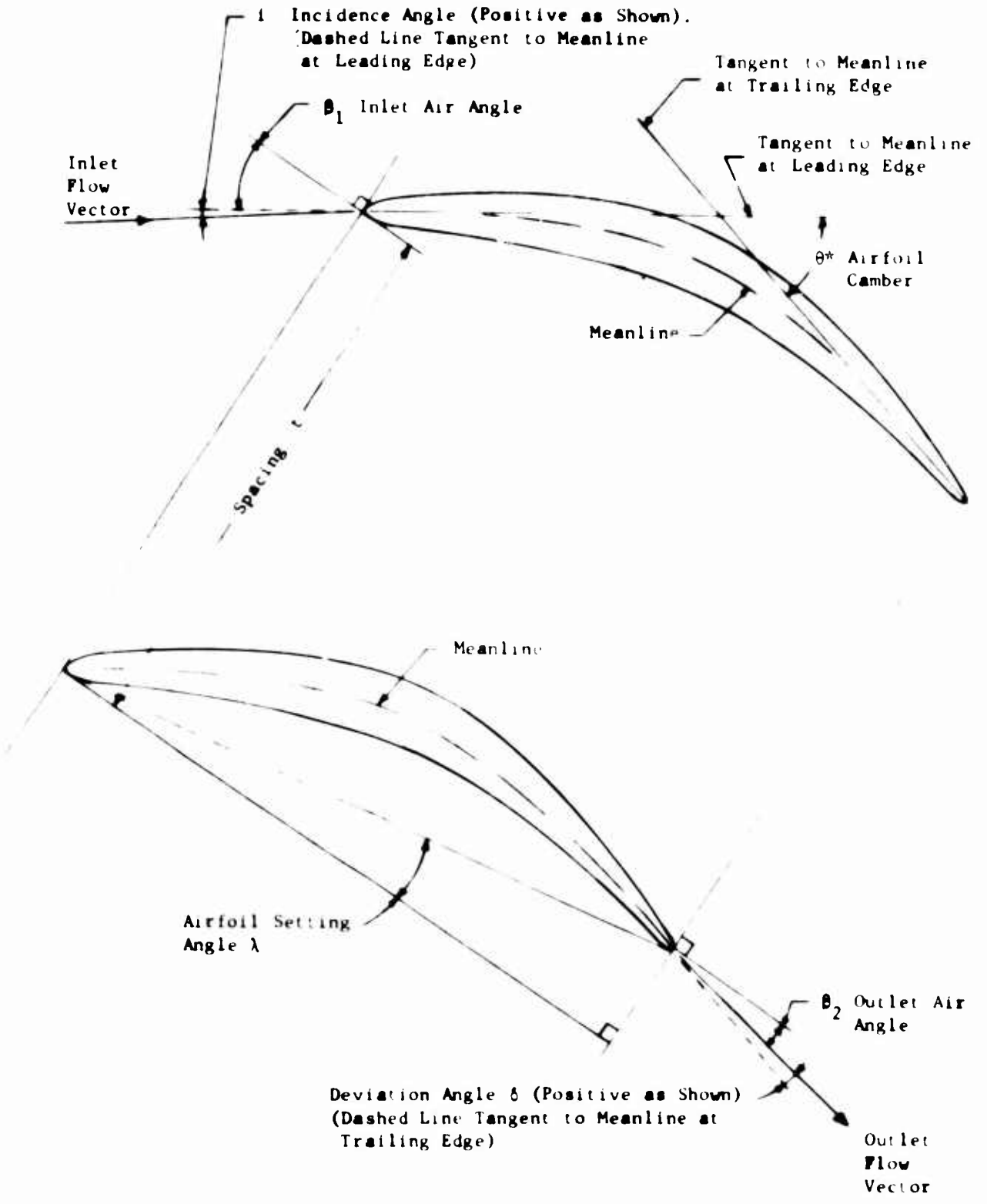

Figure 12. Cascade Geometry Nomenclature.

Figure 15. Articulated-Blade Cascade - High Camber

Figure 16. Flapped Blade.

Figure 18b. Flexible-Blade Cascade - Low Camber.

Figure 18c. Flexible-Blade Cascade - High Camber.

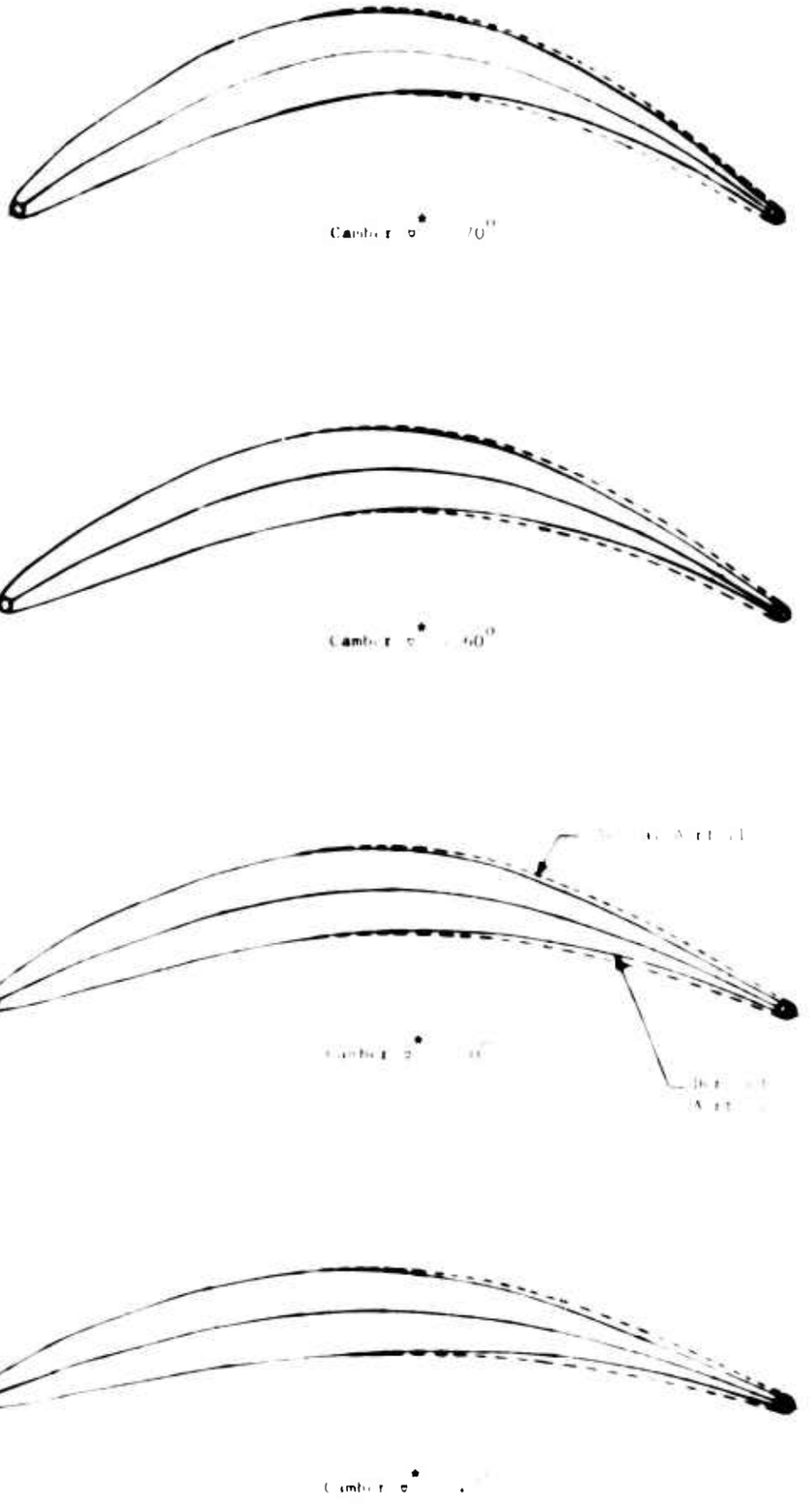

Figure 18d. Flexible Blades - Four amber Settings.

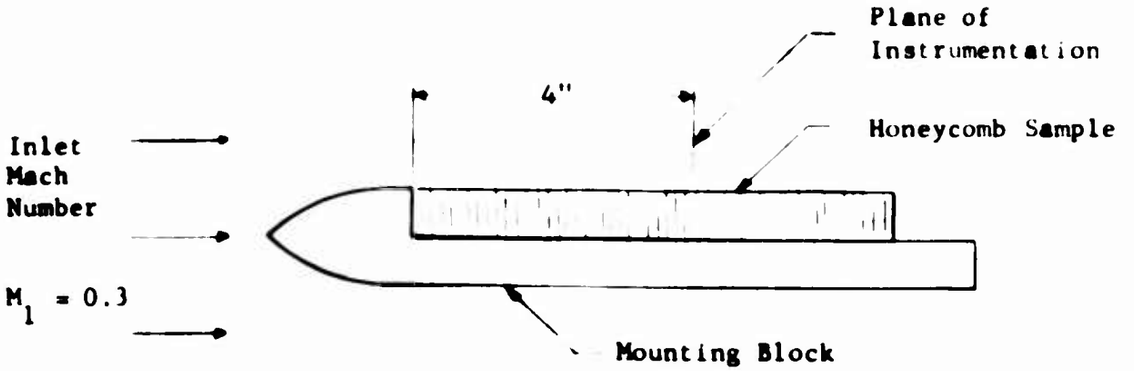

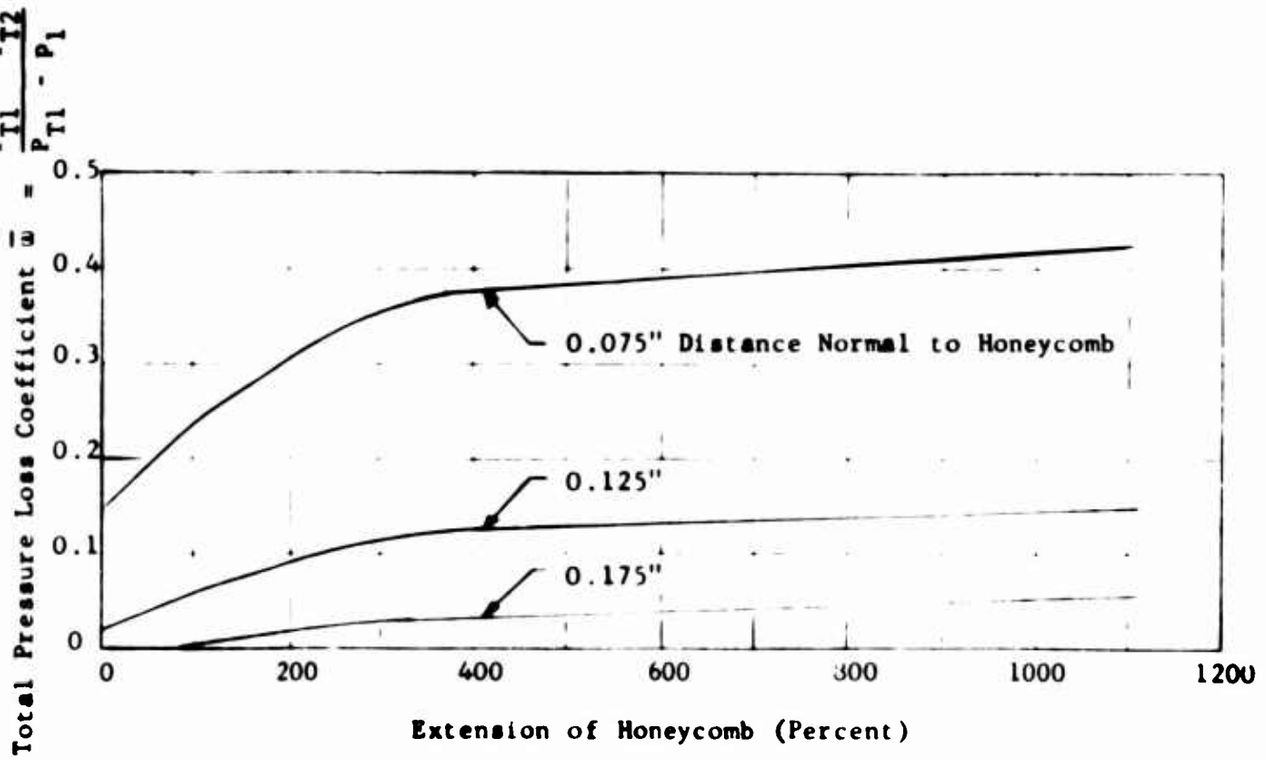

Figure 19. Experimental Evaluation of Expanded Honeycomb as an Aerodynamic Surface.

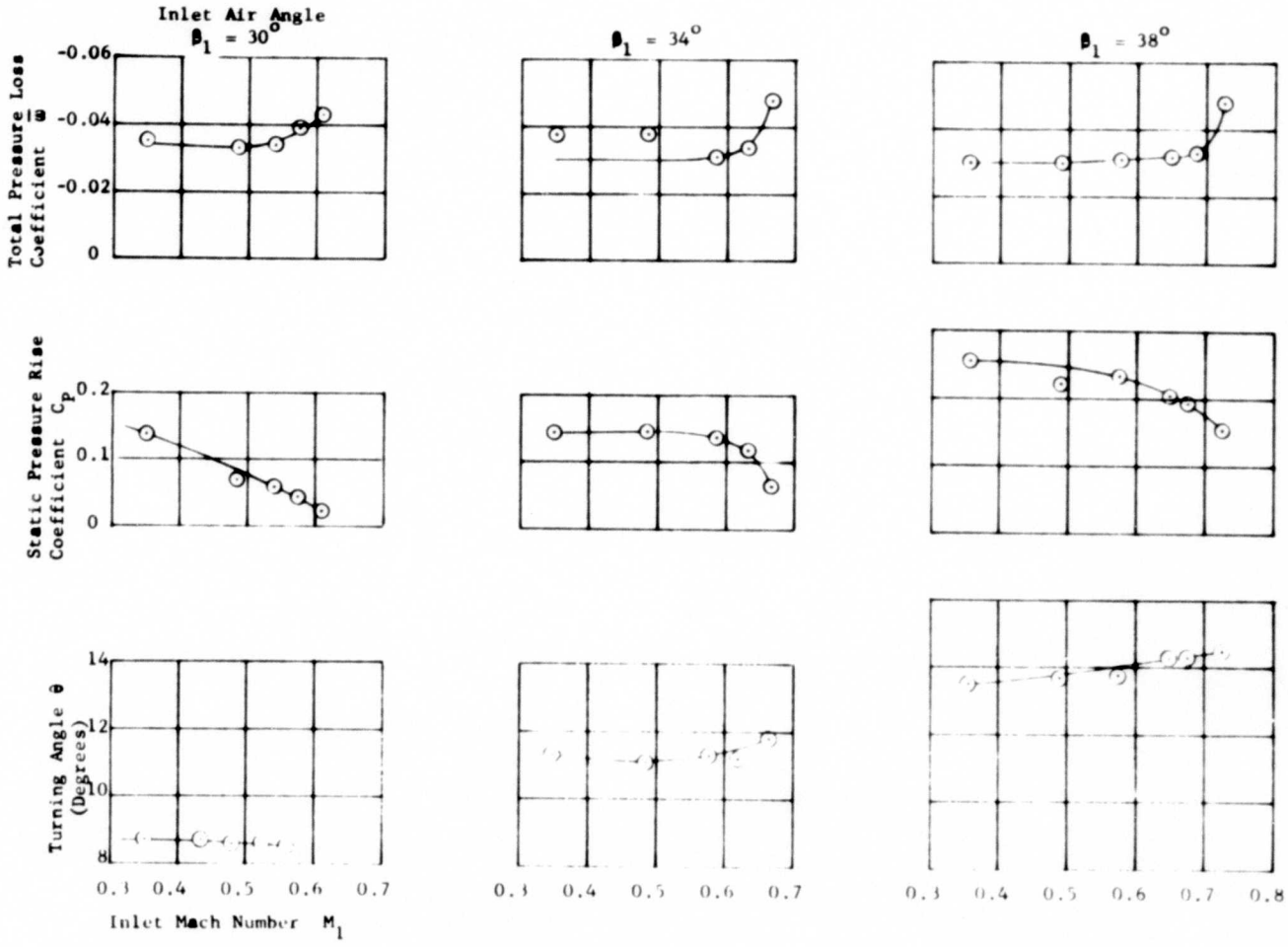

Figure 20. Articulated Airfoil. Airfoil Setting Angle $\lambda = 29^\circ$.

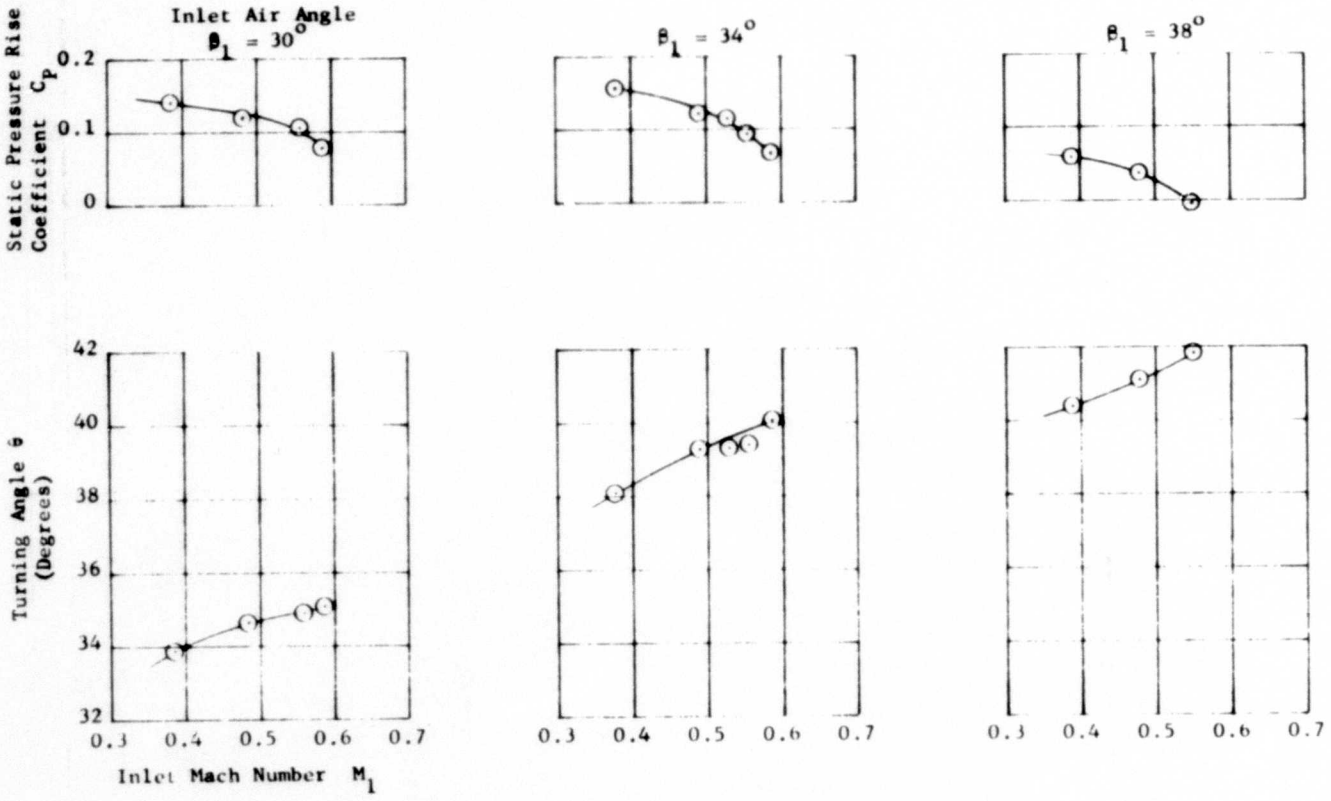

Figure 21a. **Articulated Airfoil. Airfoil Setting Angle $\lambda = 0^\circ$.**

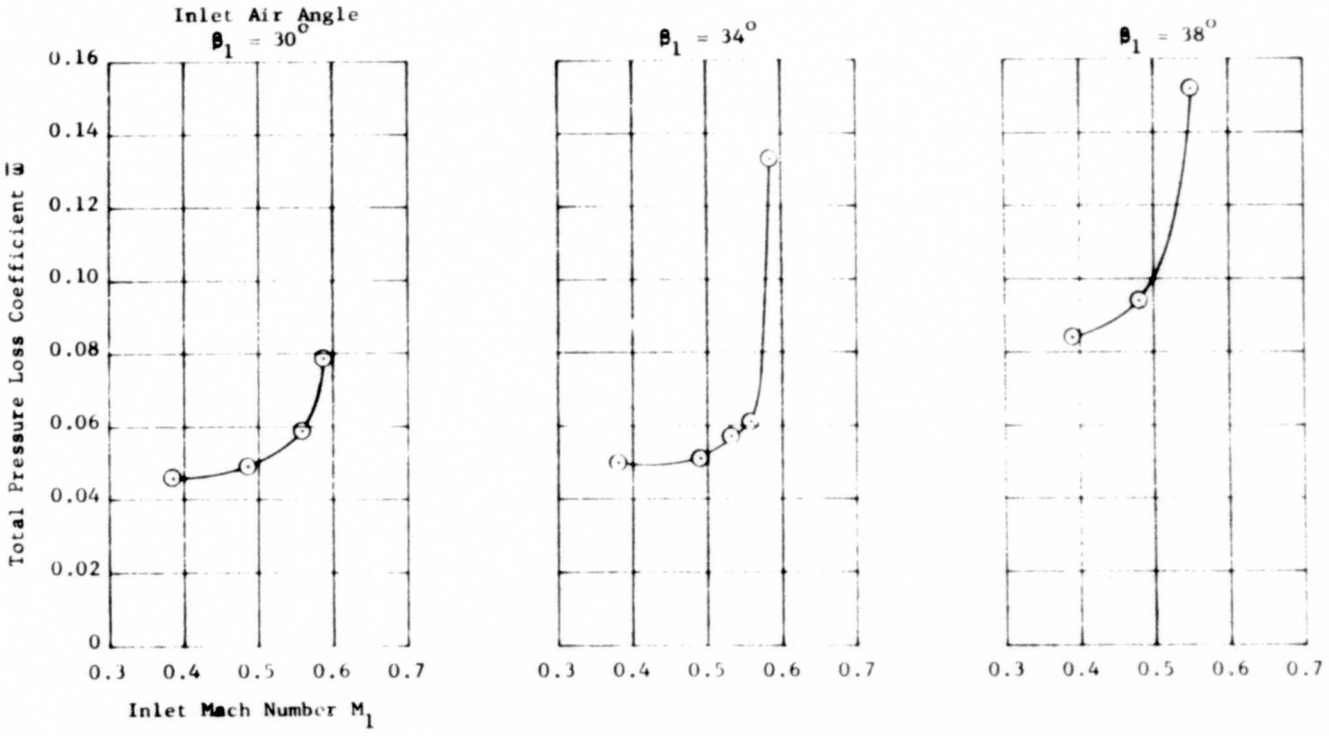

Figure 21b. Articulated Airfoil. Airfoil Setting Angle $\lambda = 0^\circ$.

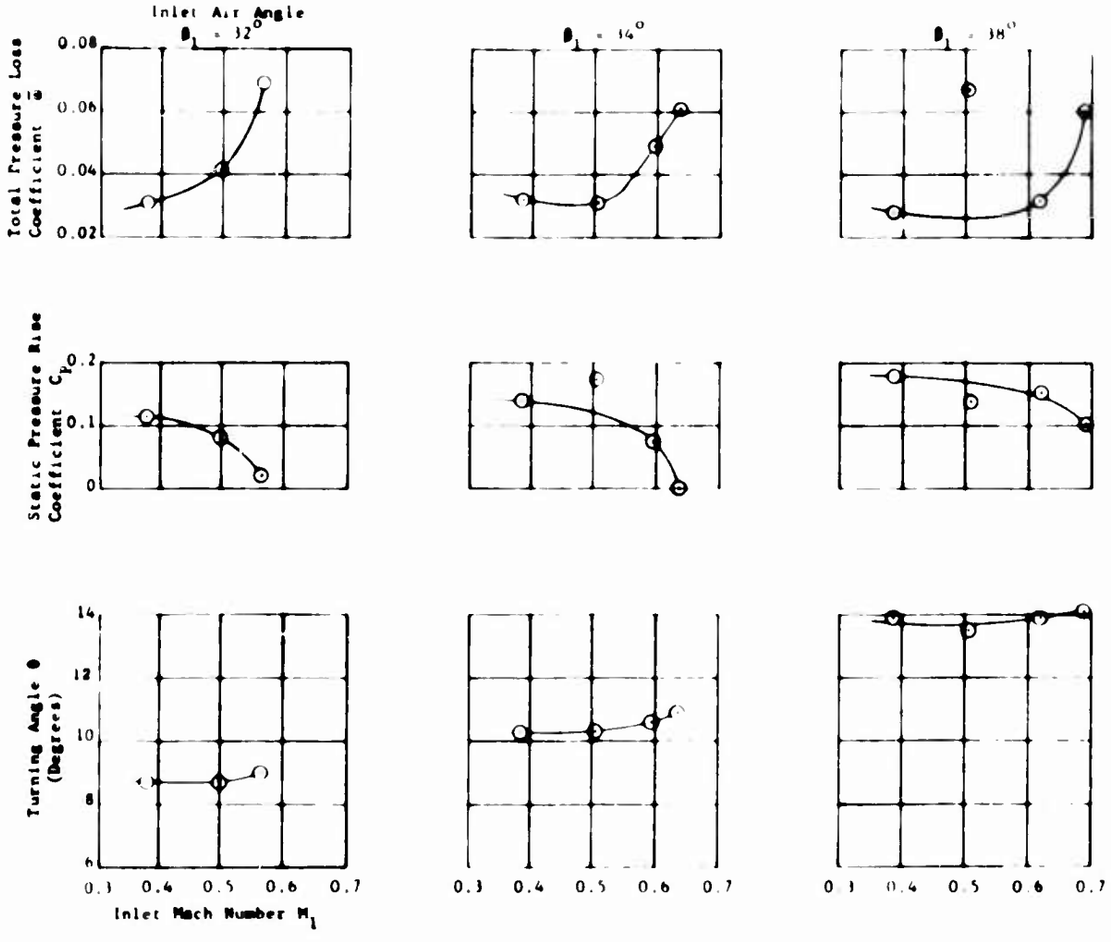

Figure 22. Flapped Airfoil. Airfoil Setting Angle $\lambda = 29^\circ$.

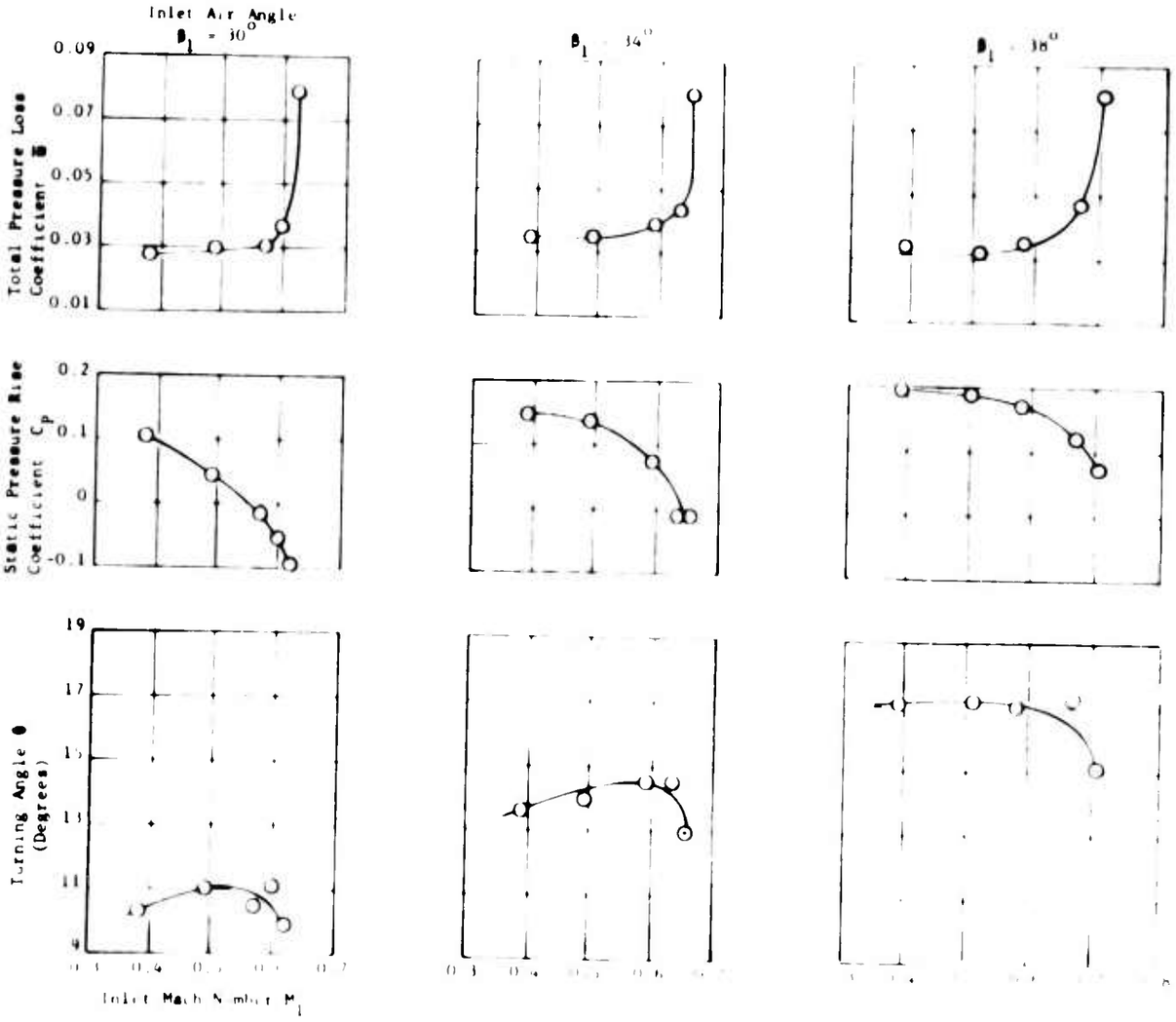

Figure 23. **Flexible Airfoil.** Camber, $\theta^* = 17^\circ$. Airfoil Setting Angle $\lambda = 29^\circ$.

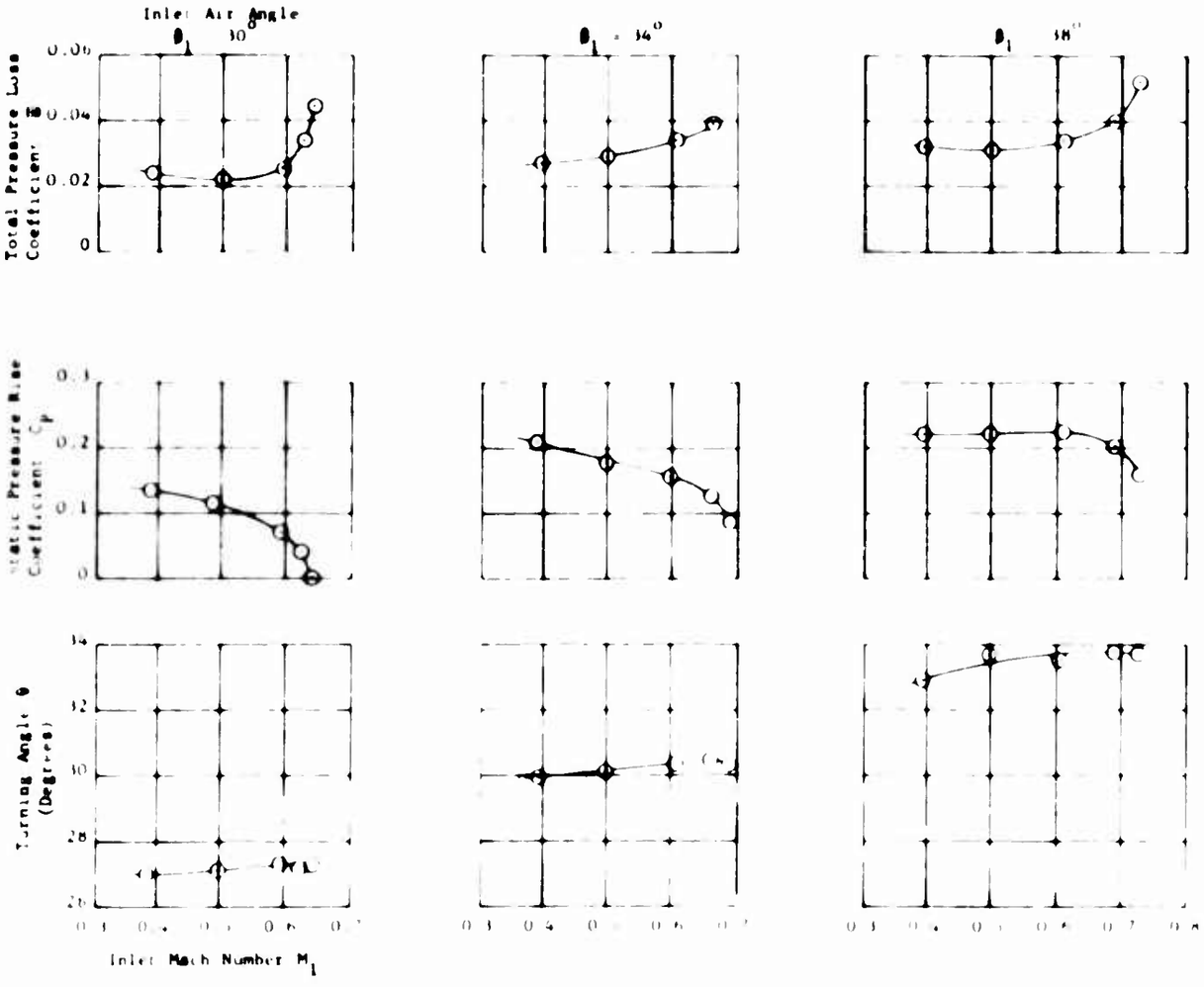

Figure 24. Flexible Airfoil. Camber, $\theta^* = 36^\circ$. Airfoil Setting Angle $\lambda = 17.25^\circ$.

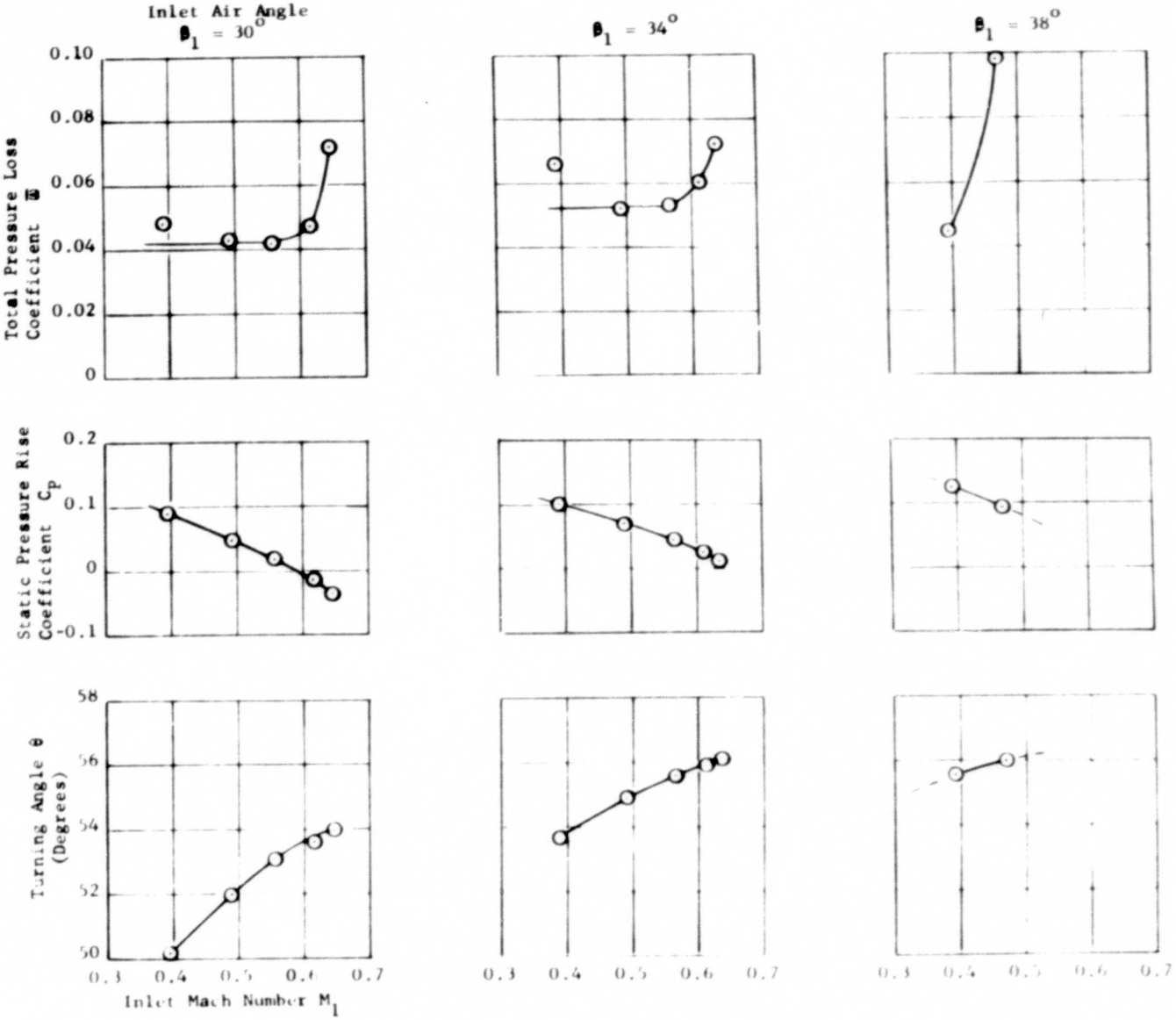

Figure 25. Flexible Airfoil. Camber, $\theta^* = 66^\circ$. Airfoil Setting Angle $\lambda = 0^\circ$.

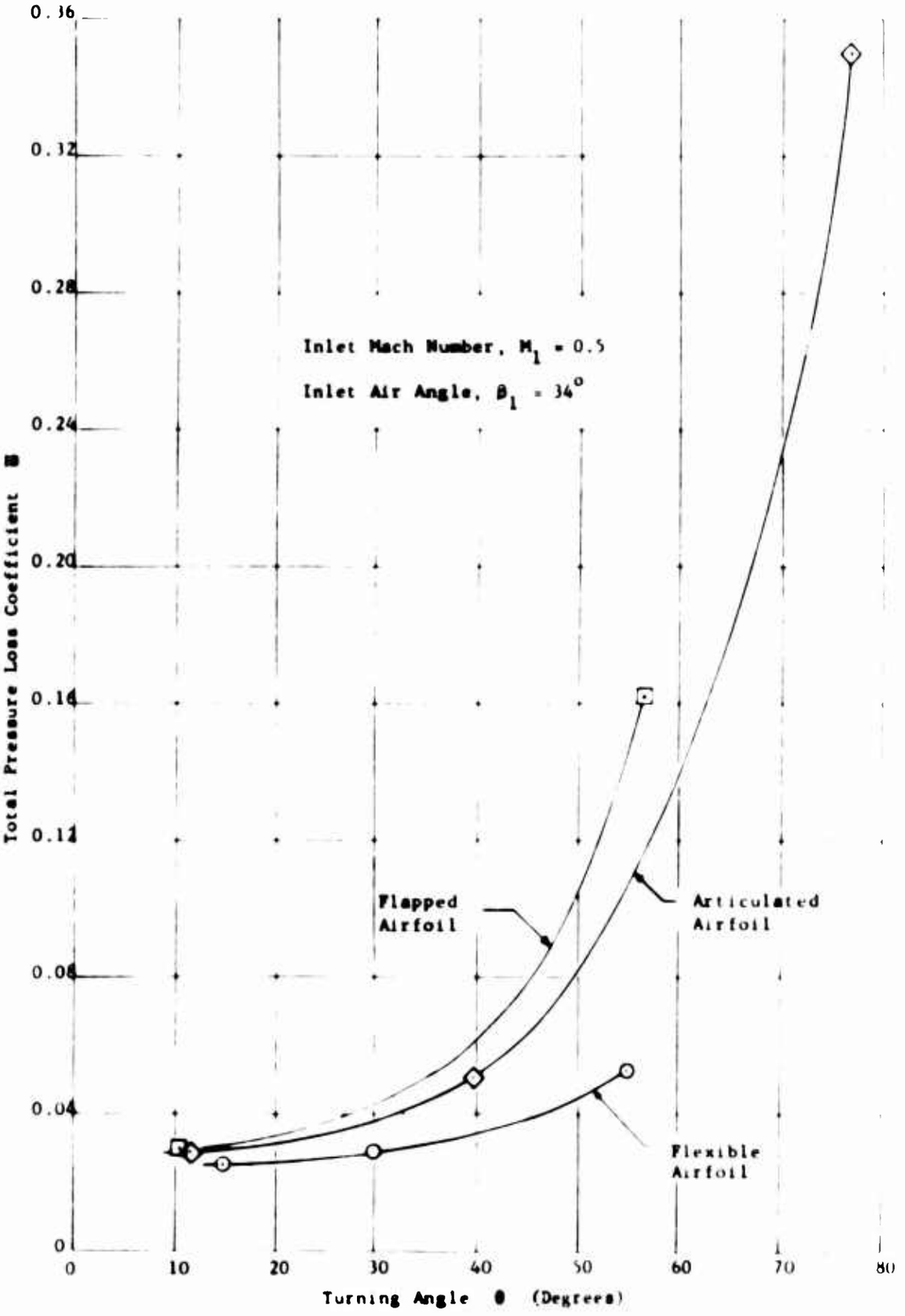

Figure 26. Total Pressure Loss Coefficient Comparison Between Airfoils.

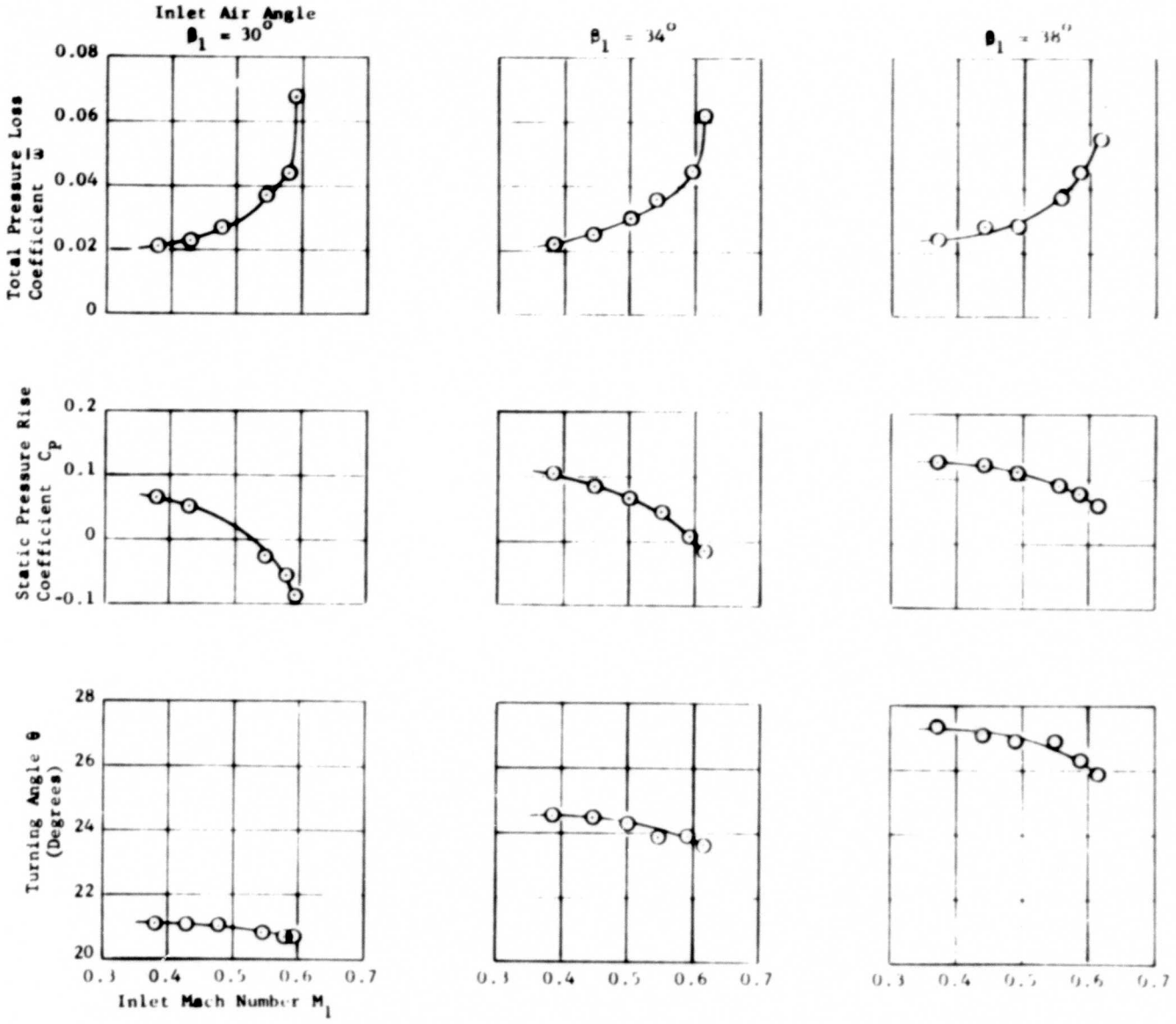

Figure 27. Tandem (Forward) Cascade. Camber, $\theta^* = 30^\circ$. Airfoil Setting Angle $\lambda = 22^\circ$.

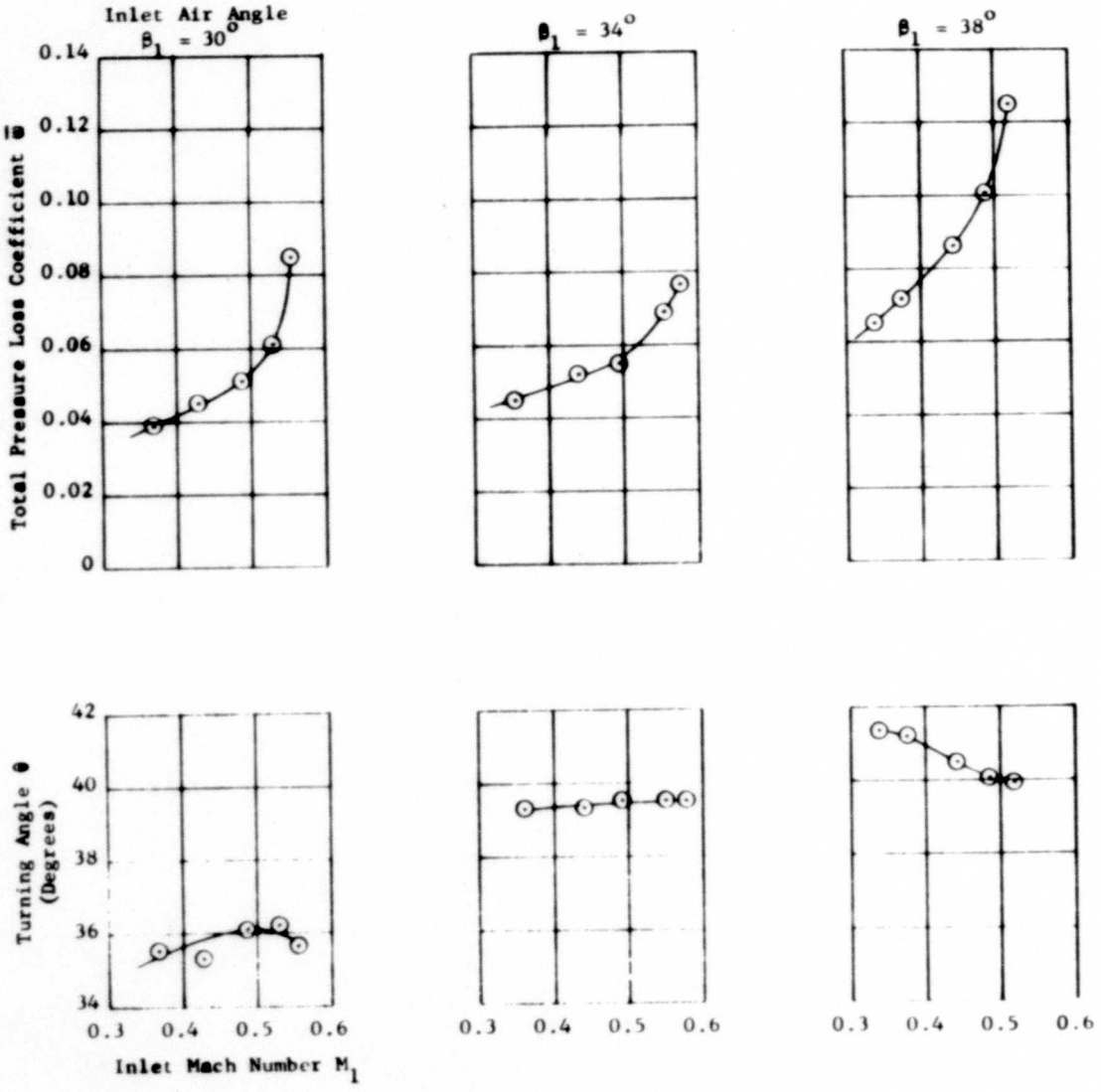

Figure 28a. Tandem (Forward) Cascade. Camber, $\theta^* = 45^\circ$. Airfoil Setting Angle $\lambda = 14.5^\circ$.

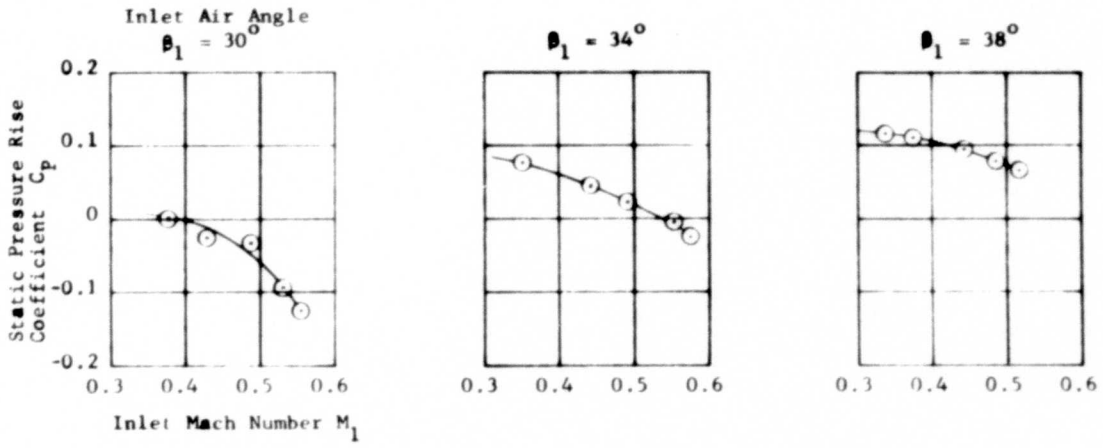

Figure 28b. Tandem (Forward) Cascade. Camber, $\theta^* = 45^\circ$. Airfoil Setting Angle $\lambda = 14.5^\circ$.

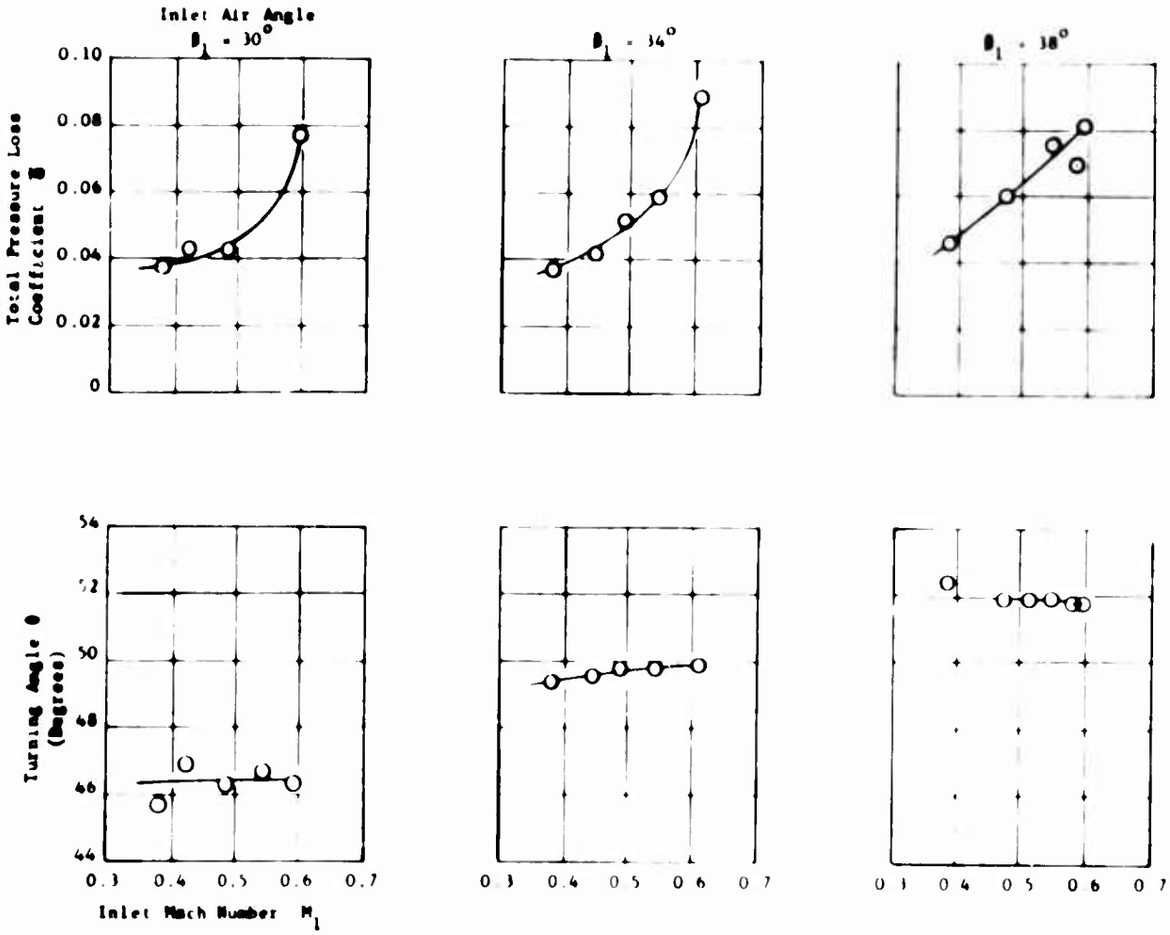

Figure 29a. Tandem (Forward) Cascade. Camber, $\theta^* = 60^\circ$. Airfoil Setting Angle $\lambda = 7^\circ$.

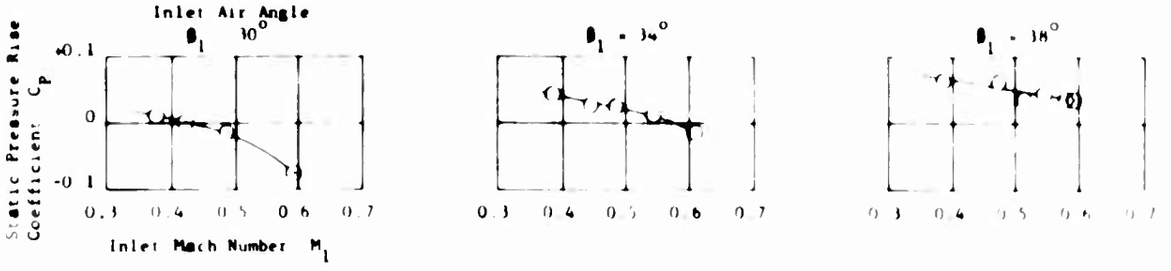

Figure 29b. Tandem (Forward) Cascade. Camber, $\theta^* = 60^\circ$. Airfoil Setting Angle $\lambda = 7^\circ$.

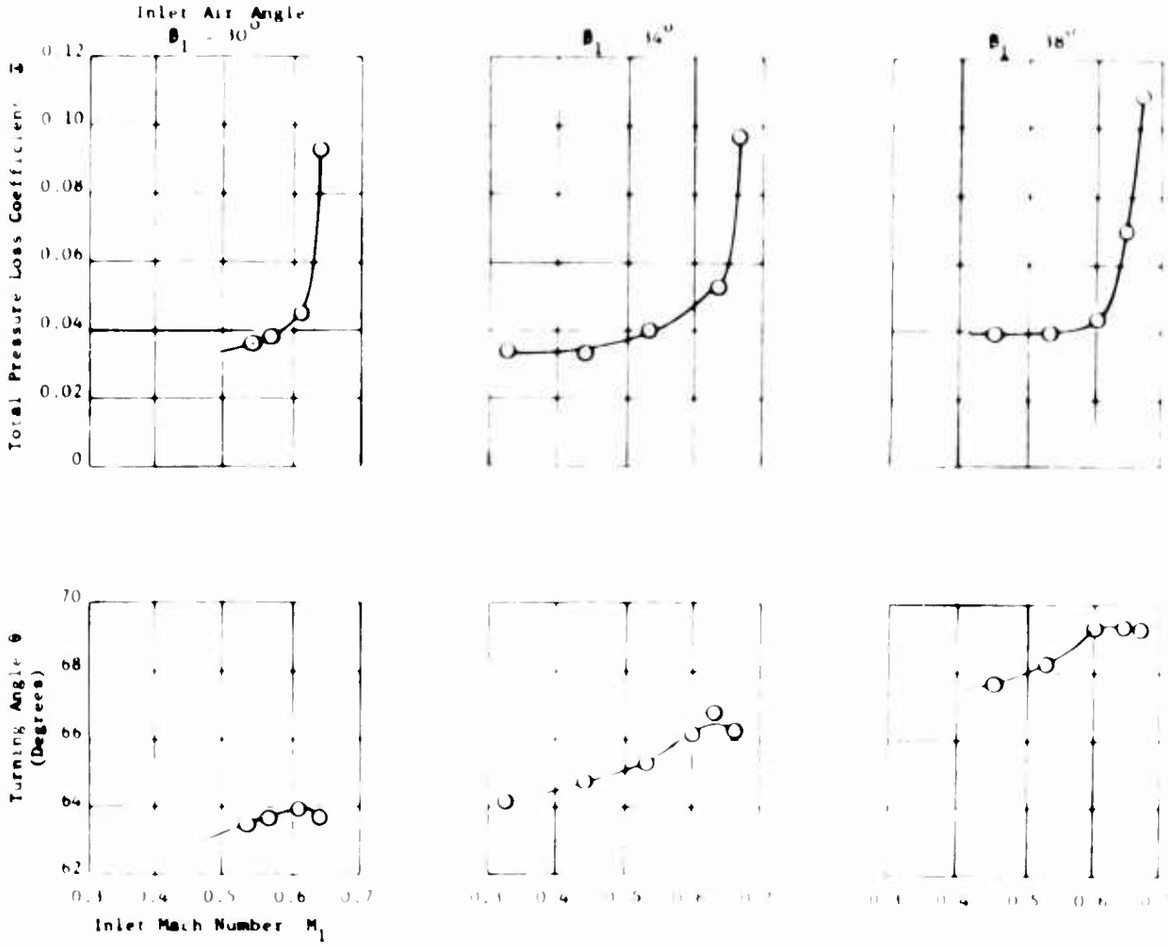

Figure 30a. Tandem (Forward) Cascade. Camber, $\theta^* = 73^\circ$. Airfoil Setting Angle $\lambda = -2^\circ$.

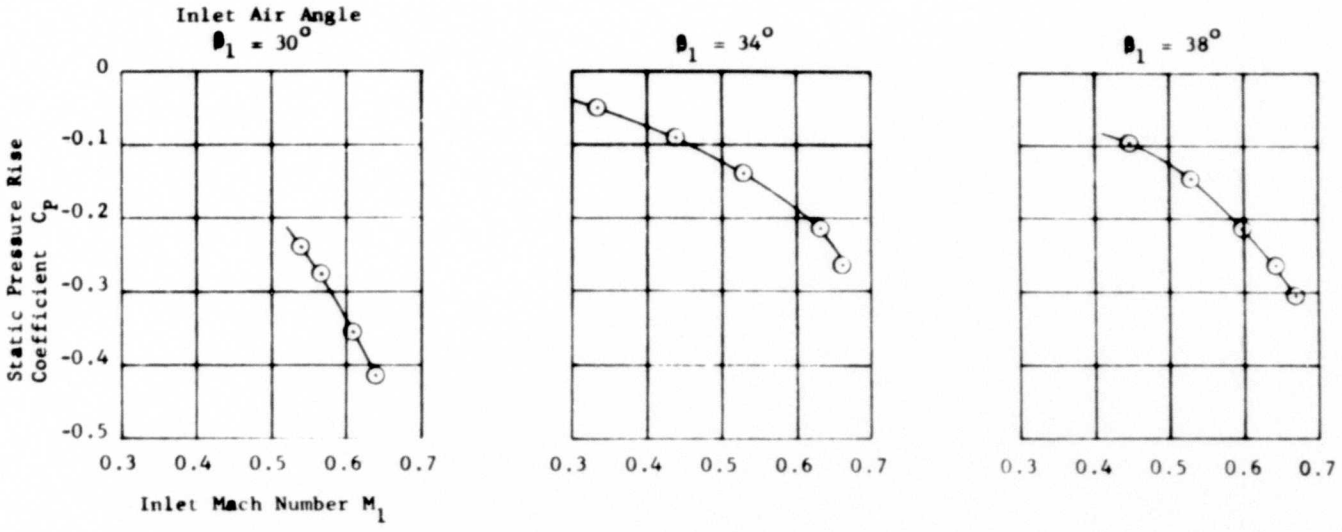

Figure 30b. Tandem (Forward) Cascade. Camber, $\theta^* = 78^\circ$. Airfoil Setting Angle $\lambda = -2^\circ$.

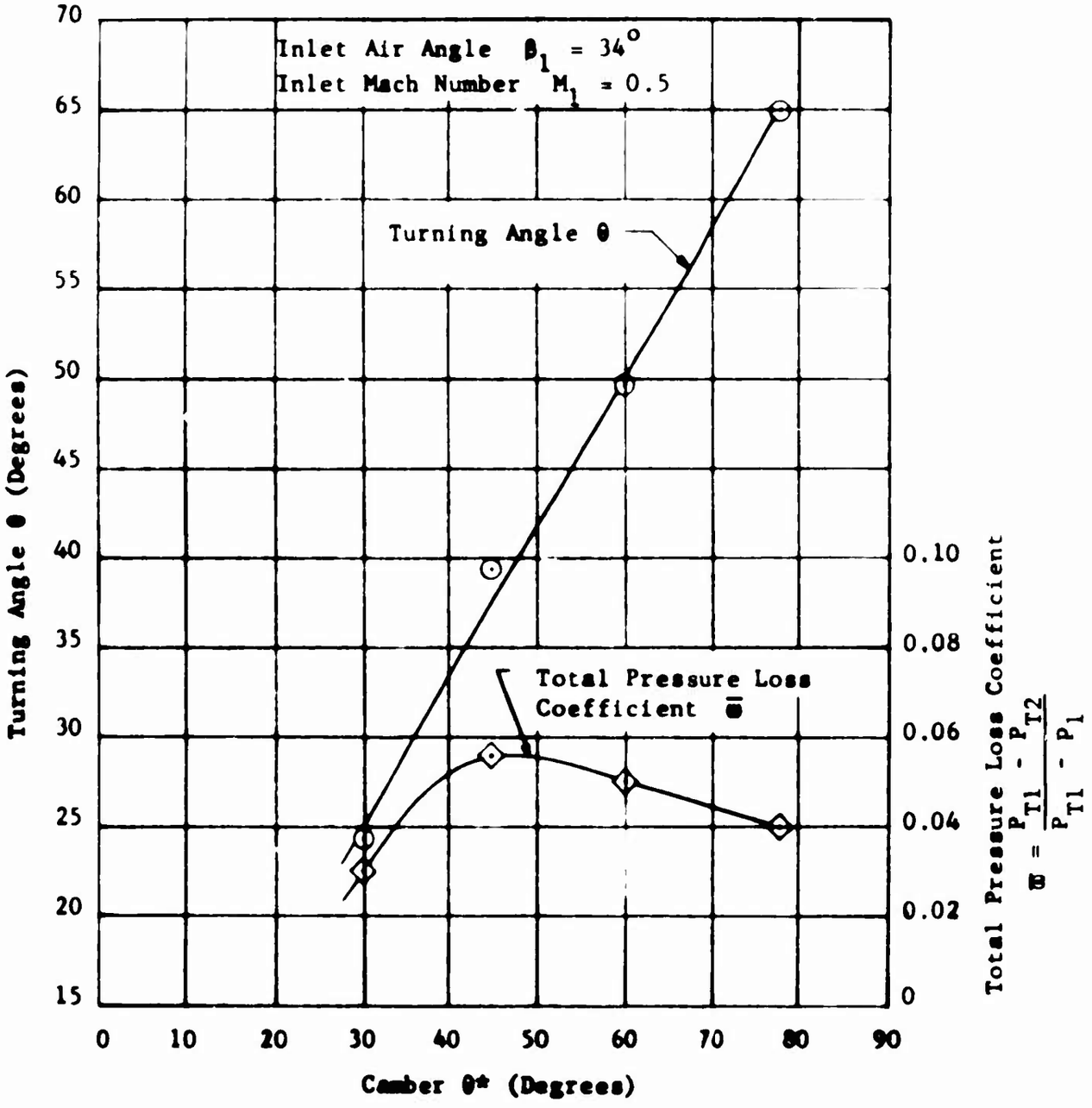

Figure 31. Flexible Airfoil. Single Cascade.

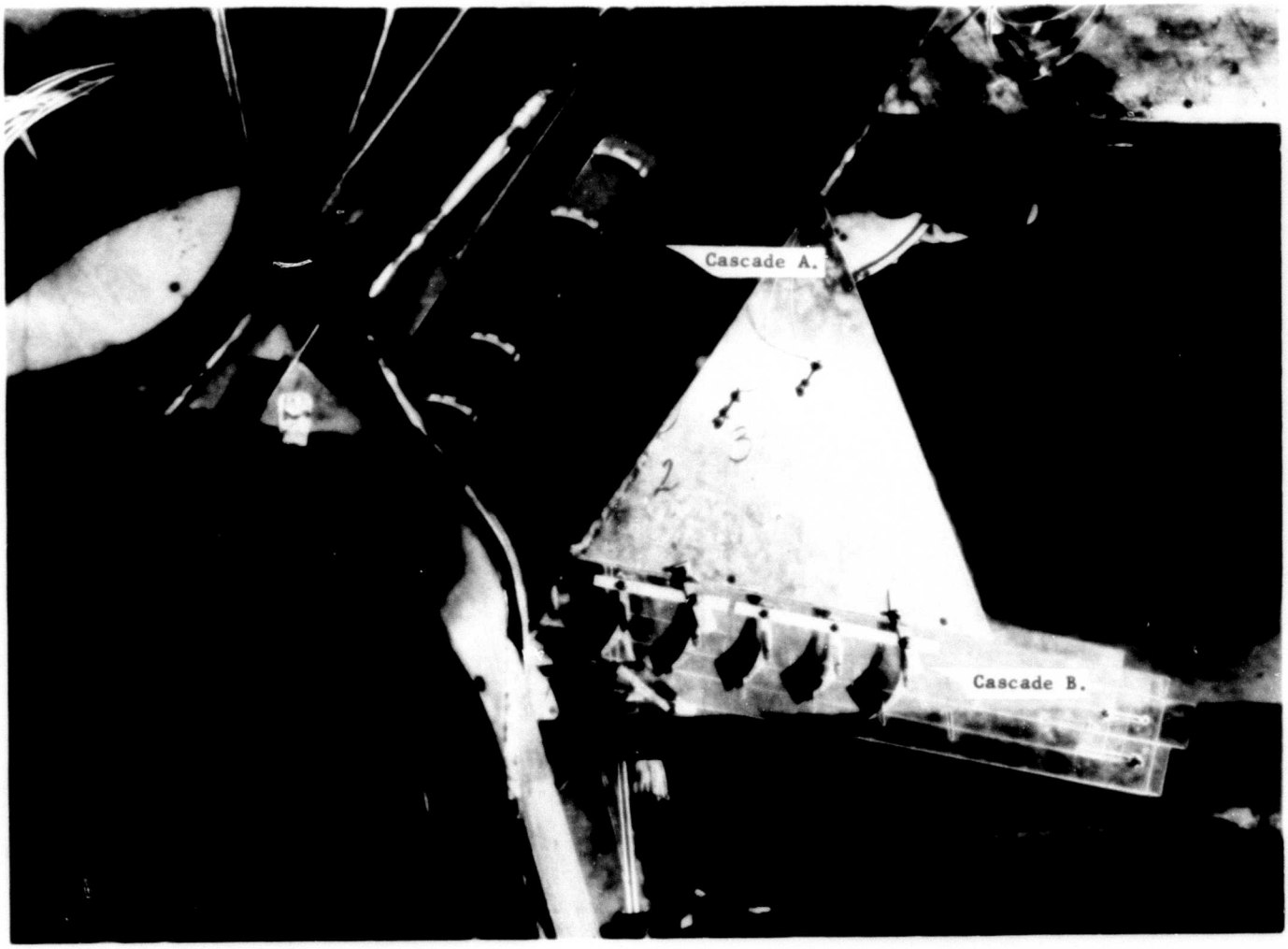

Figure 32. Tandem Cascade of Flexible Blades Installed in Transonic Cascade Tunnel.

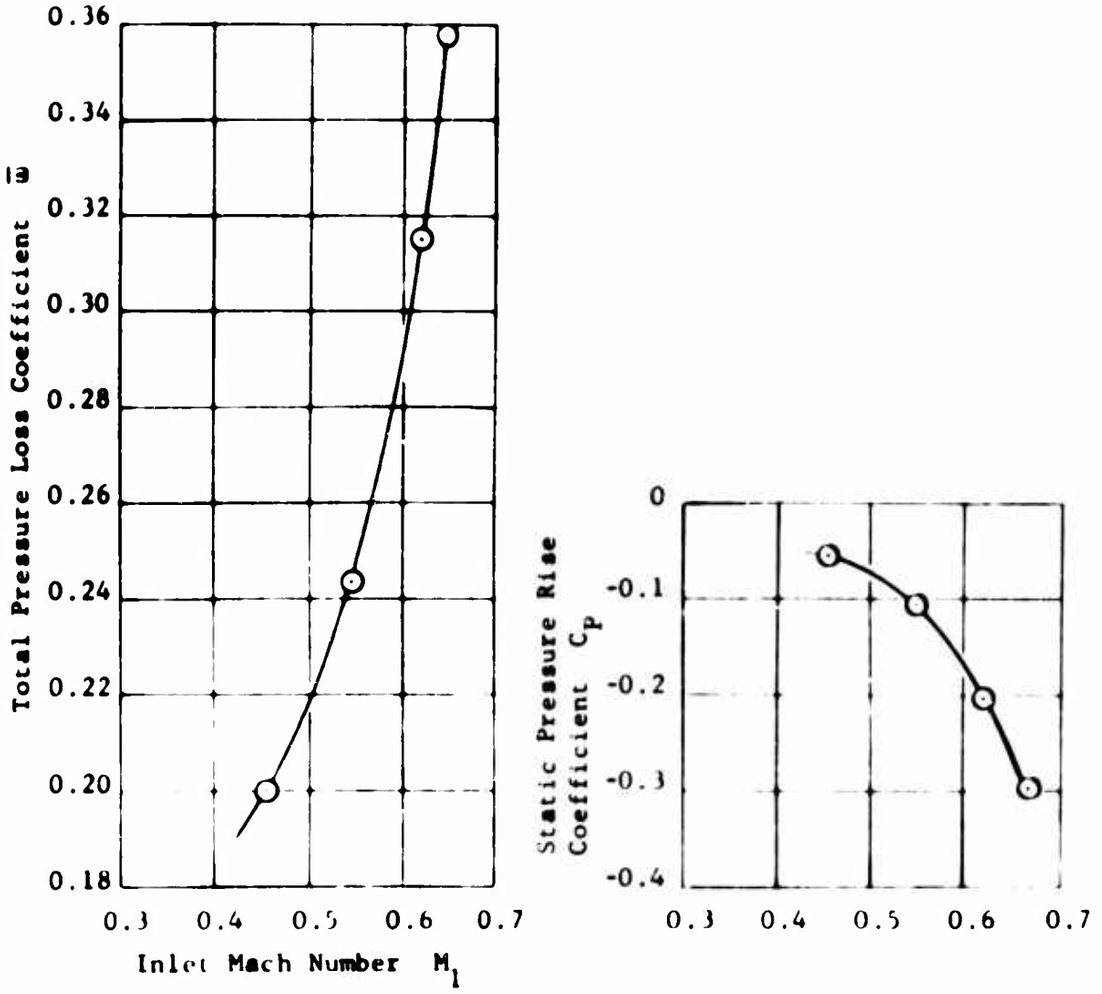

Figure 33. Tandem Cascade. Forward Camber, $\theta_A^* = 60^\circ$. Aft Camber, $\theta_B^* = 8^\circ$. Turning Angle, $\beta_J = \theta_A + \theta_B = 50^\circ$.

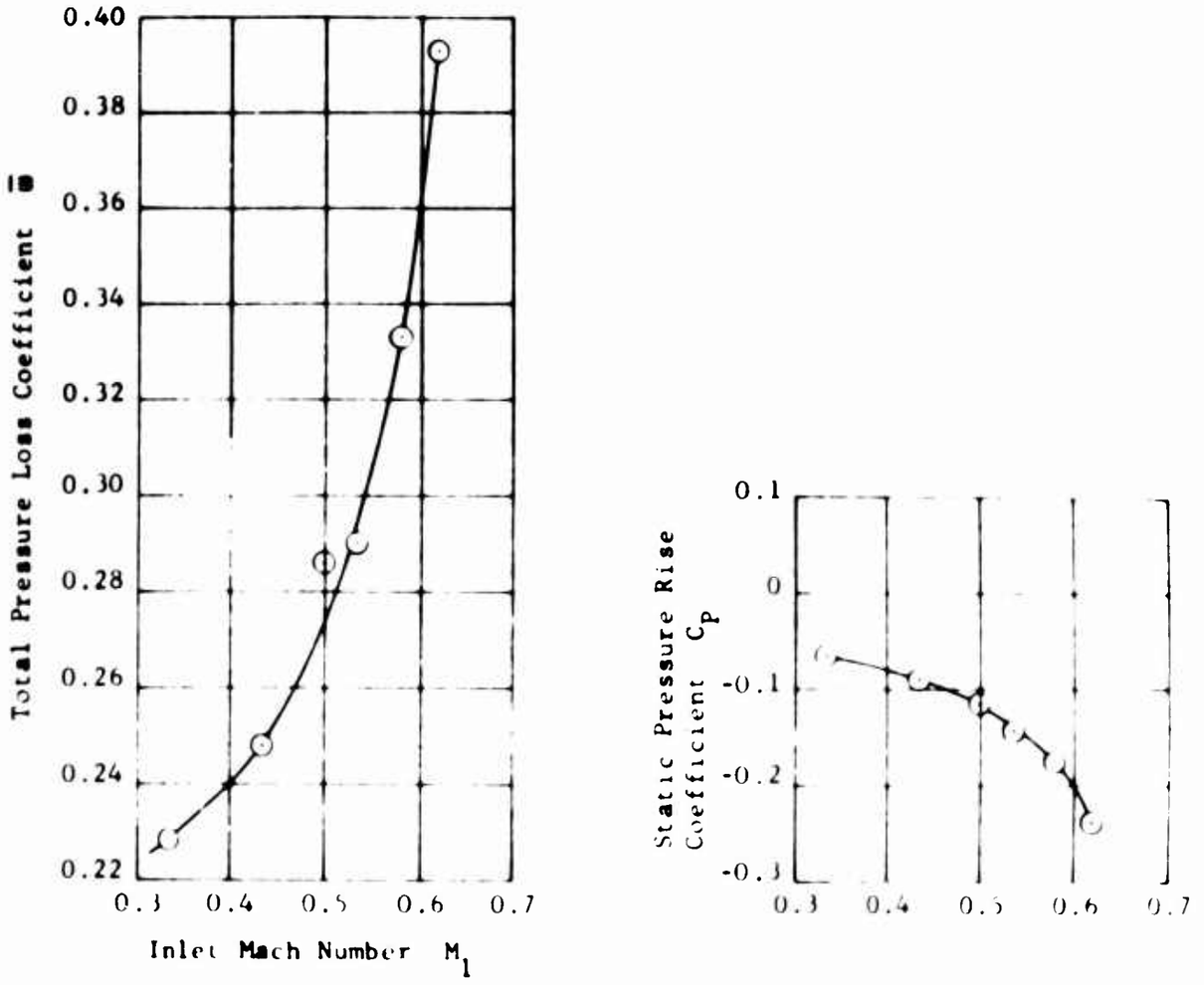

Figure 34. Tandem Cascade. Forward Camber, $\theta_A^* = 60^\circ$. Aft Camber, $\theta_B^* = 30^\circ$. Turning Angle, $\theta_J = \theta_A + \theta_B = 70^\circ$.

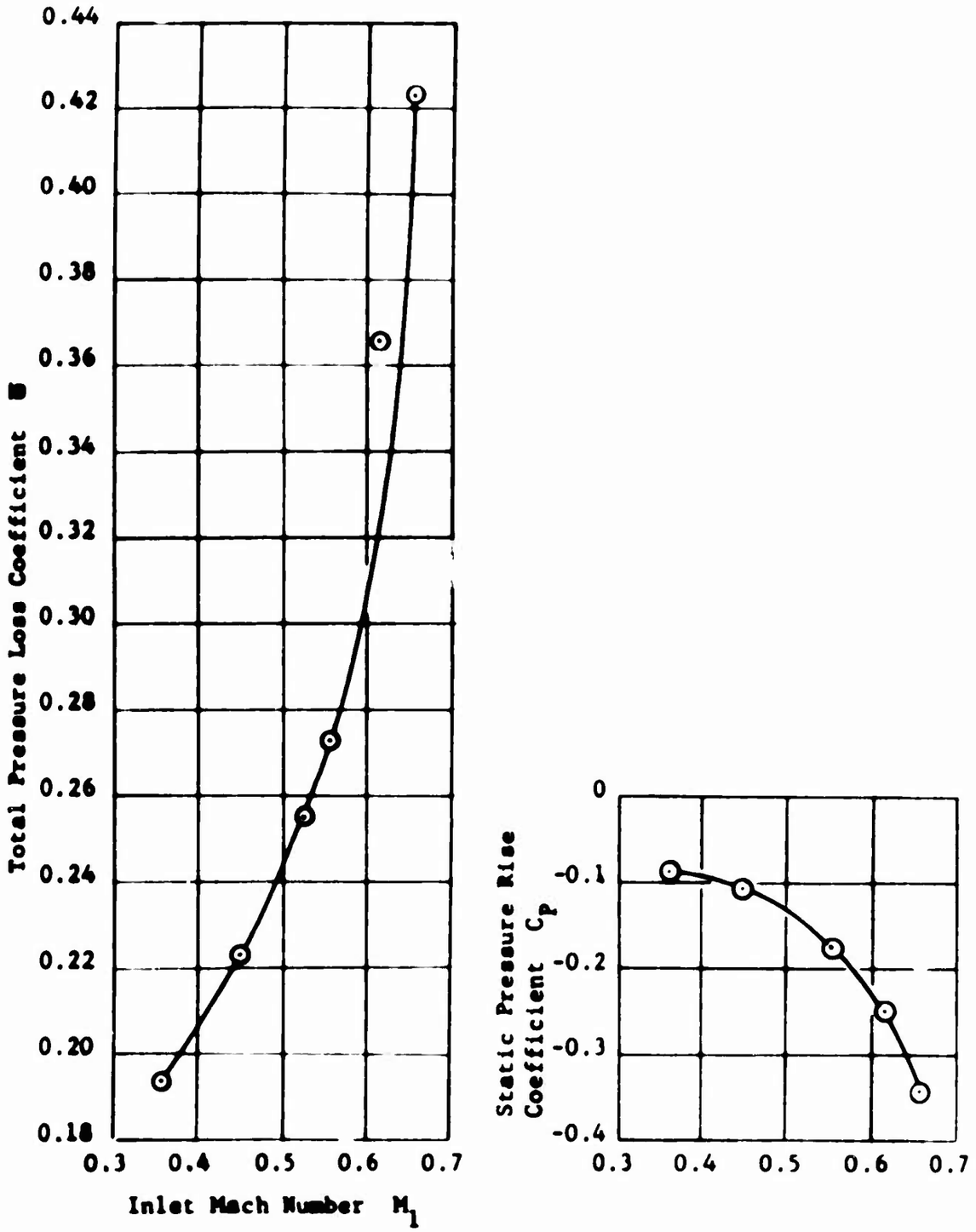

Figure 35. Tandem Cascade. Forward Camber, $\theta_A^* = 60^\circ$. Aft Camber, $\theta_B^* = 52^\circ$. Turning Angle, $\beta_J = \theta_A + \theta_B = 90^\circ$.

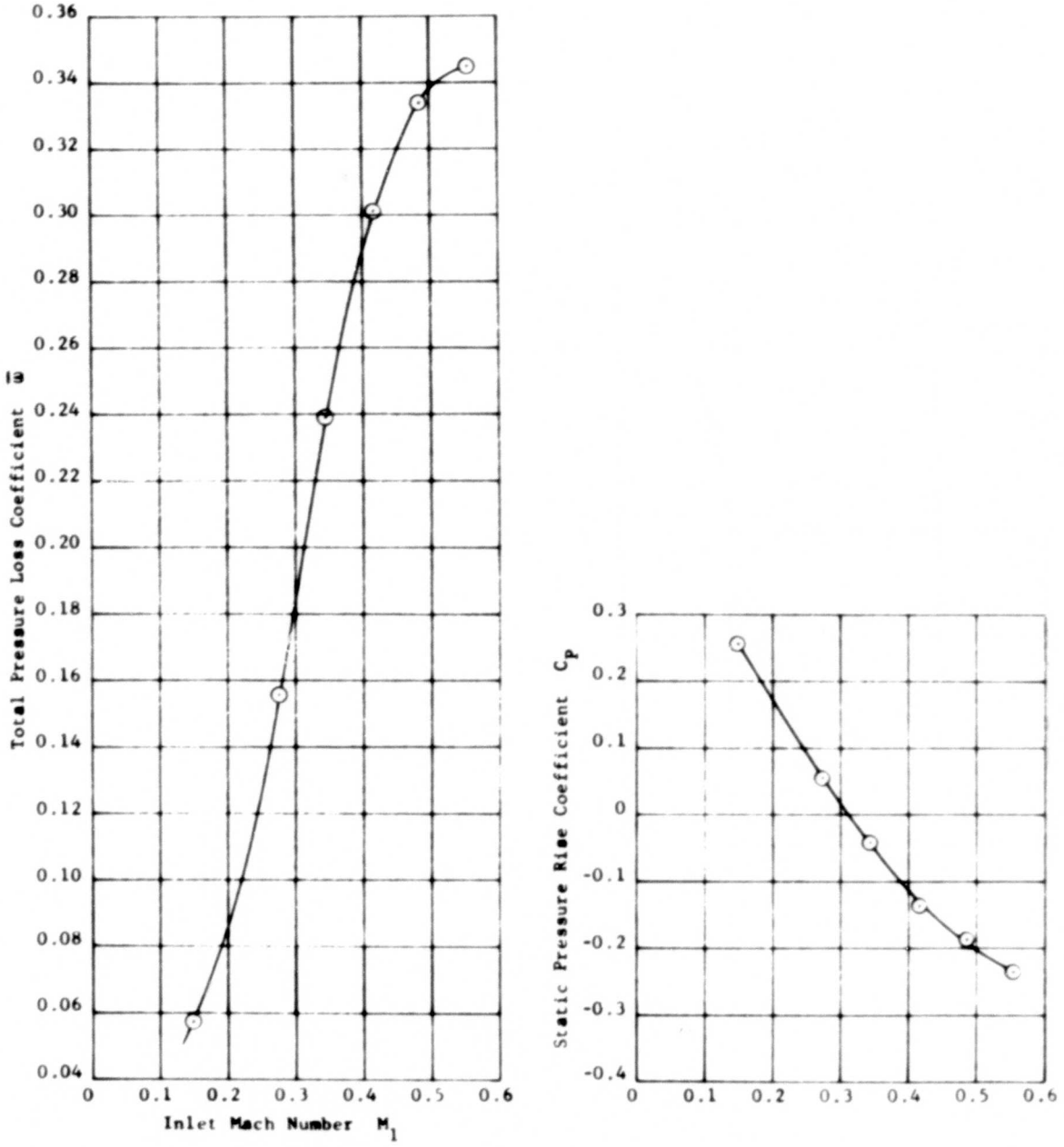

Figure 36. Tandem Cascade. Forward Camber $\theta_A^* = 78^o$ Aft Camber $\theta_B^* = 66^o$. Turning Angle $\beta_J = \theta_A + \theta_B = 130^o$

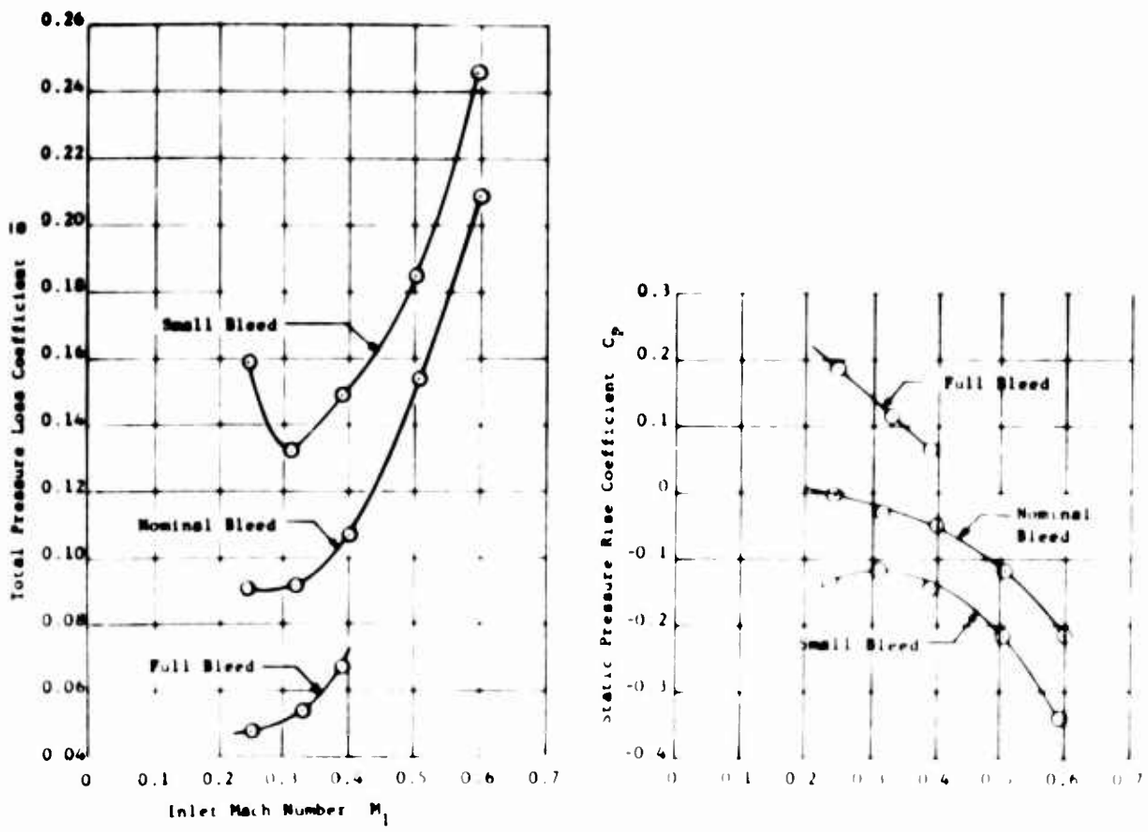

Figure 37. Tandem Cascade. Forward Camber, $\theta_A^* = 60^\circ$. Aft Camber, $\theta_B^* = 52^\circ$. Turning Angle, $\beta_J = \theta_A + \theta_B = 90^\circ$.

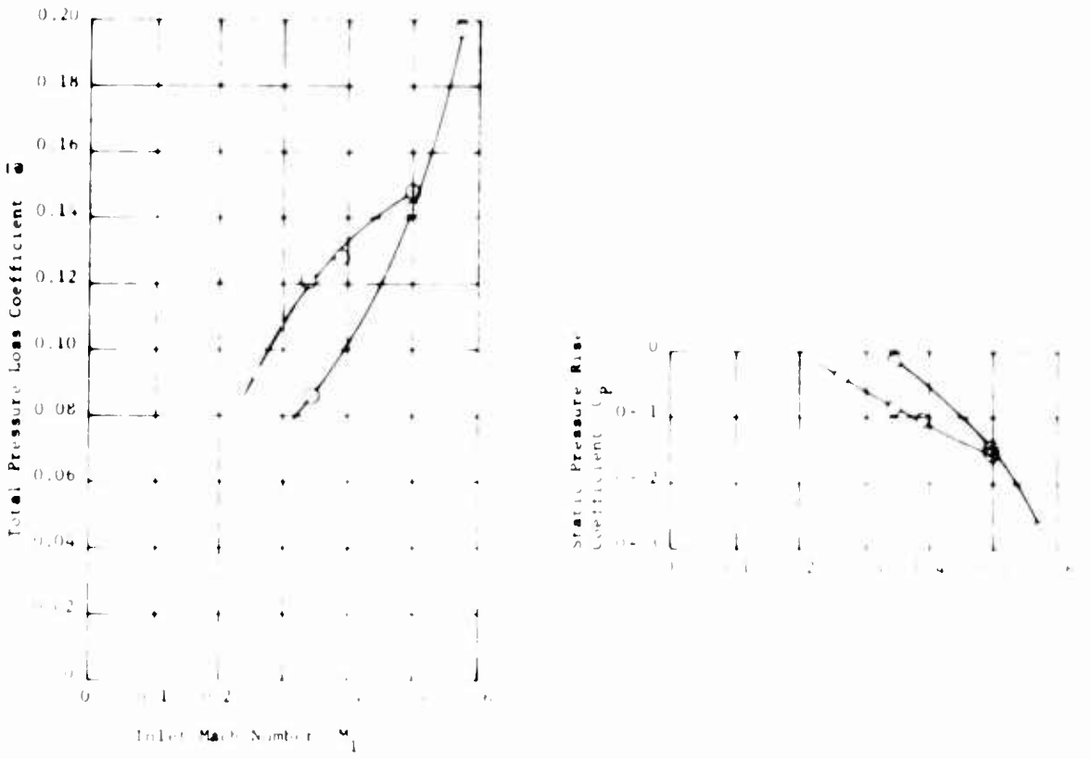

Figure 38. Tandem Cascade. Forward Camber, $\theta_A^* = 78^\circ$. Aft Camber, $\theta_B^* = 66^\circ$. Turning Angle, $\beta_J = \theta_A + \theta_B = 129^\circ$.

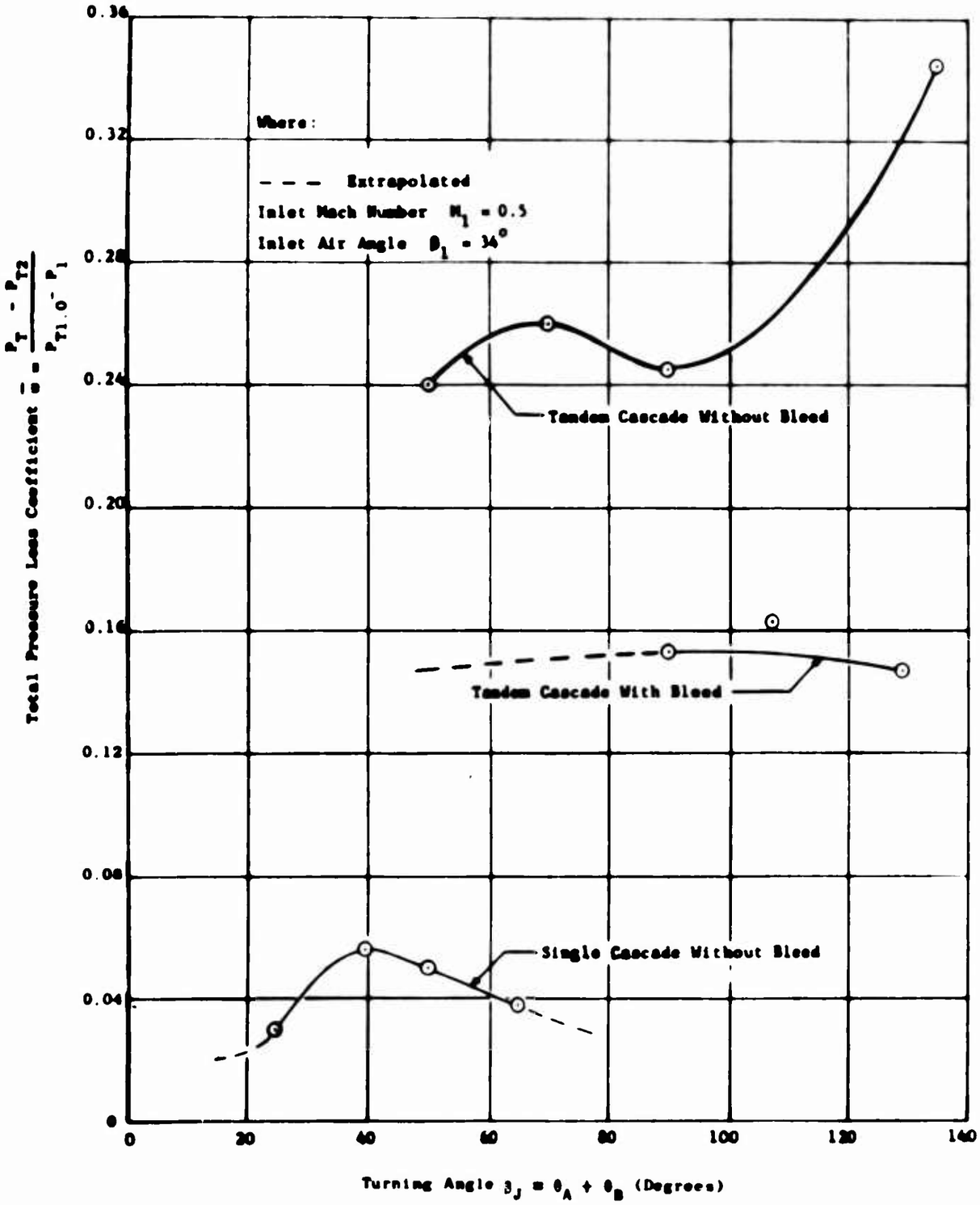

Figure 39. Summary of Flexible-Airfoil Tandem Cascade Results Obtained in the Transonic Cascade Tunnel.

Figure 40. Schematic of Tandem Cascade Test Facility.

Figure 41. Scale-Model **Tandem Cascade** Facility - Plan View.

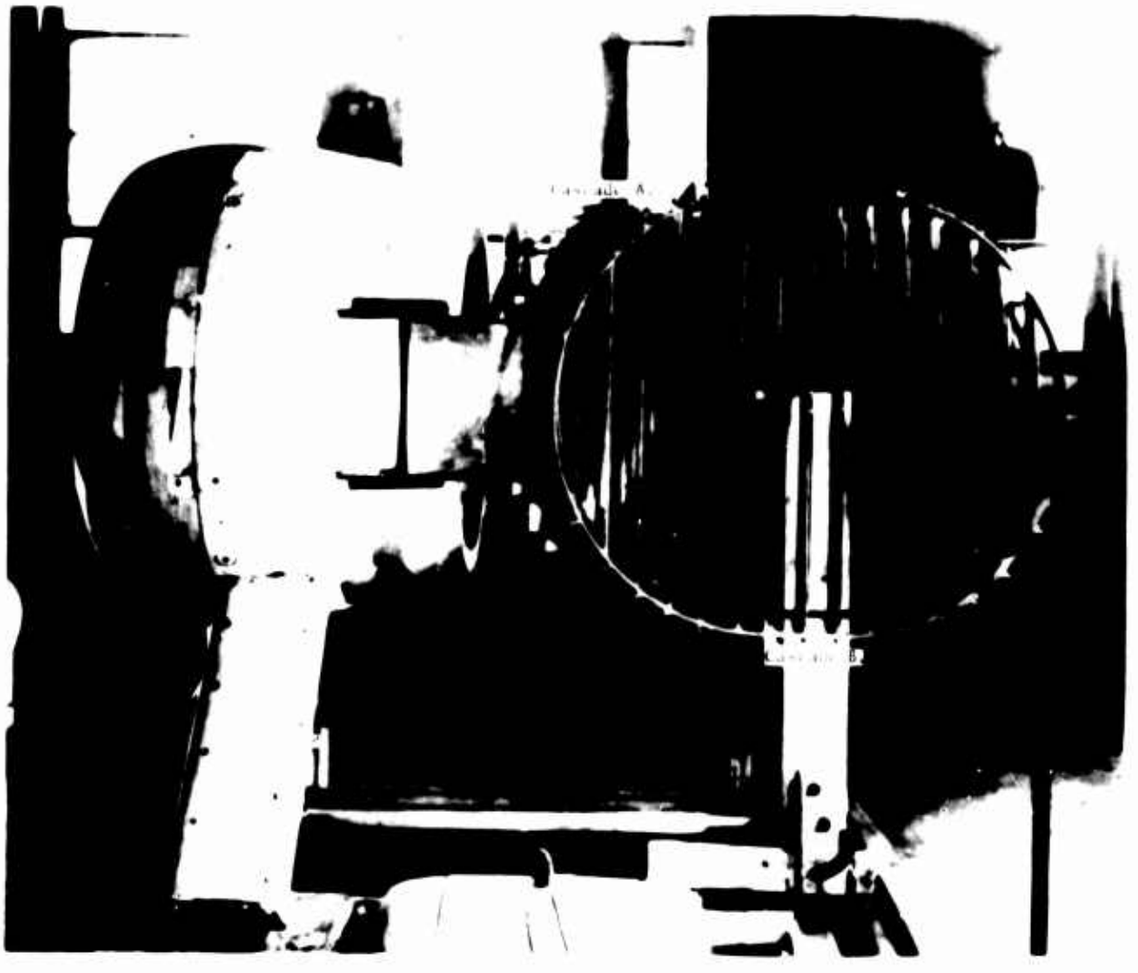

Figure 42 View Looking into Cascade B Discharge.

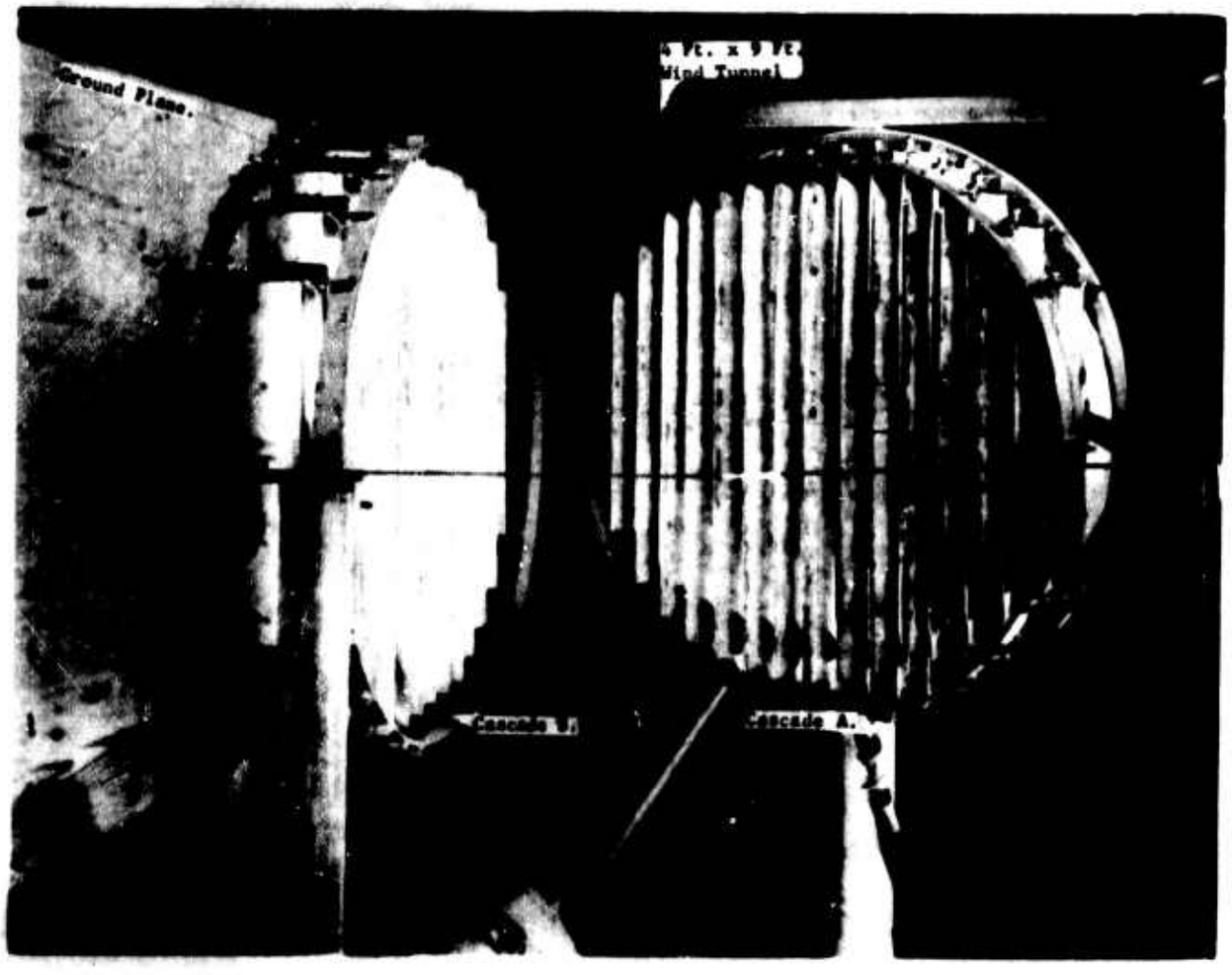

Figure 43. View Looking Upstream Between Cascades A and B.

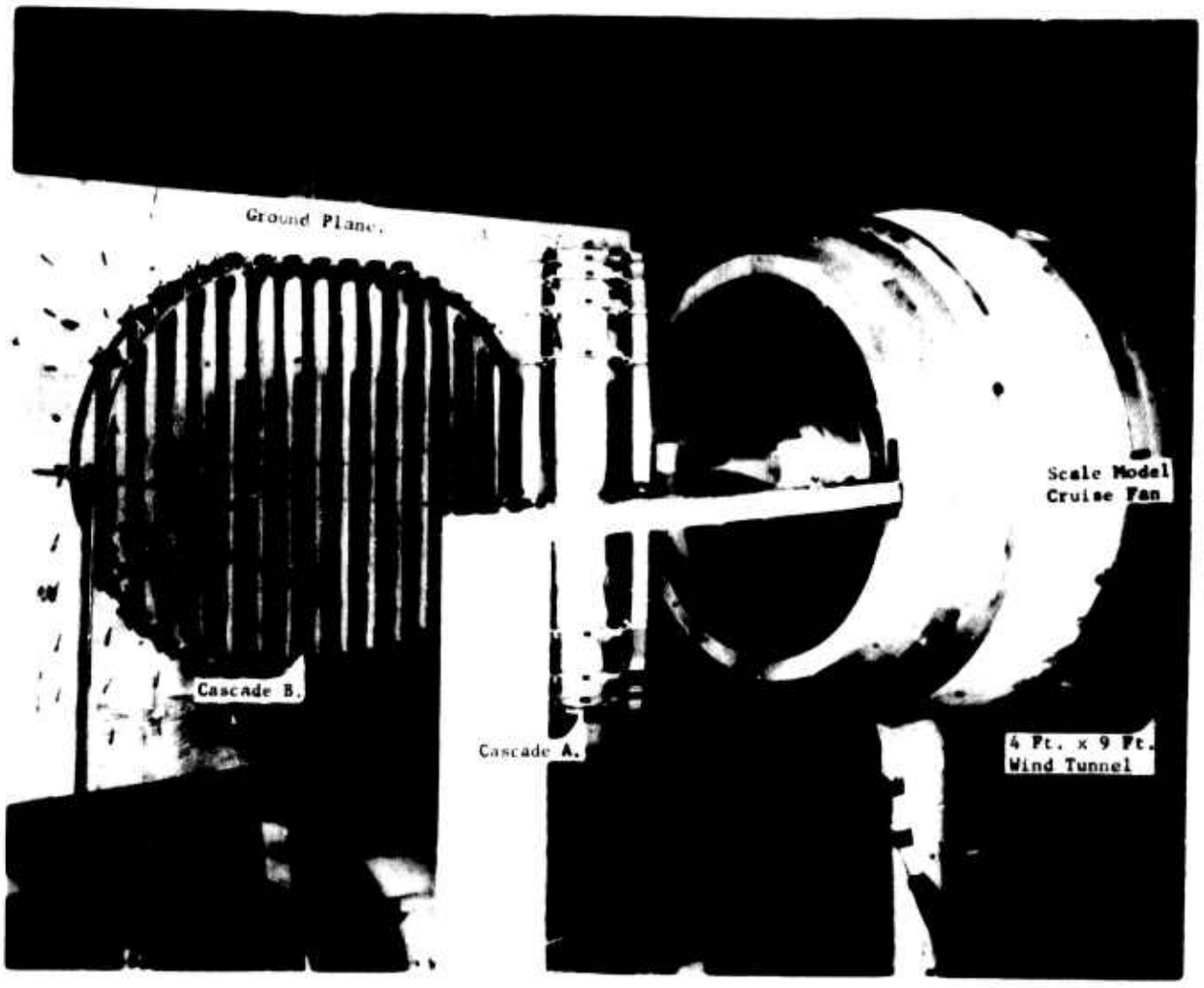

Figure 44. Scale-Model Tandem Cascade Facility - Side View.

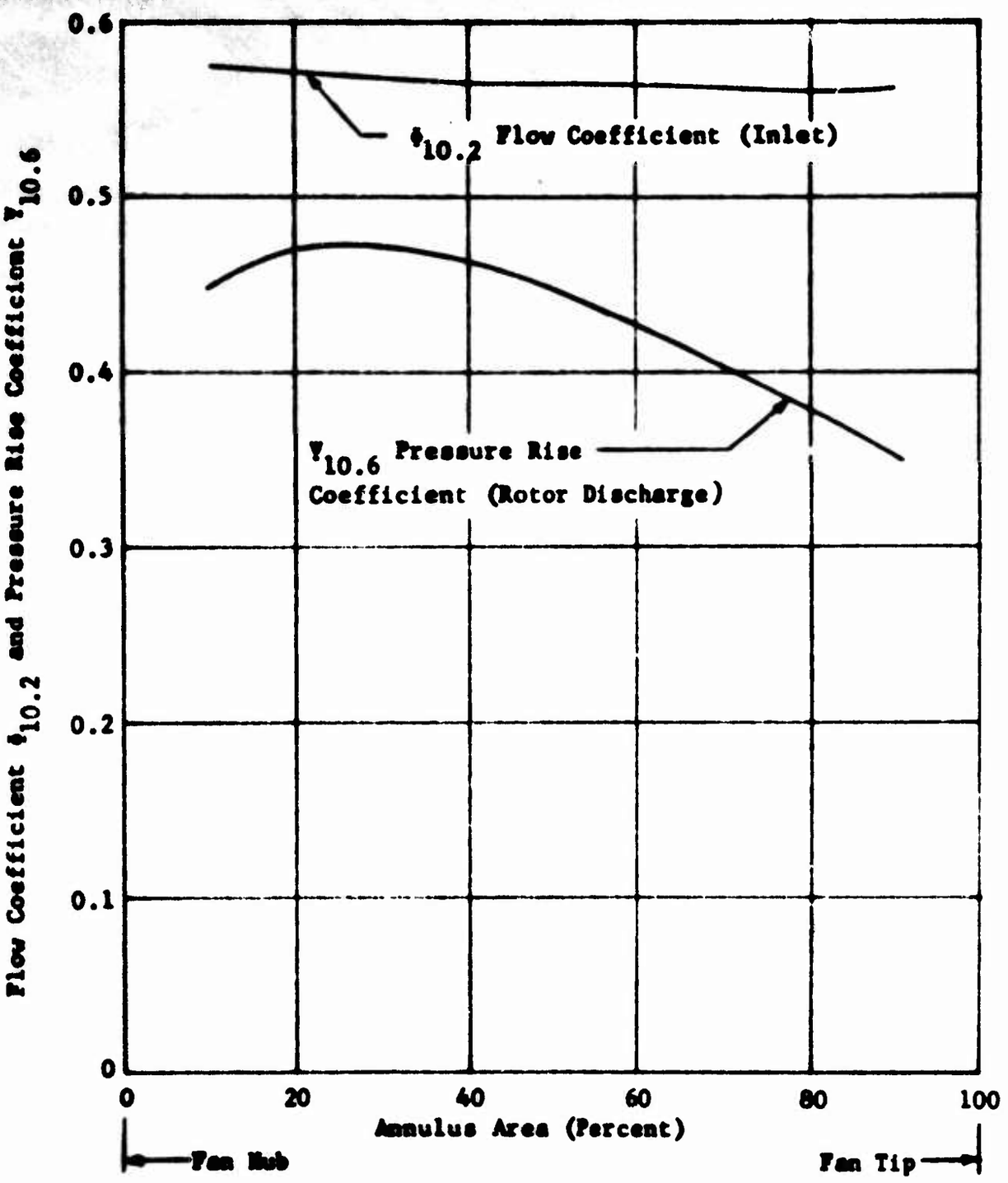

Figure 45. Flow and Pressure Rise Coefficients for 26-Inch-Tip-Diameter Fan.

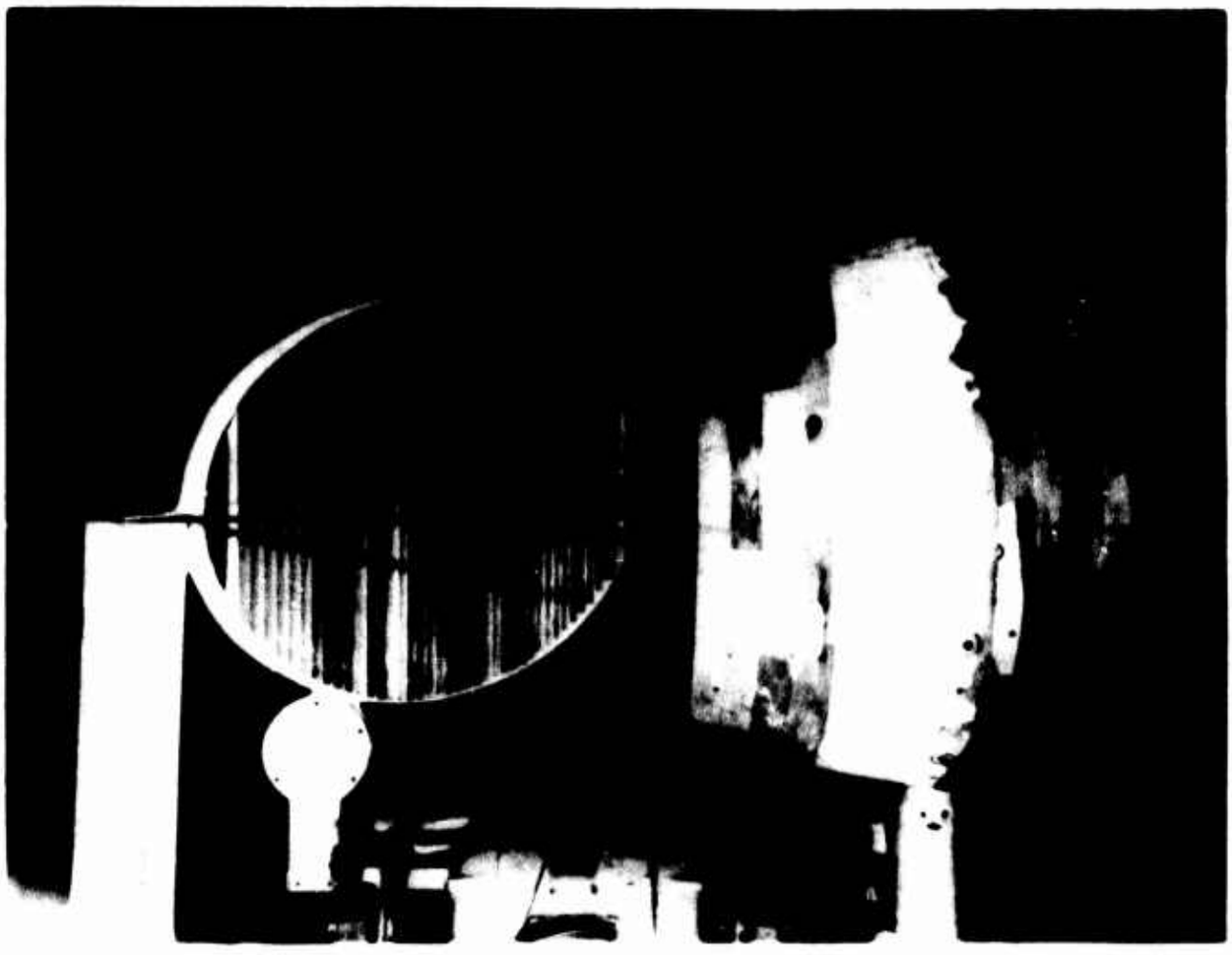

Figure 46. Fixed-Camber Cascade with Molded Plastic Blades. Camber, $\theta^* = 90^\circ$. Solidity, $\sigma = 2.14$.

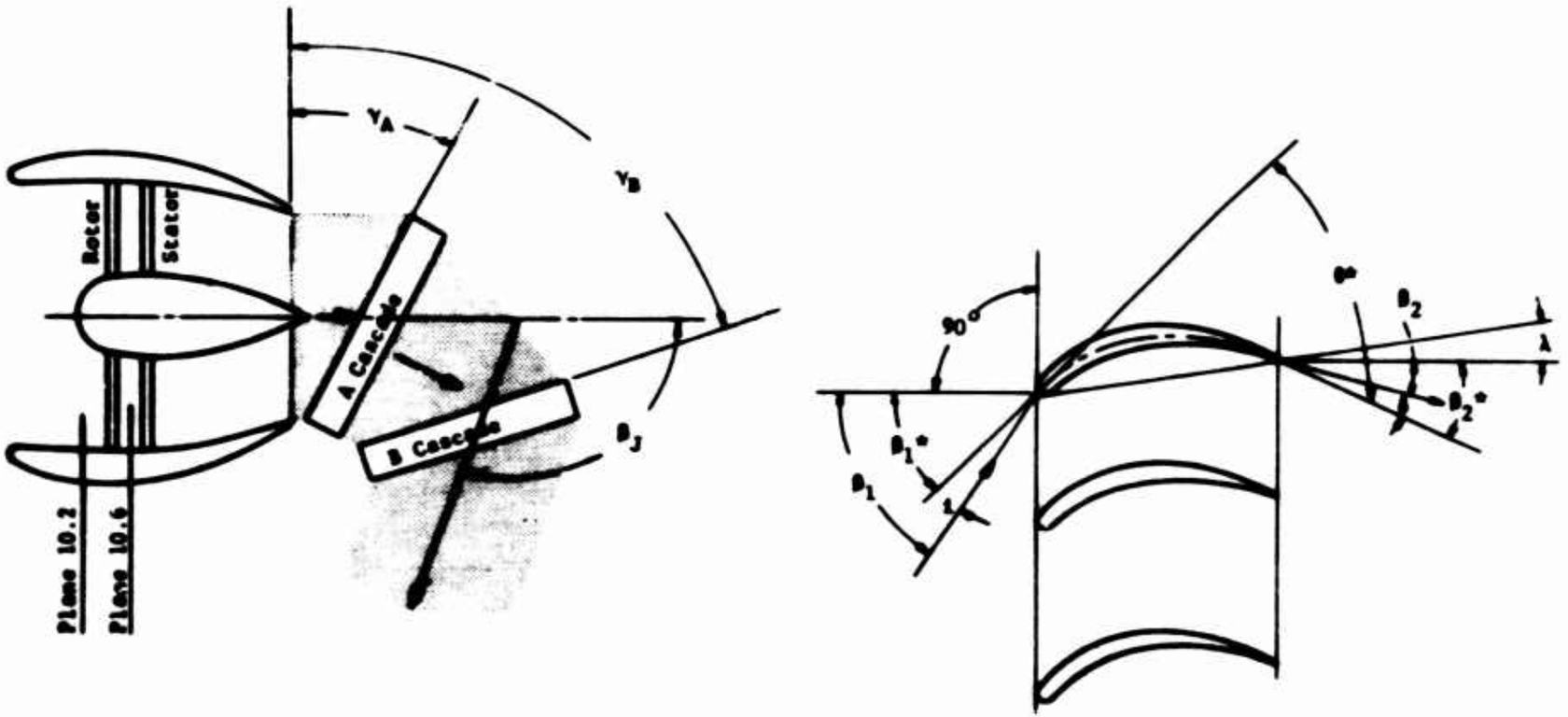

Angles Measured Relative to Fan

γ = Cascade Orientation Angle (A&B)

β_J = Jet Efflux Angle (Thrust Deflection)

Angles Measured Relative to Each Cascade

β_1 = Air Inlet Angle

β_2 = Air Exit Angle

θ = $\beta_1 + \beta_2$ = Air Turning Angle

i = Incidence ($\beta_1 - \beta_1^*$)

λ = Blade Setting Angle

β_1^* = Blade Inlet Angle

β_2^* = Blade Exit Angle

θ^* = Blade Camber Angle

δ = Deviation ($\beta_2^* - \beta_2$)

Figure 47. Tandem Cascade Geometry Nomenclature.

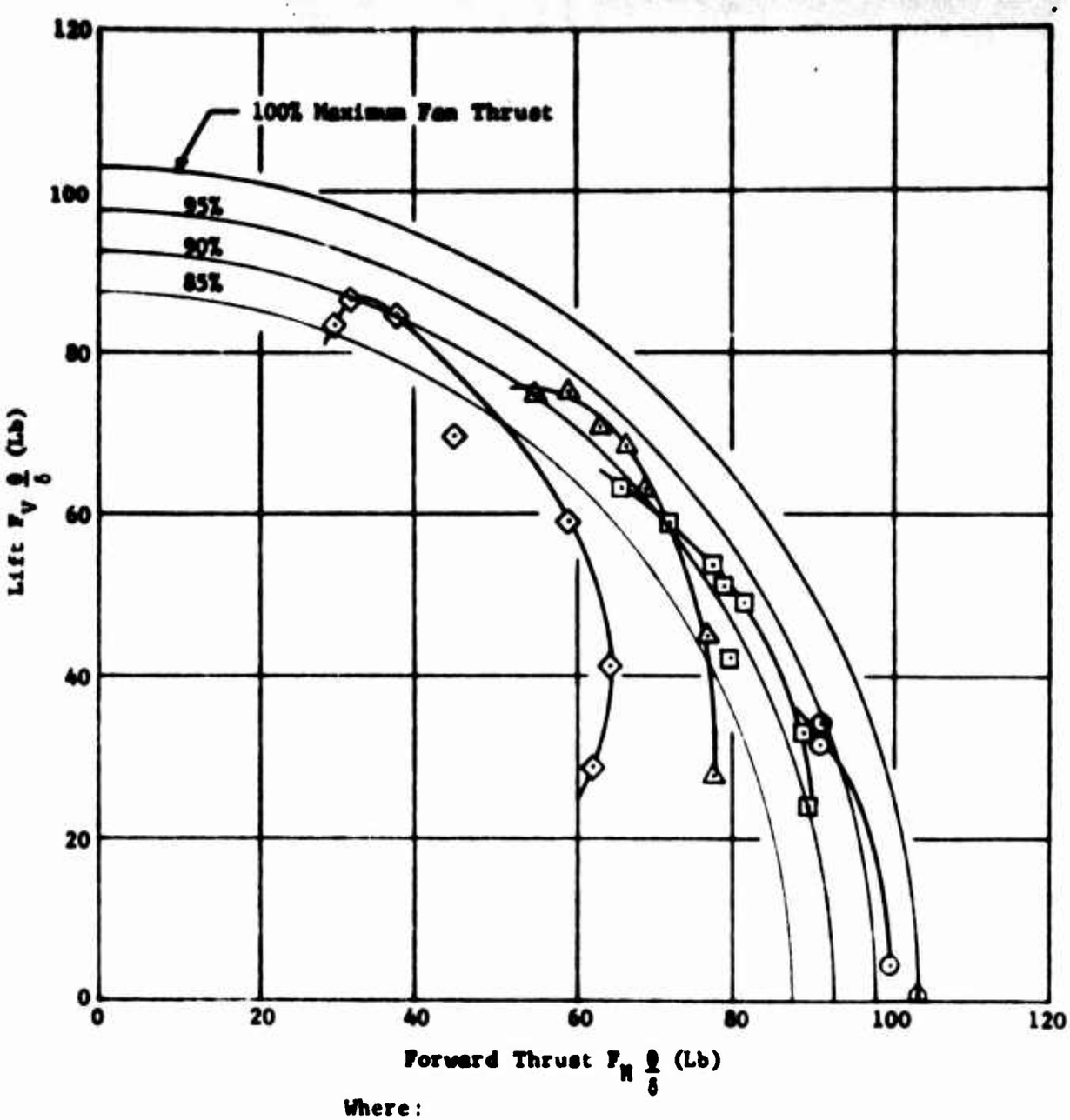

Where:

Mark	Run	θ_A^*	β_1^*
○	1	0°	10°
□	5	35°	16.5°
△	8	56°	31.5°
◇	8	80°	39.5°
⌂	—	No Cascades Mounted	

Figure 48. Vectored Thrust.

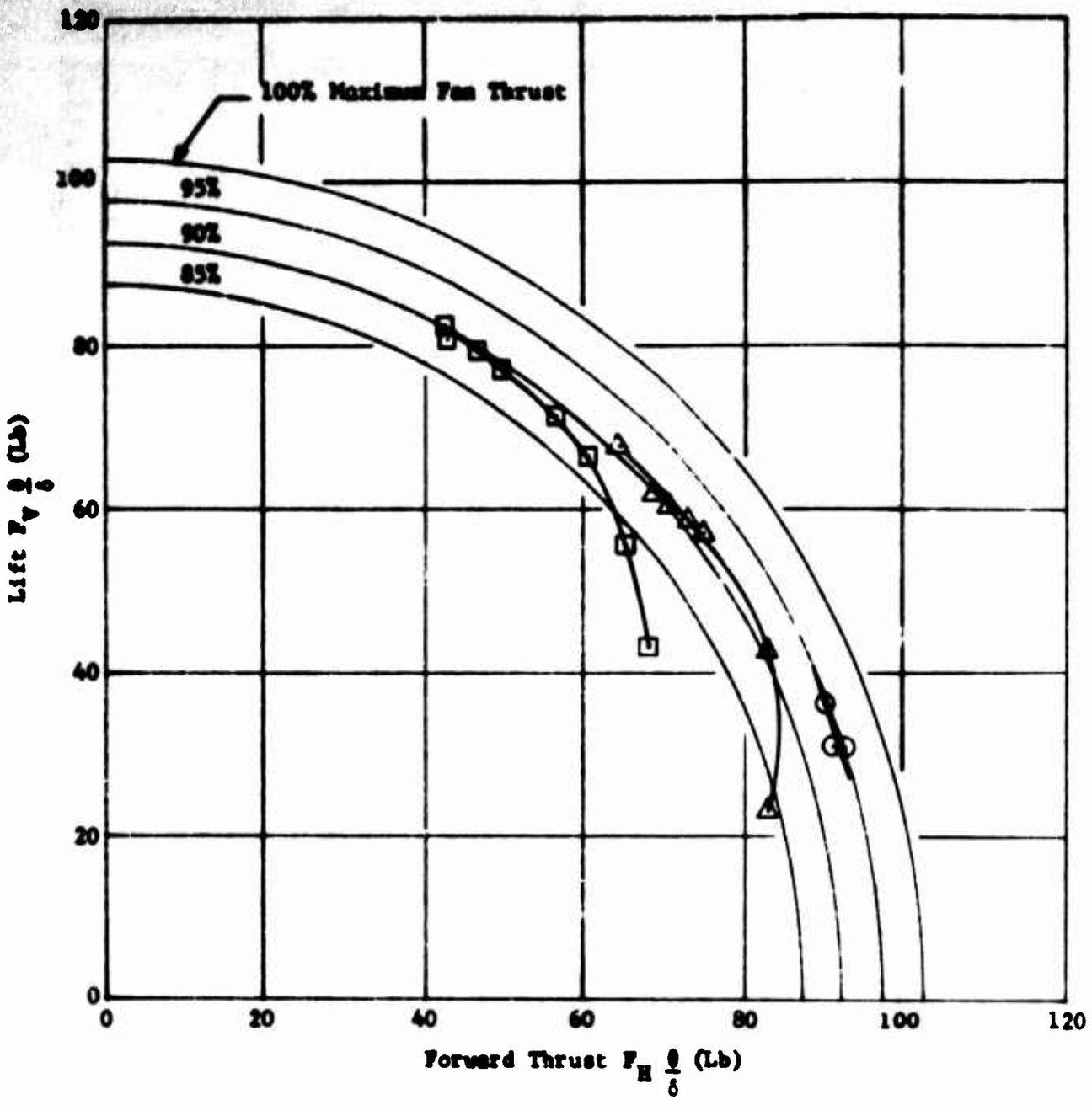

Where:

Mark	Run	θ_A^*	β_1^*
○	2	25°	13.5°
□	3	78°	39°
△	6	48°	22°

Figure 49. Vectored Thrust

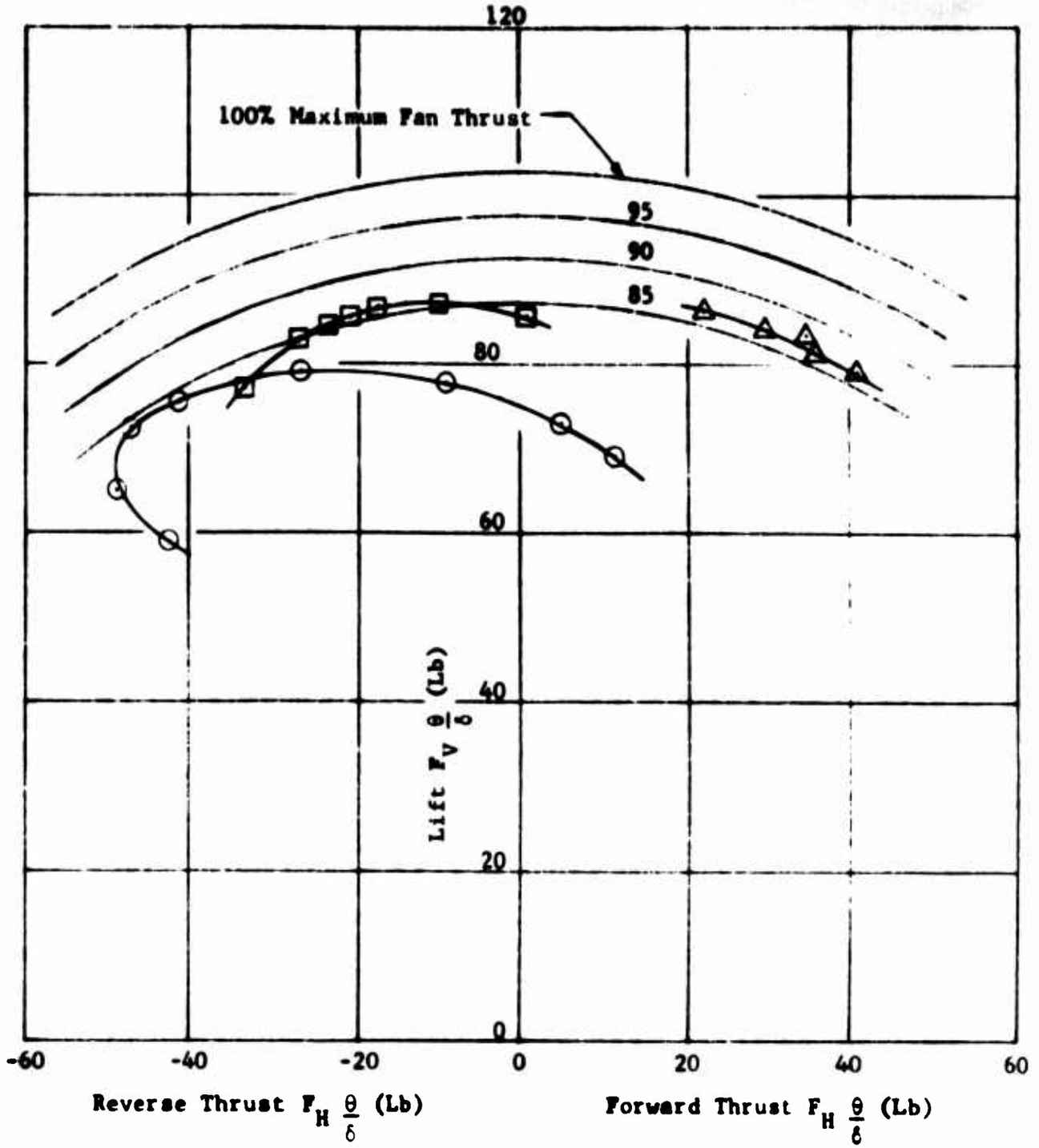

Where:

		1st Cascade		2nd Cascade	
Mark	Run	θ_A^*	β_1^*	θ_B^*	β_1^*
△	4	78°	39°	0°	0°
□	6	78°	39°	48°	22°
○	8	78°	39°	78°	39°

Figure 50. Vectored Thrust.

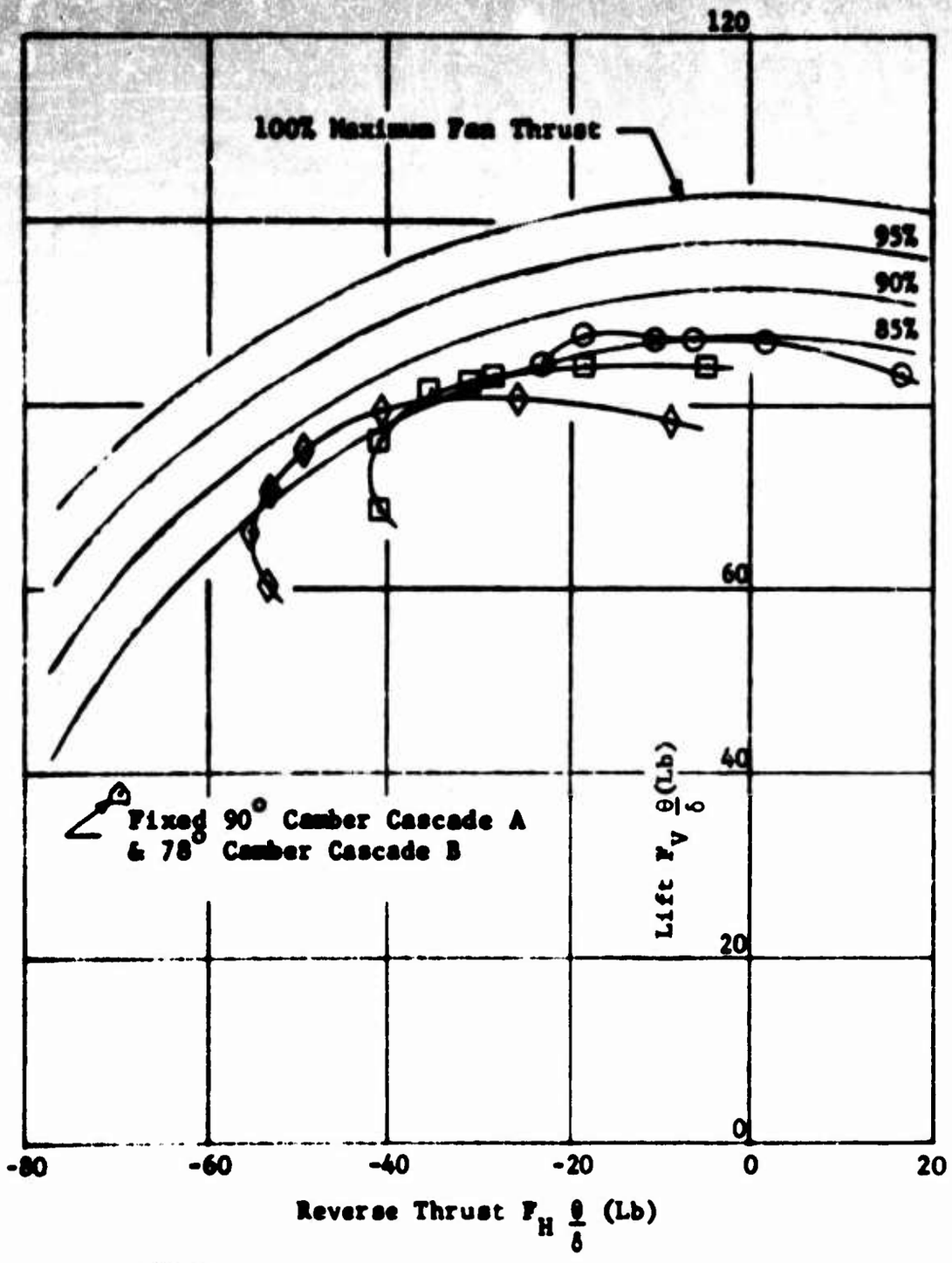

Where:

		1st Cascade		2nd Cascade	
Mark	Run	θ_A^*	β_1^*	θ_B^*	β_1^*
○	5	78°	39°	35°	16.5°
□	7	78°	39°	56°	31.5°
◇	14	80°	39.5°	78°	39°
⌂	8	90°	45°	78°	39°

Figure 51. Vectored Thrust.

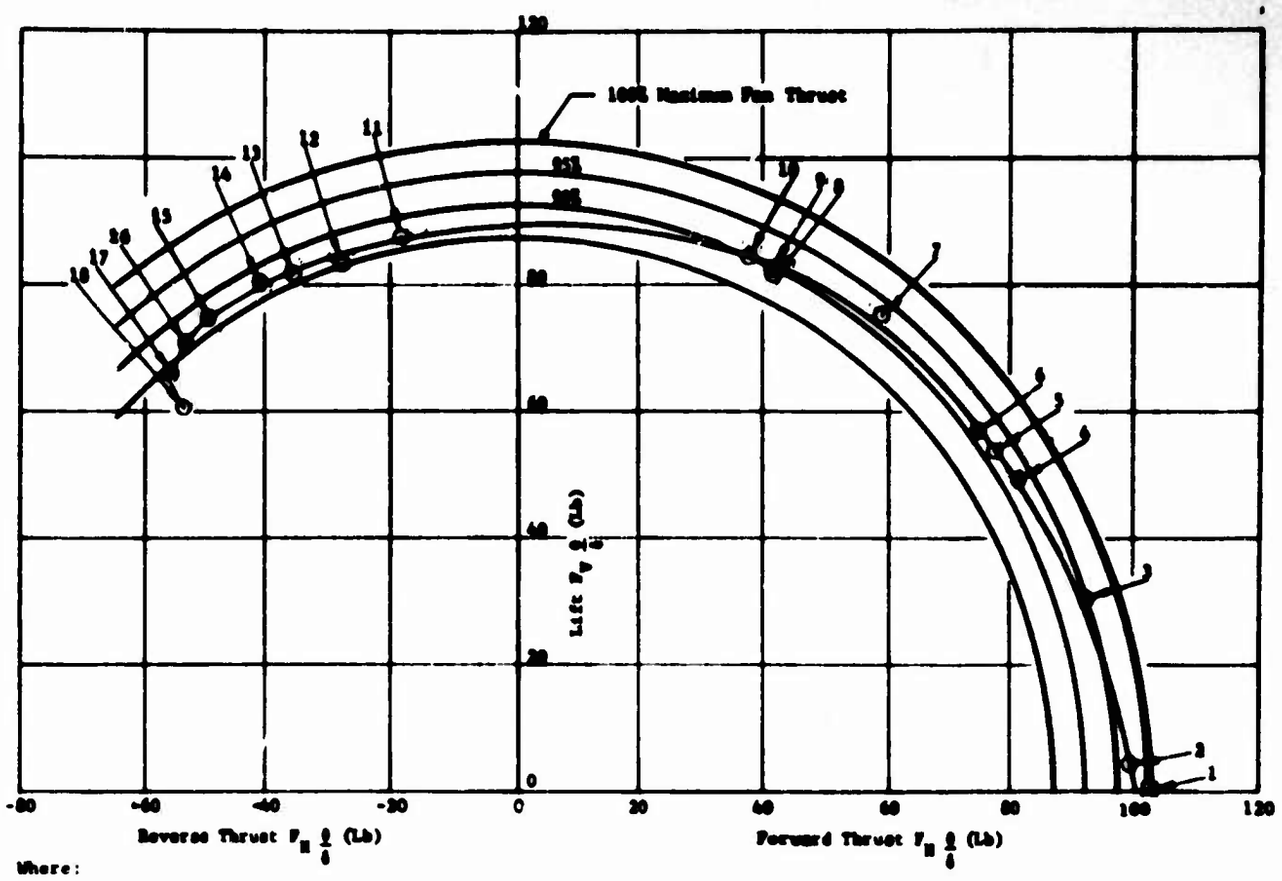

Where:

Mark	Run-Reading	1st Cascade θ_A^*	1st Cascade β_1^*	1st Cascade γ_A	2nd Cascade θ_B^*	2nd Cascade β_1^*	2nd Cascade γ_B
1	1-2	(No Cascades Mounted - Maximum Fan Thrust)					
2	1-1	0°	13.5°	0°			
3	2-2	25°	13.5°	9°			
4	5-11	35°	16.5°	16°			
5	5-7	35°	16.5°	20°			
6	6-3	48°	22°	20°			
7	7-9	56°	31.5°	33°			
8	8-5	78°	39°	35°			
9	3-1	78°	39°	37°			
10	14-2	78°	39°	35°	80°	39°	35°
11	5-2	78°	39°	35°	35°	16.5°	83°
12	6-13	78°	39°	35°	48°	22°	90°
13	7-3	78°	39°	35°	56°	31.5°	91°
14	14-3	78°	39°	35°	80°	39.5°	90°
15	14-18	80°	39.5°	38°	79°	39°	95°
16	14-19	80°	39.5°	38°	79°	39°	100°
17	14-20	80°	39.5°	38°	79°	39°	105°
18	14-21	80°	39.5°	38°	79°	39°	110°

Figure 52. Maximum Vectored Thrust for Tandem Cascade Testing, Runs 1-14.

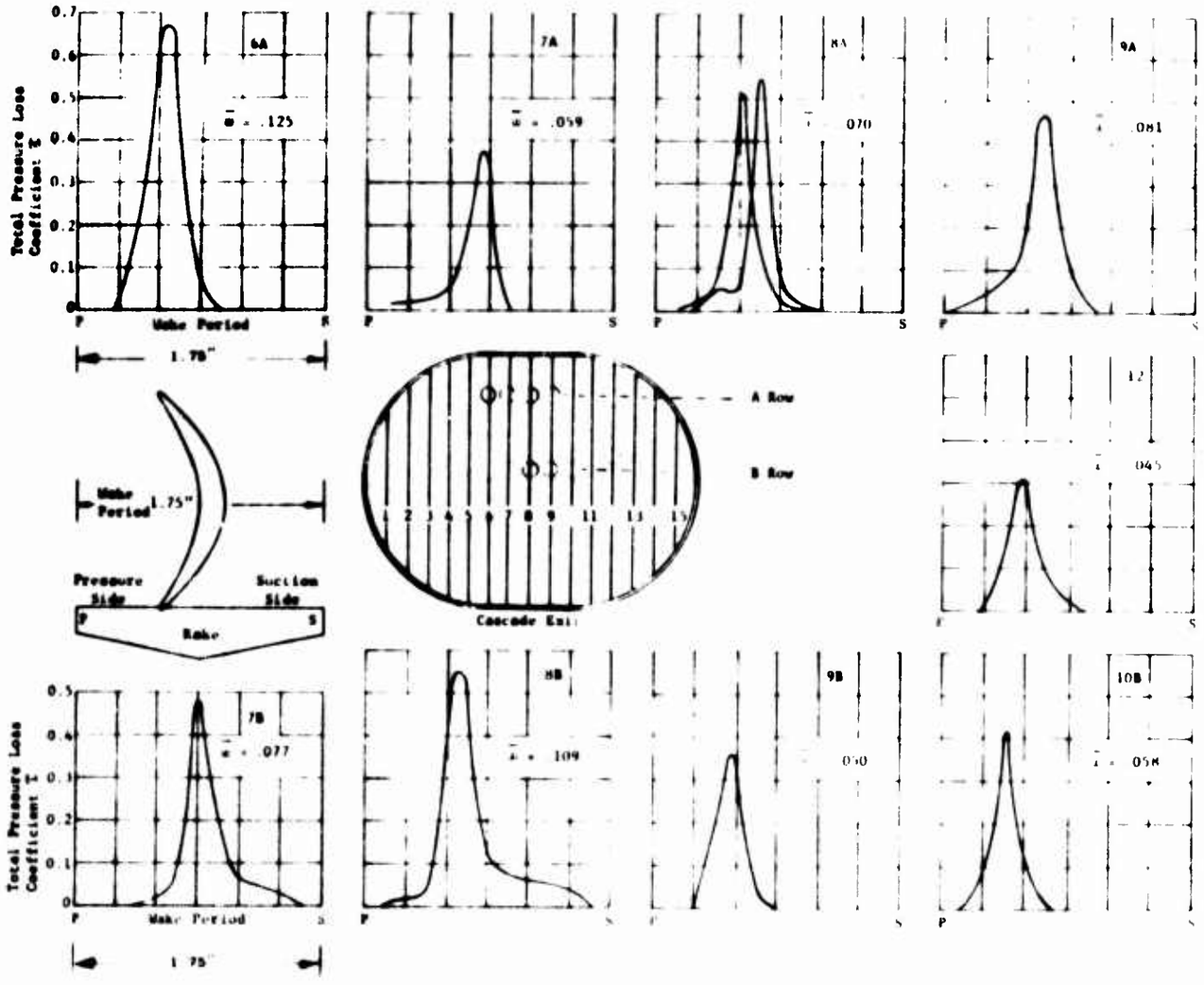

Figure 53. Blade Wake Profiles. Single Cascade. $\theta^* = 78^\circ$, $\beta_1^* = 39^\circ$, and $\gamma_A = 35^\circ$.

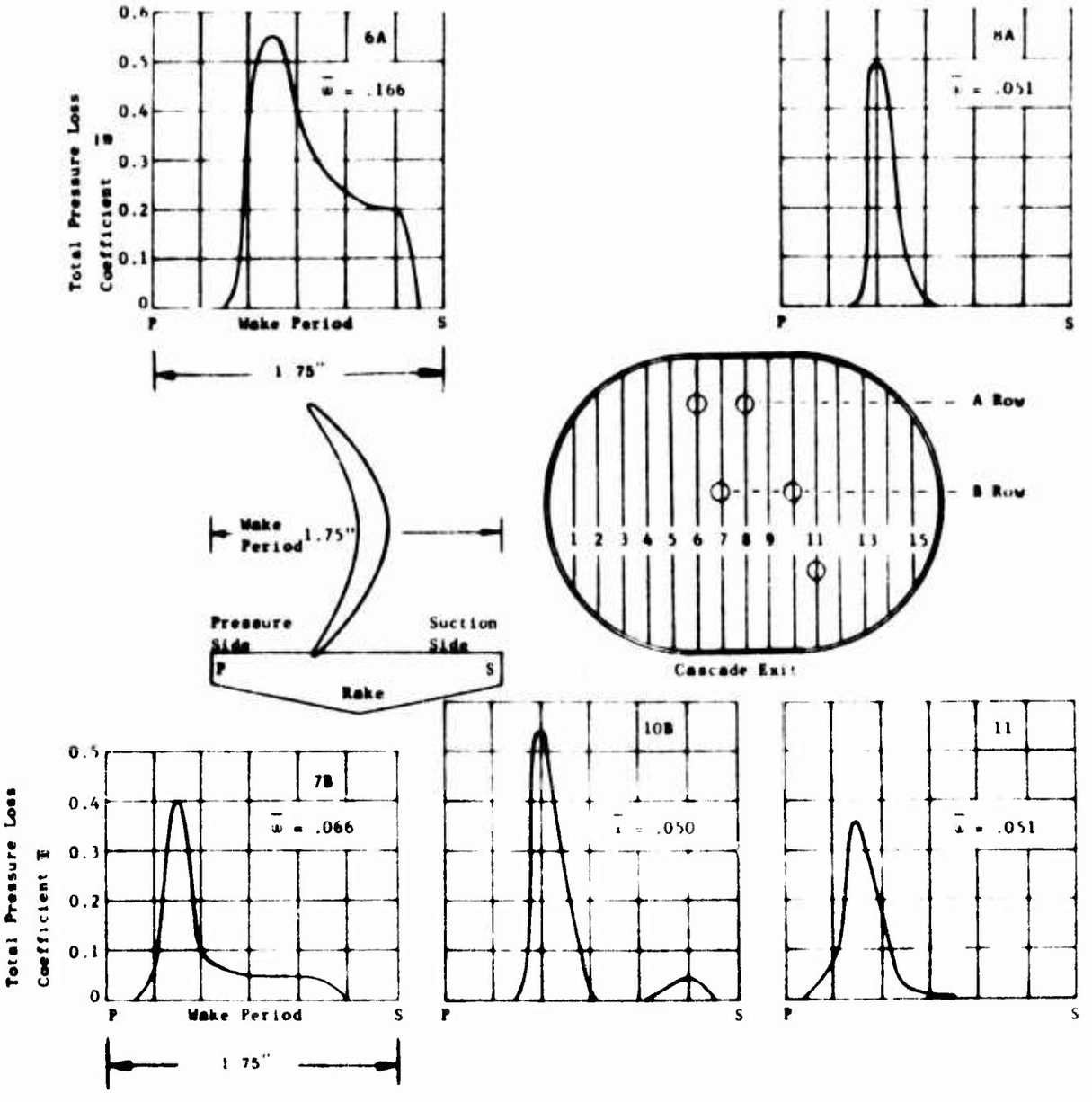

Figure 54 Blade Wake Profiles. Tandem Cascade. $\theta_B^* = 78^o$, $\theta_1^* = 39^o$, and $\gamma_B = 95^o$.

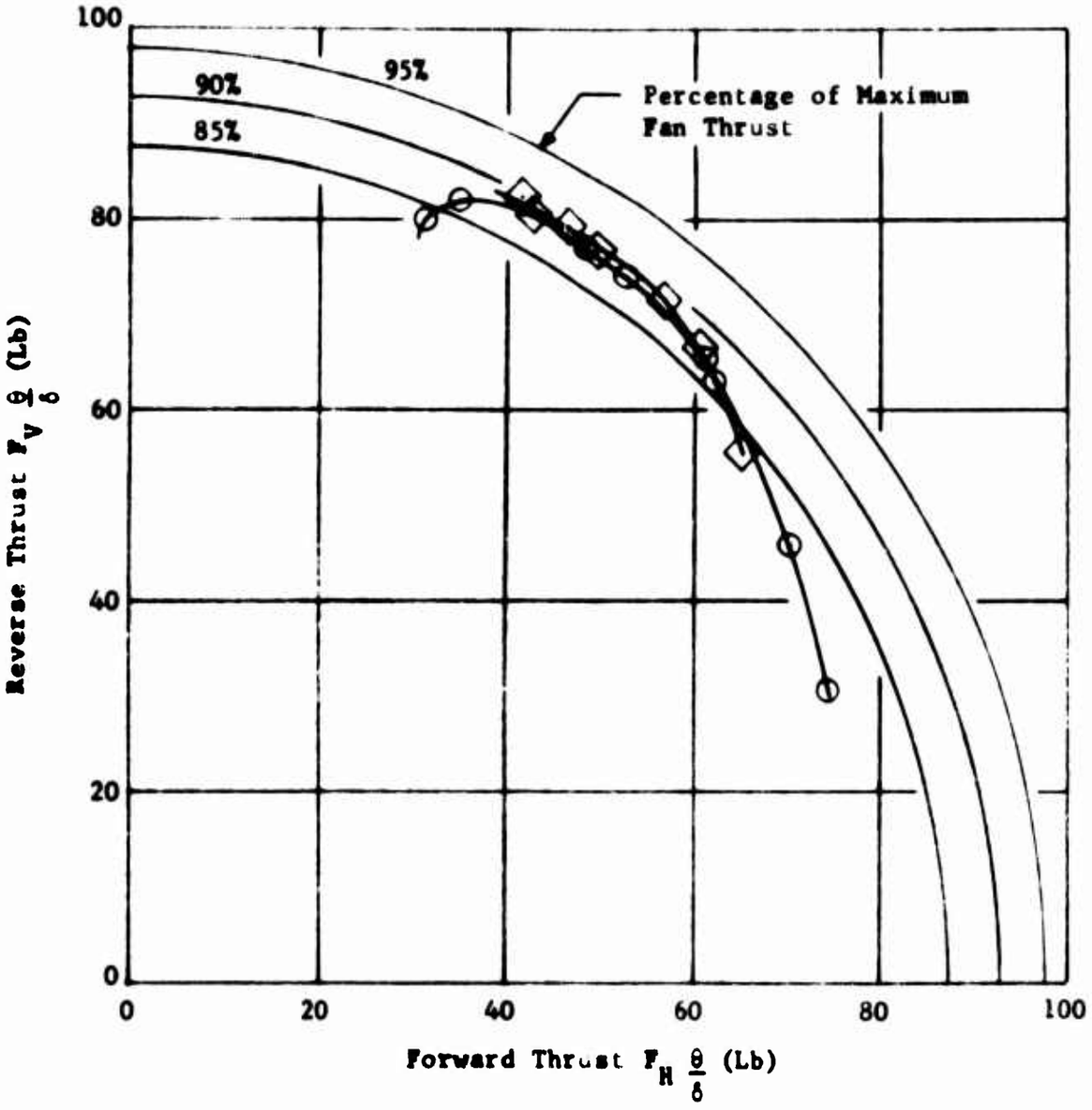

Where:

Mark	Run	θ_A^*	β_1^*	Shift
◇	3	78°	39°	0 Inches
○	12	78°	39°	12 Inches

Figure 55. Vectored Thrust Comparison - Cascade A Shifted Aft.

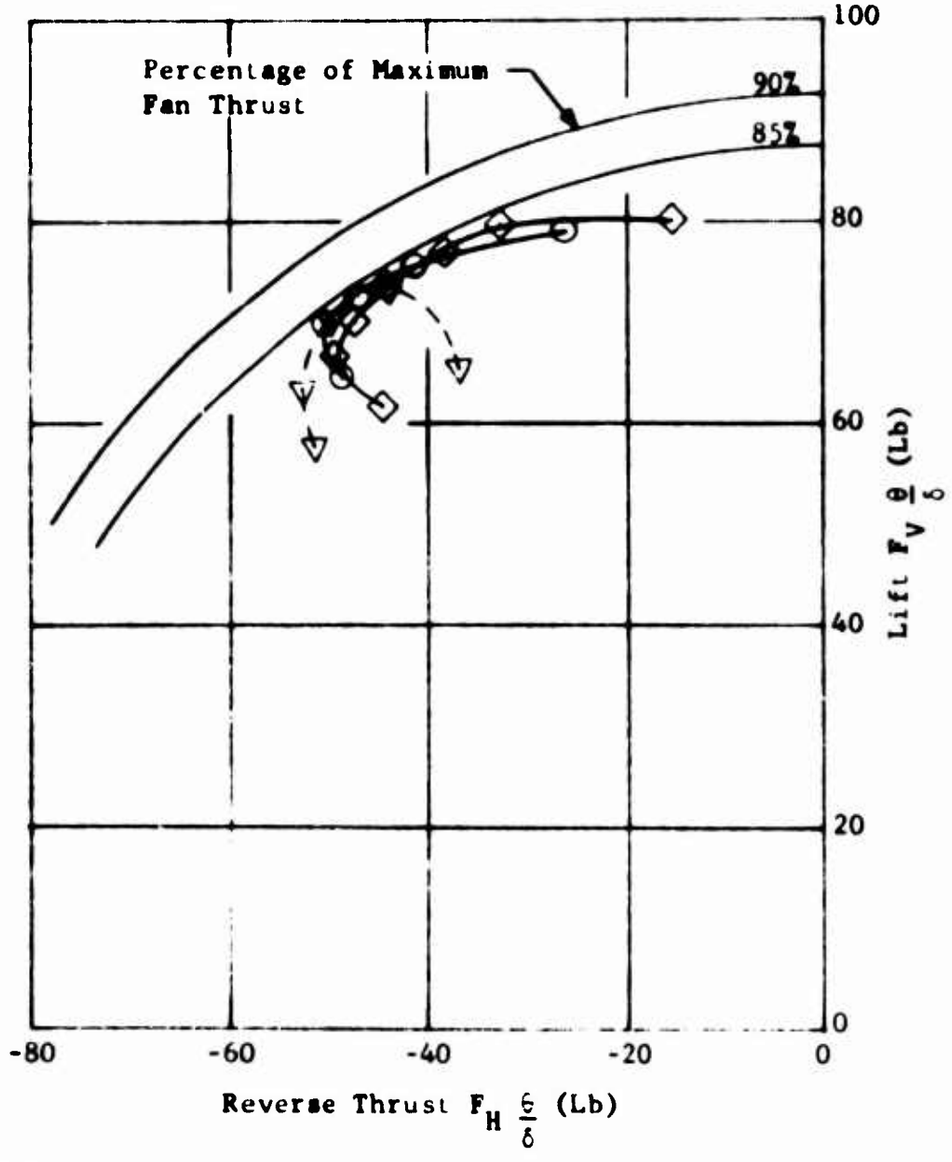

Where:

		1st Cascade		2nd Cascade		
Mark	Run	θ_A^*	β_1^*	θ_B^*	β_1^*	Shift
○	8	78°	39°	78°	39°	0
◇	12	78°	39°	78°	39°	12 Inches Aft
▽	13	78°	39°	78°	39°	3 Inches Aft

Figure 56. Vectored Thrust Comparison - Cascade B Shifted Aft.

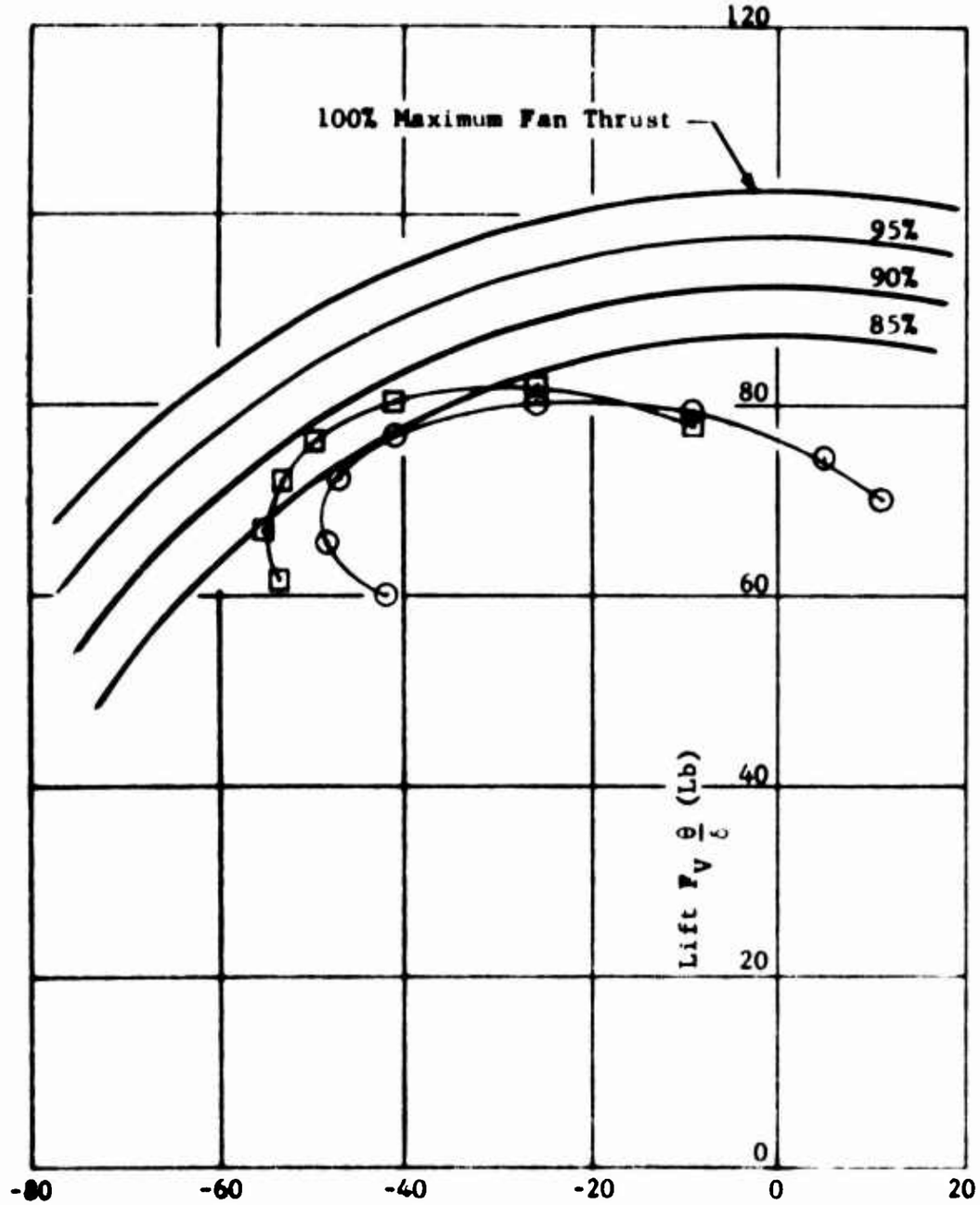

Where:

		1st Cascade		2nd Cascade	
Mark	Run	θ_A^*	β_1^*	θ_B^*	β_1^*
□	14	80°	39.5°	78°	39°
○	15	78°	39°	78°	39°

Figure 57 Vectored Thrust.

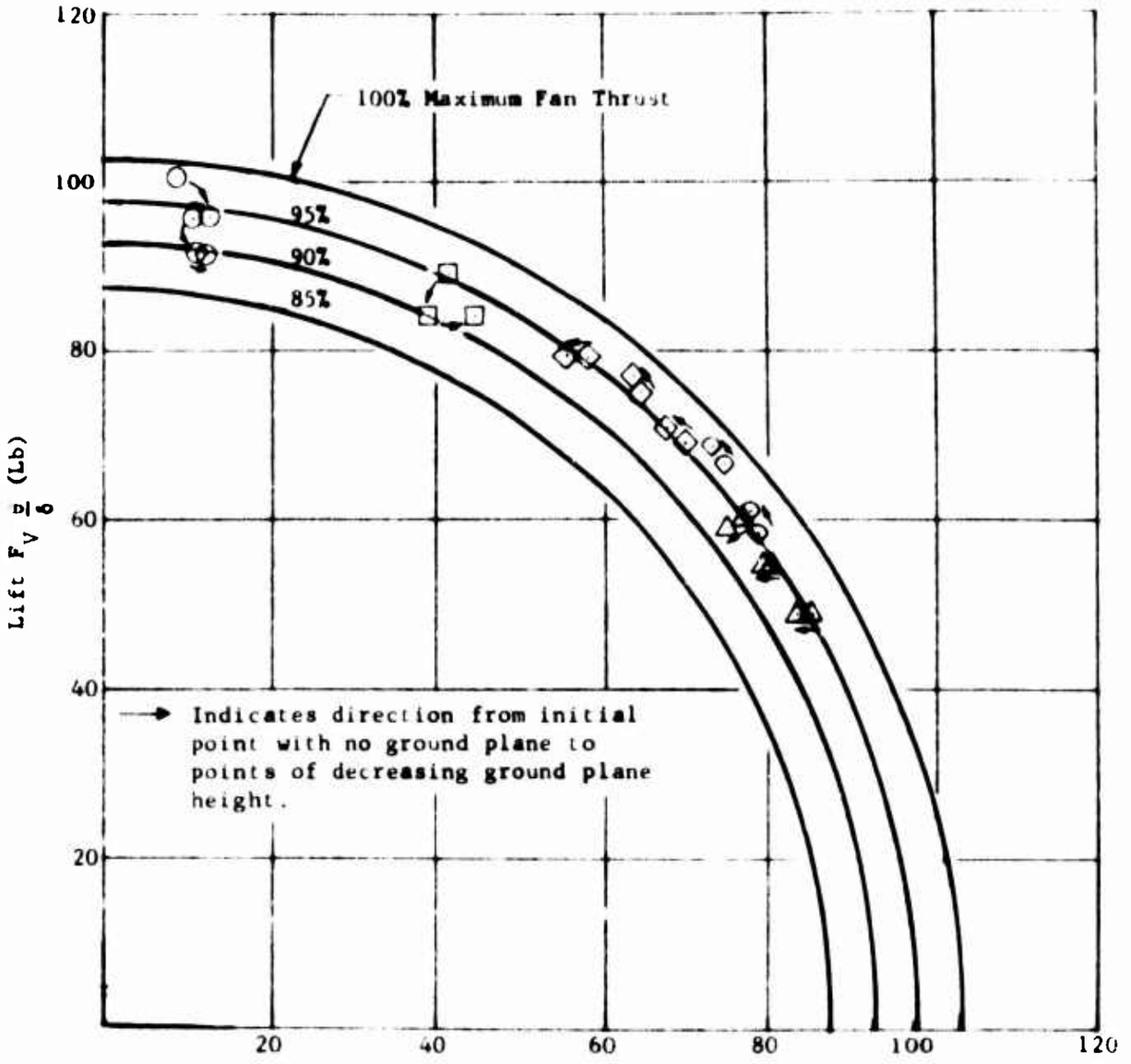

Where:

Mark	Run	θ_A^*	β_1^*
□	18	80°	39.5°
○	19	90°	45° (Fixed Camber)
△	20	42°	37°
◇	23	48°	37°
◇	25	61°	37°

Figure 58. Vectored Thrust - Ground Effect.

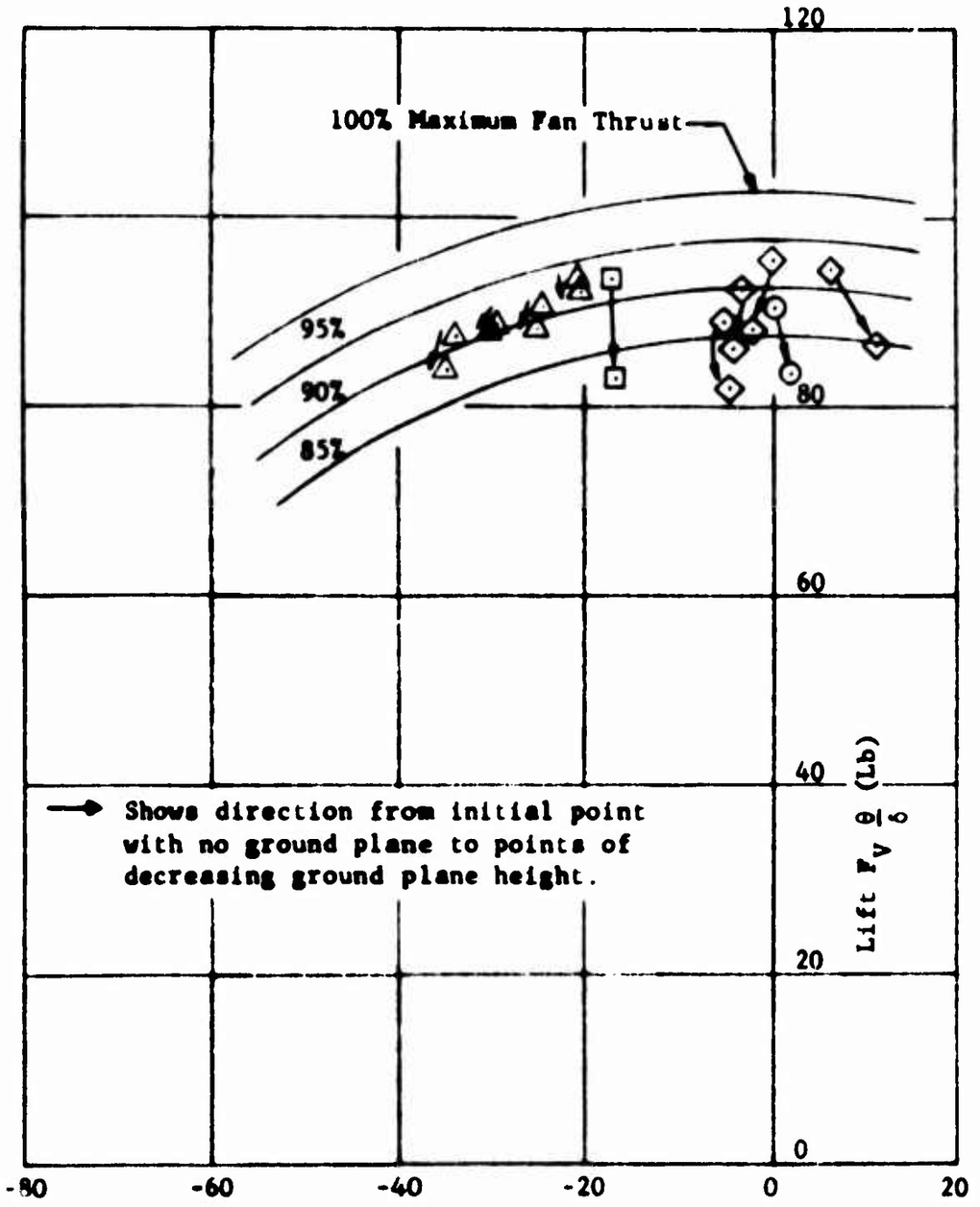

Where:

		Cascade A		Cascade B	
Mark	Run	θ_A^*	β_1^*	θ_B^*	β_1^*
○	21	78°	39°	42°	37°
□	22	78°	39°	48°	37°
△	24	78°	39°	48°	25°
◇	26	61°	37°	48°	25°

Figure 59. Vectored Thrust - Ground Effect.

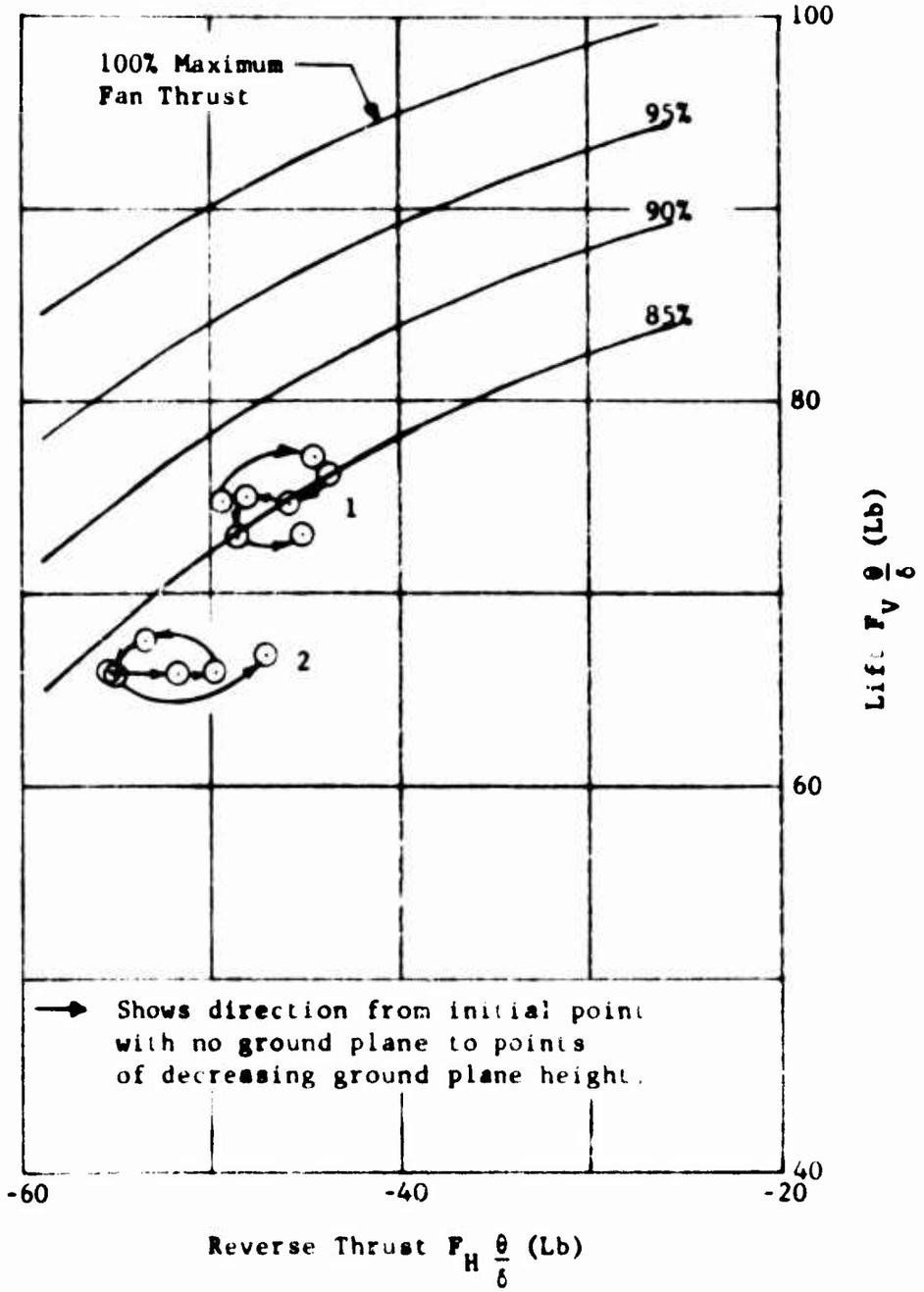

Where:

		1st Cascade		2nd Cascade		
Mark	Run	θ_A^*	β_1^*	θ_B^*	β_1^*	γ_B
1	16	80°	39.5°	78°	39°	95°
2	17	80°	39.5°	78°	39°	105°

Figure 60. Vectored Thrust - Ground Effect.

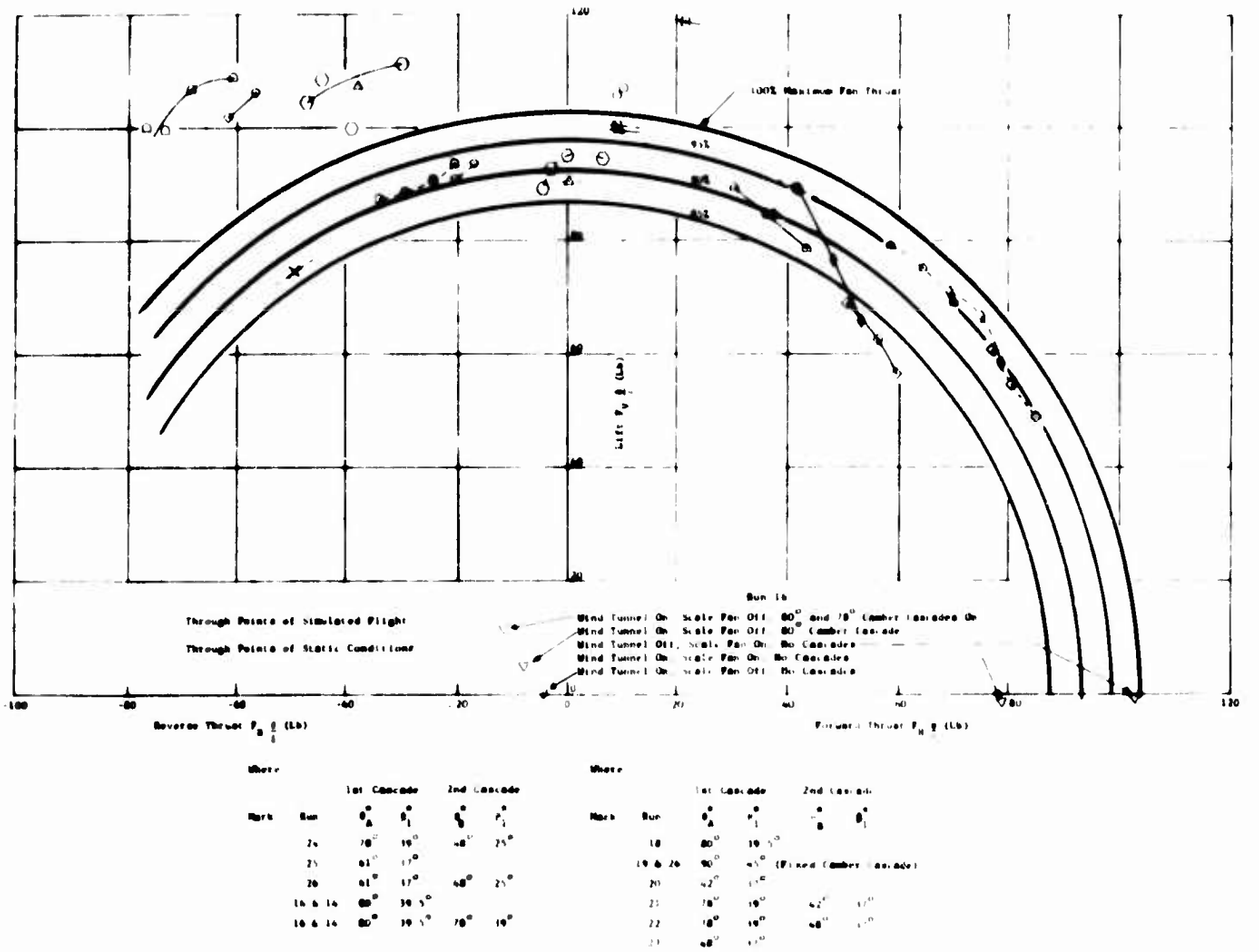

Figure 61. Vectored Thrust Comparison of Simulated Flight and Static Test Conditions.

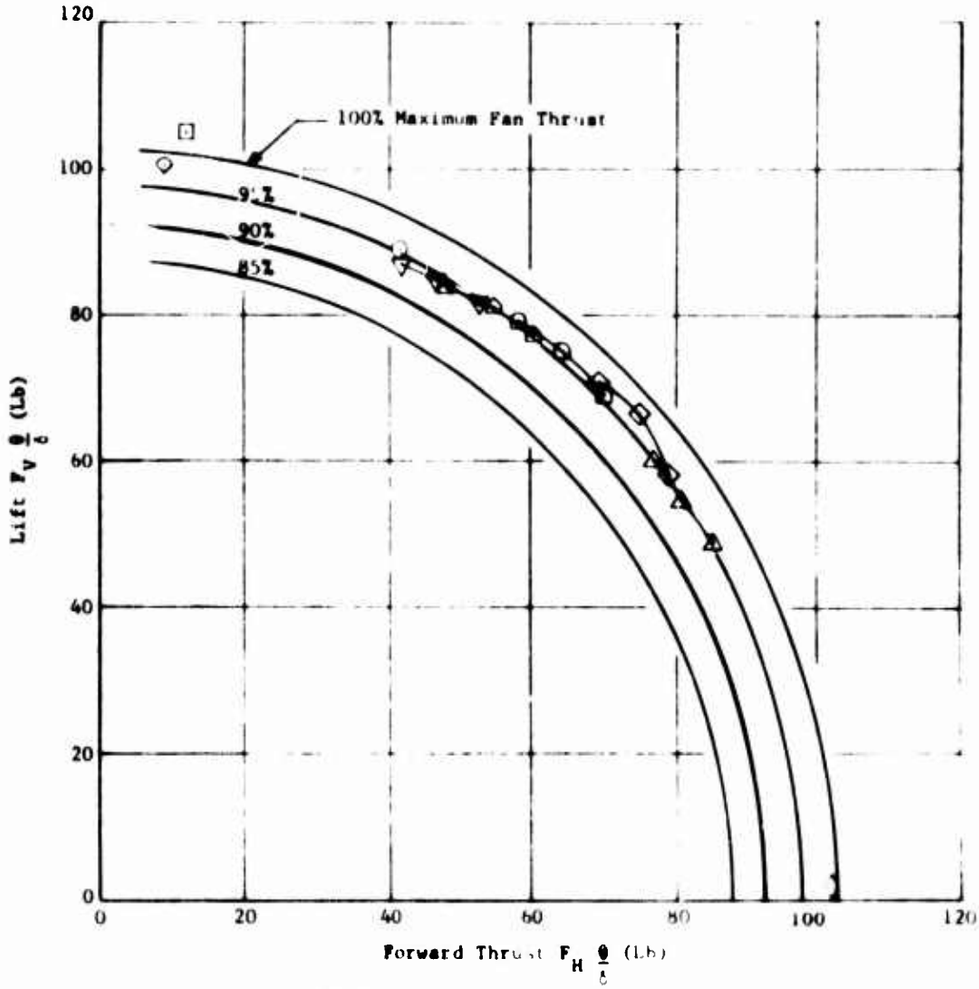

Where:

Mark	Run	θ_A^*	β_1^*	
○	18	80°	39.5°	
□	19	90°	45°	(Fixed Camber)
△	20	42°	37°	
◇	21	48°	37°	
⌂	25	61°	37°	
◇	26	No Cascade		
◇	26	90°	45°	(Fixed Camber)
▽	27	78°	39°	
⌂	27	60°	35°	

Figure 62. Vectored Thrust

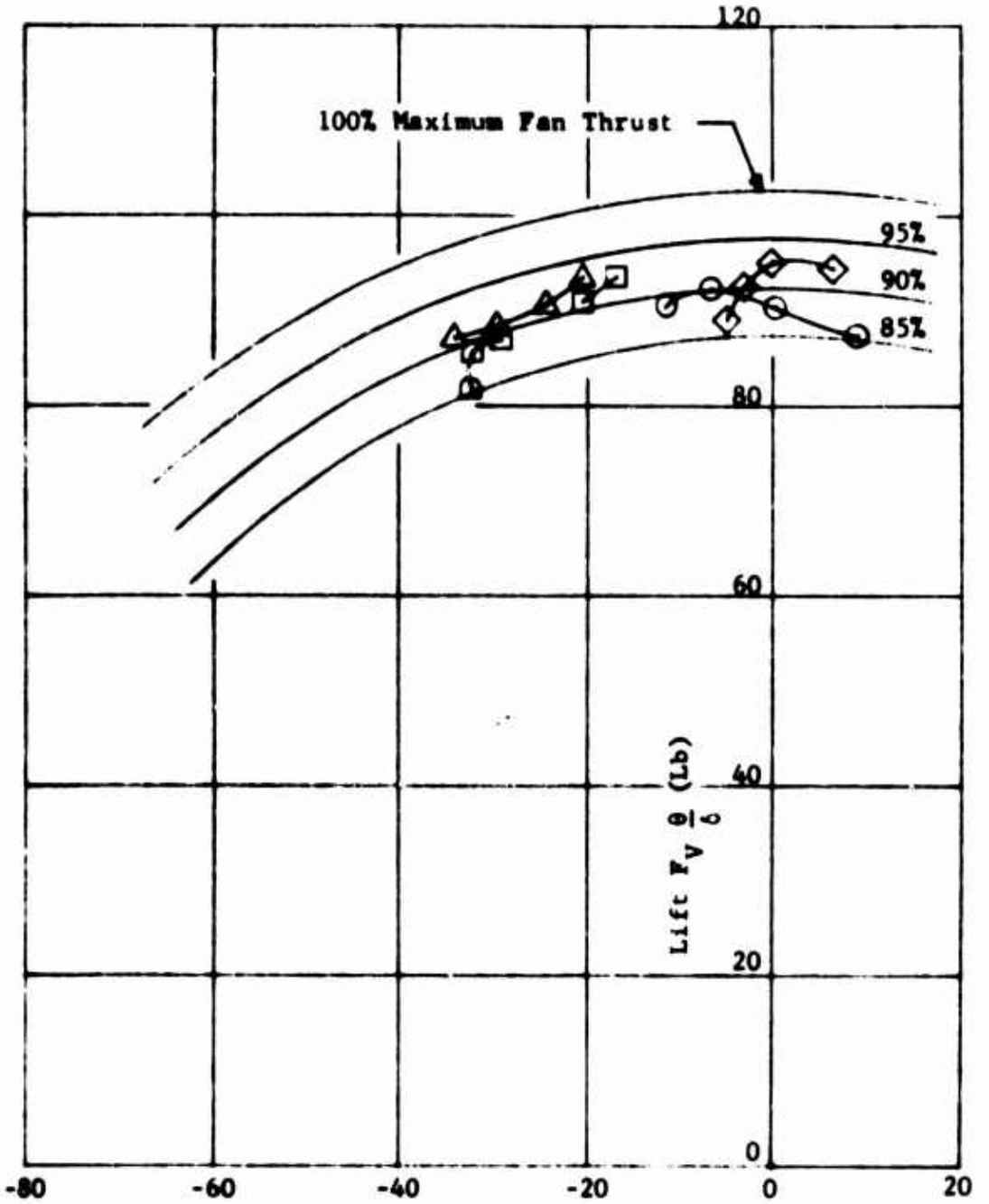

Where:

Mark	Run	1st Cascade θ_A^*	1st Cascade β_1^*	2nd Cascade θ_B^*	2nd Cascade β_1^*
○	21	78°	39°	42°	37°
□	22	78°	39°	48°	37°
△	24	78°	39°	48°	25°
◇	26	61°	37°	48°	25°
⬠	27	78°	39°	60°	35°

Figure 63. Vectored Thrust.

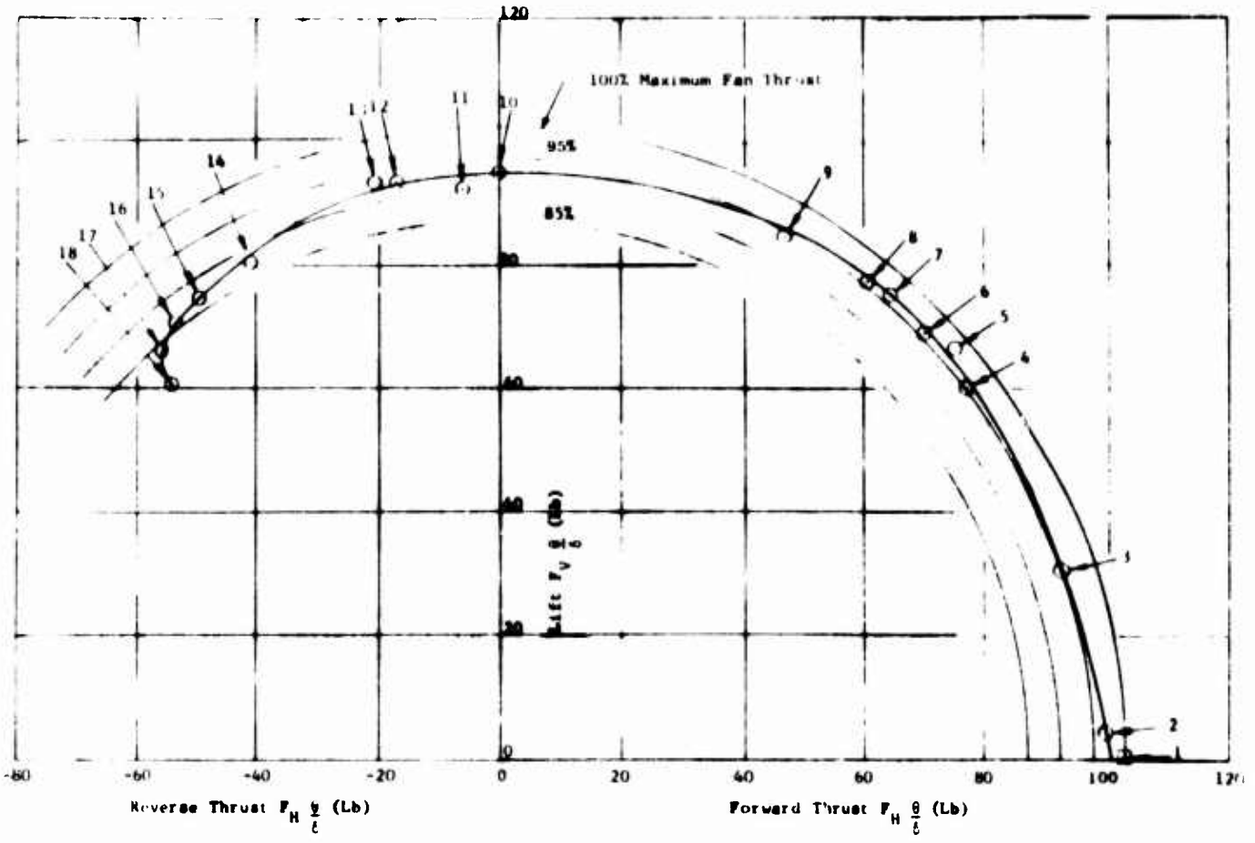

Where:

Mark	Run-Reading	1st Cascade θ_A^*	1st Cascade β_1^*	1st Cascade γ_A	2nd Cascade θ_B^*	2nd Cascade β_1^*	2nd Cascade γ_B
1	1-2	(No Cascades Mounted, Maximum Fan Thrust)					
2	1-1	0°	13.5°	0°			
3	2-2	25°	13.5°	9°			
4	20-7	42°	37°	35°			
5	23-5	48°	37°	35°			
6	25-1	61°	37°	30°			
7	25-5	61°	37°	35°			
8	27-1	60°	35°	30°			
9	27-2	78°	39°	35°			

Mark	Run-Reading	1st Cascade θ_A^*	1st Cascade β_1^*	1st Cascade γ_A	2nd Cascade θ_B^*	2nd Cascade β_1^*	2nd Cascade γ_B
10	26-4	61°	37°	35°	48°	25°	68°
11	21-5	78°	39°	35°	42°	37°	90°
12	22-1	78°	39°	35°	48°	37°	94°
13	24-1	78°	39°	35°	48°	25°	84°
14	14-3	78°	39°	35°	80°	39.5°	90°
15	14-18	80°	39.5°	38°	78°	39°	95°
16	14-19	80°	39.5°	38°	78°	39°	100°
17	14-20	80°	39.5°	38°	78°	39°	105°
18	14-21	80°	39.5°	38°	78°	39°	110°

Figure 64. Summary of Maximum Vectored Thrust for Phase III, Tandem Cascade Testing.

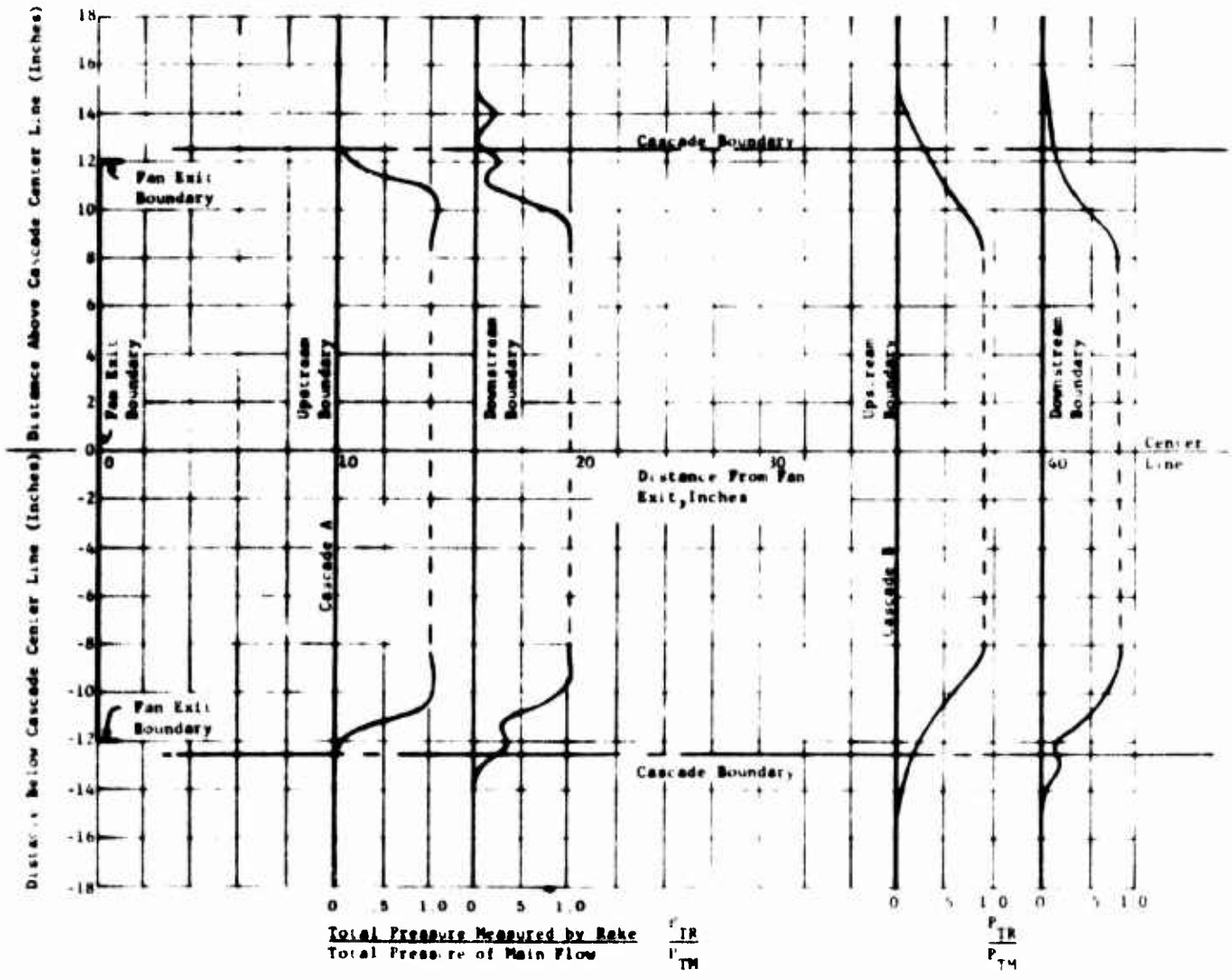

Figure 65. Flow Distribution Through Tandem Cascades.

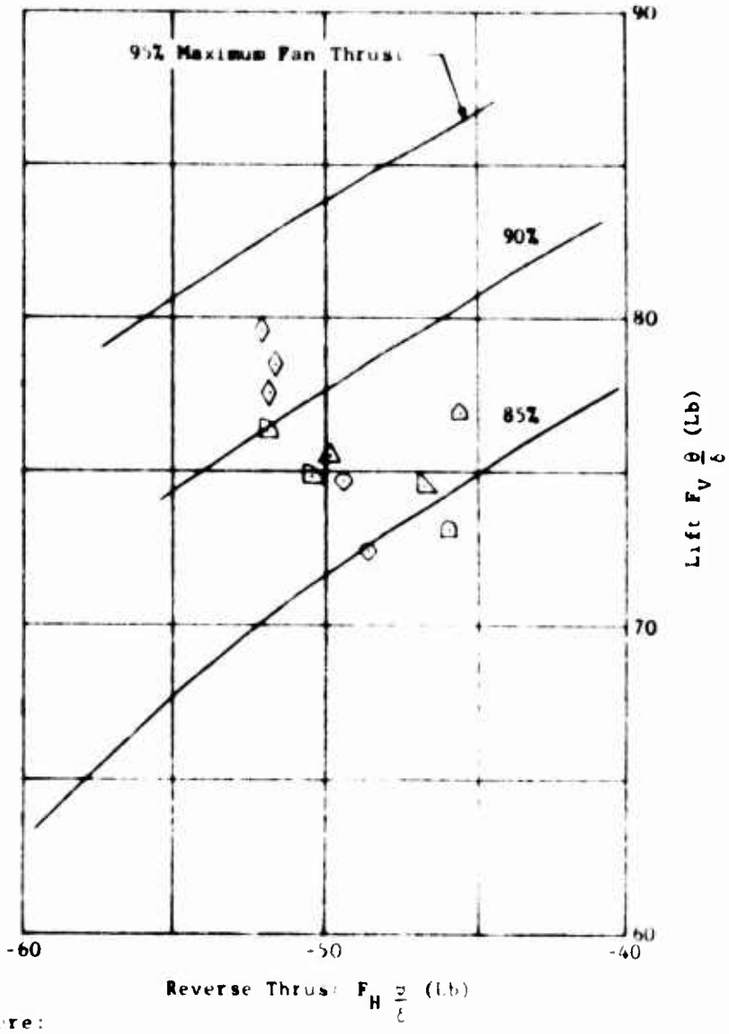

Where:

- No Ducts or End Plates.
- Ducts From Fan to Cascade A, to Cascade B End Plates on Both Cascades.
- Duct From Fan to Cascade A, End Plates on Cascade A.
- Duct From Cascade A to Cascade B, End Plates on Both.
- End Plates on Cascades A and B.
- Duct From Cascade A to Cascade B
- Ducts From Fan to Cascade A, to Cascade B, No End Plates.

Figure 66 Vectored Thrust - Ducted Flow.

Figure 67. Comparison of Run 27 Vectored Thrust with Previous Runs.

DISTRIBUTION

U. S. Army Materiel Command	1
U. S. Army Mobility Command	2
U. S. Army Aviation Materiel Command	2
U. S. Army Transportation Research Command	24
U. S. Army Research and Development Group (Europe)	2
U. S. Army Engineer Research and Development Laboratories	2
Army Research Office-Durham	1
U. S. Army Engineer Waterways Experiment Station	1
U. S. Army Combat Developments Command Aviation Agency	1
U. S. Army Aviation School	1
U. S. Army Aviation Test Board	1
U. S. Army Aviation Test Activity	1
U. S. Army Representative, Air Force Systems Command, Andrews AFB	2
Air Force Systems Command, Wright-Patterson AFB	1
Air Force Flight Test Center, Edwards AFB	1
Bureau of Naval Weapons	2
U. S. Naval Postgraduate School	1
Naval Air Test Center	1
David Taylor Model Basin	1
Marine Corps Liaison Officer, U. S. Army Transportation School	1
Ames Research Center, NASA	2
NASA-LRC, Langley Station	2
Lewis Research Center, NASA	2
Manned Spacecraft Center, NASA	2
NASA Representative, Scientific and Technical Information Facility	2
Research Analysis Corporation	1
Canadian Liaison Officer, U. S. Army Transportation School	1
Defense Documentation Center	20

General Electric Company, Cincinnati, Ohio, 45215, TANDEM CASCADE THRUST VECTORING RESEARCH PROGRAM - J.R. Erwin, D.E. Clark, R.G. Giffin, and J.G. Kirkpatrick, TRECOM Technical Report 64-59, November 1964, 134 pp. [Contract DA 44-177-AMC-73(T)] USA-TRECOM Project 1D121401A142.

Unclassified Report

Continuous thrust vectoring from horizontal through vertical, to reversed thrust can be accomplished by the use of one or two cascades in

(over)

1. Thrust Vectoring
2. Variable Camber Blades
3. Tandem Cascade
4. Contract DA 44-177-AMC-73(T)

General Electric Company, Cincinnati, Ohio, 45215, TANDEM CASCADE THRUST VECTORING RESEARCH PROGRAM - J.R. Erwin, D.E. Clark, R.G. Giffin, and J.G. Kirkpatrick, TRECOM Technical Report 64-59, November 1964, 134 pp. [Contract DA 44-177-AMC-73(T)] USA-TRECOM Project 1D121401A142.

Unclassified Report

Continuous thrust vectoring from horizontal through vertical, to reversed thrust can be accomplished by the use of one or two cascades in

(over)

1. Thrust Vectoring
2. Variable Camber Blades
3. Tandem Cascade
4. Contract DA 44-177-AMC-73(T)

General Electric Company, Cincinnati, Ohio, 45215, TANDEM CASCADE THRUST VECTORING RESEARCH PROGRAM - J.R. Erwin, D.E. Clark, R.G. Giffin, and J.G. Kirkpatrick, TRECOM Technical Report 64-59, November 1964, 134 pp. [Contract DA 44-177-AMC-73(T)] USA-TRECOM Project 1D121401A142.

Unclassified Report

Continuous thrust vectoring from horizontal through vertical, to reversed thrust can be accomplished by the use of one or two cascades in

(over)

1. Thrust Vectoring
2. Variable Camber Blades
3. Tandem Cascade
4. Contract DA 44-177-AMC-73(T)

General Electric Company, Cincinnati, Ohio, 45215, TANDEM CASCADE THRUST VECTORING RESEARCH PROGRAM - J.R. Erwin, D.E. Clark, R.G. Giffin, and J.G. Kirkpatrick, TRECOM Technical Report 64-59, November 1964, 134 pp. [Contract DA 44-177-AMC-73(T)] USA-TRECOM Project 1D121401A142.

Unclassified Report

Continuous thrust vectoring from horizontal through vertical, to reversed thrust can be accomplished by the use of one or two cascades in

(over)

1. Thrust Vectoring
2. Variable Camber Blades
3. Tandem Cascade
4. Contract DA 44-177-AMC-73(T)

series, each employing variable camber airfoils. An experimental wind tunnel evaluation of three types of variable camber airfoils, and experimental scale model investigation of the principle applied to a cruise fan is reported. Flexible camber blades are found to be most satisfactory with a cascade pressure loss coefficient of 0.4. The tandem cascade system provides efficient thrust vectoring varying from 6 percent loss at 67° vectoring, 12 percent loss at 124° vectoring and a maximum of 54 percent reversed thrust. The application of this thrust vectoring system to V/STOL applications is encouraged by these results.

series, each employing variable camber airfoils. An experimental wind tunnel evaluation of three types of variable camber airfoils, and experimental scale model investigation of the principle applied to a cruise fan is reported. Flexible camber blades are found to be most satisfactory with a cascade pressure loss coefficient of 0.4. The tandem cascade system provides efficient thrust vectoring varying from 6 percent loss at 67° vectoring, 12 percent loss at 124° vectoring and a maximum of 54 percent reversed thrust. The application of this thrust vectoring system to V/STOL applications is encouraged by these results.

series, each employing variable camber airfoils. An experimental wind tunnel evaluation of three types of variable camber airfoils, and experimental scale model investigation of the principle applied to a cruise fan is reported. Flexible camber blades are found to be most satisfactory with a cascade pressure loss coefficient of 0.4. The tandem cascade system provides efficient thrust vectoring varying from 6 percent loss at 67° vectoring, 12 percent loss at 124° vectoring and a maximum of 54 percent reversed thrust. The application of this thrust vectoring system to V/STOL applications is encouraged by these results.

series, each employing variable camber airfoils. An experimental wind tunnel evaluation of three types of variable camber airfoils, and experimental scale model investigation of the principle applied to a cruise fan is reported. Flexible camber blades are found to be most satisfactory with a cascade pressure loss coefficient of 0.4. The tandem cascade system provides efficient thrust vectoring varying from 6 percent loss at 67° vectoring, 12 percent loss at 124° vectoring and a maximum of 54 percent reversed thrust. The application of this thrust vectoring system to V/STOL applications is encouraged by these results.